Energy, Mines and Resources Canada

Énergie, Mines et Ressources Canada

CANMET

Canada Centre for Mineral and Energy Technology

Centre canadien de la technologie des minéraux et de l'énergie

Mining Research Laboratories

Laboratoires de recherche minière

Canada

HIGH TEMPERATURE UNIAXIAL AND TRIAXIAL COMPRESSION TESTS ON URL ROCK SAMPLES FROM BOREHOLE 401-009-HF1

J.S.O. Lau and B. Gorski January 1990

Mining Research Laboratories
Divisional Report MRL 90-5(TR)

MICROMEDIA

This document is an unedited interim report prepared primarily for discussion and internal reporting purposes. It does not represent a final expression of the opinion of the Canada Centre for Mineral and Energy Technology (CANMET)

Ce document est un rapport provisoire non revisé et rédigé principalement pour la diffusion et la documentation interne. Il ne représente nullement l'expression définitive de l'opinion du Centre canadien de la technologie des minéraux et de l'énergie (CANMET)

100 pp

90-06010/

HIGH TEMPERATURE UNIAXIAL AND TRIAXIAL COMPRESSION TESTS ON URL ROCK SAMPLES FROM BOREHOLE 401-009-HF1

by

J.S.O. Lau[1] and B. Gorski[2]

ABSTRACT

A series of ambient and high temperature uniaxial compression tests and triaxial compression tests were conducted on grey granitic core samples obtained from Borehole 401-009-HF1 located at the 420 level of Atomic Energy of Canada Limited's Underground Research Laboratory (URL). Twelve sets of tests were carried out at three temperatures (21°, 75° and 125° C) and four confining pressures (0.0, 3.5, 17.0 and 35.0 MPa) to study the thermo-mechanical properties of the rock at the 420 level of the URL.

The failure deviator stress, axial strain at failure and Poisson's ratio were found to increase with increasing confining pressure, but decrease with increasing temperature. The largest decrease in the failure deviator stress occurred at the unconfined condition.

The tangent Young's modulus and pseudo Young's modulus increased with increasing confining pressure at stress levels below 0.8 times the failure deviator stress. Temperature had no effect on these two moduli.

The strength properties of the intact rock material were expressed in terms of the Hoek and Brown failure criterion. The uniaxial compressive strength of the intact rock material σ_c decreased only when the temperature was raised from 75° to 125° C. It appeared that temperature had no effect on the material constant m. The cohesive strengths and angles of internal friction of the rock samples were measured from the Mohr failure envelopes generated by using equations suggested by Hoek and Brown. The cohesive strength appeared to decrease with increasing temperature, while the angle of internal friction remained unaffected.

---

[1]Geotechnical Engineer, Atomic Energy of Canada Limited, on attachment to Canadian Mine Technology Laboratory, Mining Research Laboratories, CANMET, Energy, Mines and Resources Canada, Ottawa, Ontario.

[2]Rock Mechanics and Development Technologist, Canadian Mine Technology Laboratory, Mining Research Laboratories, CANMET, Energy, Mines and Resources Canada, Ottawa, Ontario.

The effect of stress relaxation on the rock specimens was found to be greater at the 420 level than at the 240 level of the URL, resulting in higher crack porosity, lower p-wave and s-wave velocities, larger deformations and lower Young's modulus values.

Keywords: uniaxial, triaxial, compression, temperature, confining pressure, strength, deformation, modulus, micro-crack, wave velocity

ESSAIS DE COMPRESSION UNIAXIALE ET TRIAXIALE A HAUTE TEMPÉRATURE SUR DES ECHANTILLONS DE ROCHE DU SONDAGE 401-009-HF1 DU LRS

par

J.S.O. Lau[1] et B. Gorski[2]

RÉSUMÉ

Une série d'essais de compression uniaxiale et triaxiale à température ambiante et élevée ont été menés sur des échantillons de carottes de granit gris prélevées dans le sondage 401-009-HF1 au niveau 420 du Laboratoire de recherche sousterrain (LRS) d'Energie atomique du Canada limitée. Douze ensembles d'essais ont été effectués à trois température (21°, 75° et 125° C) et quatre pressions de confinement (0.0, 3.5, 17.0 et 35.0 MPa) pour étudier les propriétés thermo-mécaniques de la roche au niveau 420 du LRS.

Les essais ont révélé que la contrainte de distorsion de rupture, la déformation axiale de rupture et le rapport de Poisson augmentent en fonction de la pression de confinement, mais diminuent en fonction de la température. La plus forte diminution de la contrainte de distorsion de rupture s'est produite en l'absence de confinement.

Le module tangent d'Young et le pseudo-module d'Young ont augmenté en fonction de la pression de confinement sous des contraintes inférieures á 0.8 fois la contrainte de distorsion de rupture. La température n'a eu aucun effet sur ces deux modules.

La résistance de la roche intacte a été exprimée en termes du critère de rupture de Hoek et Brown. La résistance à la compression uniaxiale de la roche intacte σ_c n'a diminué que lorsque la température a été porté de 75° á 125° C. Il semble que la température n'eu aucun effet sur la constant du matériau m. Les forces de cohésivité

---

[1]Ingénieur géotechnique, L'Énergie atomique de Canada Limitée, détaché au Laboratoire canadien de la technologie minière, Laboratories de recherche miniére, CANMET, Énergie, Mines et Ressources Canada, Ottawa, Ontario.

[2]Spécialiste en mécanique des roches et technique de développement, Laboratoire canadien de la technologie minière, Laboratoires de recherche minière, CANMET, Énergie, Mines et Ressources Canada, Ottawa, Ontario.

et les angles de frottement interne des échantillons de roche ont été mesurés à l'aide des enveloppes de rupture de Mohr générées par les équations proposées par Hoek et Brown. La force de cohésivité semble diminuer en fonction de la température, tandis que l'angle de frottement interne demeure inchangé.

L'effet de la ralaxation des contraintes sur les éprouvettes de roche s'est avéré plus important au niveau 420 qu'au niveau 240 du LRS, donnant lieu à une porosité plus grande des fissures, à des vitesses réduites des ondes P et S, à des déformations plus fortes et à des valeurs plus faibles du module d'Young.

Mots clés: uniaxiale, triaxiale, compression, température, pression de confinement, résistance, déformation, module, microfissure, vitesse d'une onde.

TABLE OF CONTENTS

	Page No.
Abstract	i
Résumé	iii
Table of contents	v
List of tables	vi
List of figures	vii
1. Introduction	1
2. Sampling and specimen preparation	1
3. Dynamic elastic properties	2
4. Test apparatus and procedure	4
5. Testing program	5
6. Results and discussion	5
6.1 Test results	5
6.2 Failure deviator stress	6
6.3 Axial strain at failure	7
6.4 Tangent Young's modulus	7
6.5 Pseudo Young's modulus	9
6.6 Poisson's ratio	10
6.7 Strength properties of intact rock material	10
7. Conclusions	13
8. Recommendations	14
Acknowledgements	14
References	15
Appendix A	51

LIST OF TABLES

Table		Page No.
1.	Dimensions, densities and dynamic elastic properties of rock specimens.	17
2.	Results of ambient temperature and high temperature uniaxial and triaxial compression tests.	18
3.	Mean failure deviator stresses, mean axial strains at failure and mean Poisson's ratios.	20
4.	Tangent Young's moduli at stress levels ranging from 10% to 90% of the failure deviator stress.	21
5.	Pseudo Young's moduli at stress levels ranging from 10% to 90% of the failure deviator stress.	23
6.	Values of σ_c, m, s and r^2 derived from the Hoek and Brown failure criterion.	25
7.	Angles of internal friction and cohesive strengths measured from Mohr failure envelopes.	26

LIST OF FIGURES

Figure		Page No.
1.	Plots of failure deviator stress versus temperature.	27
2.	Plots of tangent Young's modulus versus normalized deviator stress at 21° C.	28
3.	Plots of tangent Young's modulus versus normalized deviator stress at 75° C.	29
4.	Plots of tangent Young's modulus versus normalized deviator stress at 125° C.	30
5.	Plots of tangent Young's modulus versus normalized deviator stress at the unconfined condition.	31
6.	Plots of tangent Young's modulus versus normalized deviator stress at the confining pressure of 3.5 MPa.	32
7.	Plots of tangent Young's modulus versus normalized deviator stress at the confining pressure of 17.0 MPa.	33
8.	Plots of tangent Young's modulus versus normalized deviator stress at the confining pressure of 35.0 MPa.	34
9.	Plots of tangent Young's modulus at $0.5(\sigma_1 - \sigma_3)_f$ versus temperature.	35
10.	Plots of pseudo Young's modulus versus normalized deviator stress at 21° C.	36
11.	Plots of pseudo Young's modulus versus normalized deviator stress at 75° C.	37
12.	Plots of pseudo Young's modulus versus normalized deviator stress at 125° C.	38
13.	Plots of pseudo Young's modulus versus normalized deviator stress at the unconfined condition.	39
14.	Plots of pseudo Young's modulus versus normalized deviator stress at the confining pressure of 3.5 MPa.	40
15.	Plots of pseudo Young's modulus versus normalized deviator stress at the confining pressure of 17.0 MPa.	41
16.	Plots of pseudo Young's modulus versus normalized deviator stress at the confining pressure of 35.0 MPa.	42
17.	Plots of pseudo Young's modulus at $0.5(\sigma_1 - \sigma_3)_f$ versus temperature.	43
18.	Plots of Poisson's ratio at $0.4(\sigma_1 - \sigma_3)_f$ versus temperature.	44

19. Hoek and Brown failure envelope at 21° C. 45
20. Hoek and Brown failure envelope at 75° C. 46
21. Hoek and Brown failure envelope at 125° C. 47
22. Mohr circles and failure envelope at 21° C. 48
23. Mohr circles and failure envelope at 75° C. 49
24. Mohr circles and failure envelope at 125° C. 50

1. Introduction

The Canadian Nuclear Fuel Waste Management Program (CNFWMP) is concerned with the safe, long term disposal of high level nuclear wastes in vaults located at depth in plutonic rock. As part of the program, Atomic Energy of Canada Limited (AECL) has constructed the Underground Research Laboratory (URL) located near to Lac du Bonnet, Manitoba to provide a representative environment in which to conduct in situ investigations. Some of these investigations will provide rock mass mechanical properties and will assess the accuracy of mathematical models by comparison with field measurements (Simmons and Soonawala, 1982). In support of these investigations, a joint laboratory testing and analysis program has been undertaken by the Canada Centre for Mineral and Energy Technology (CANMET) and AECL to provide data on the mechanical properties of the rock mass surrounding the URL excavation under both ambient and high temperature conditions. This information is required by numerical modellers for input into mechanical models and by engineers for the design of the experiments to be carried out at the URL.

The majority of high temperature uniaxial and triaxial tests have been conducted on rock core samples obtained from the 240 level at the URL and from the upper 300 m in the rock mass surrounding the URL excavation (Jackson, 1984; Annor and Jackson, 1985; Annor and Jackson, 1987; Lau et al., 1988a; Lau et al. 1988b; Lau and Gorski, 1989). In February 1989, the necessity of studying the effect of high temperatures as well as stress relaxation on the mechanical properties of the rock mass at greater depth was identified. A series of uniaxial compression and triaxial compression tests at the confining pressures of 3.5, 17.0 and 35.0 MPa and at the test temperatures of 21°, 75° and 125° C were carried out in September 1989. Rock core samples were obtained from Borehole 401-009-HF1 drilled at the 420 level in the URL. This report presents the results of the program, compares the thermo-mechanical properties of the rock samples from the 420 level with those from the 240 level, and recommends what further laboratory work will be required to determine the thermo-mechanical properties of the rock in the URL characterization program during the operating phase of the URL.

2. Sampling and specimen preparation

Samples used in these tests were supplied by AECL. They are NQ rock cores obtained from Borehole 401-009-HF1 between the downhole lengths of 32.1 and 40.7 m. The rock is a massive, grey, medium to coarse grained granite, composed of quartz, K-feldspar, plagioclase and biotite. Specimens with ends ground parallel to within 0.025

mm were prepared from those samples in accordance to the procedure described in the Pit Slope Manual Supplement 3-5 (Gyenge and Ladanyi, 1977) and the method suggested by the International Society for Rock Mechanics (Brown, 1981).

The lengths, diameters and bulk densities of the specimens are shown in Table 1. The lengths of the specimens varied from 105.15 to 111.21 mm and the diameters varied from 44.90 to 45.0 mm, with length to diameter ratios ranging from 2.3 to 2.5.

The three specimens to be used for uniaxial compression tests at room temperature were gauged, using Micro-measurements type EA-06-500BH-120 gauges. Two diametrically opposite axial strain gauges were mounted at the mid-height of each of the specimens and were connected in series to form a single active gauge. Two circumferential strain gauges were similarly mounted at 90° to the axial gauges.

3. Dynamic elastic properties

Prior to the uniaxial and triaxial compression testing, compression (p) and shear (s) wave velocity measurements were made on the rock specimens. The purposes of the p-wave and s-wave velocity measurements are to estimate various mechanical rock properties non-destructively prior to actual testing and to detect the presence of microcracks in the specimens. The velocity measurements were made in accordance with the procedures described in the Instruction Manual - Sonic Velocity Equipment (Terrametric, 1980) and the Pit Slope Manual Supplement 3-2 (Gyenge and Herget, 1977). The p-wave and s-wave velocities were determined from p-wave and s-wave transit times made along the longitudinal axes of the specimens. The dynamic elastic constants were computed from the wave velocities using the following equations:

Dynamic Young' modulus of elasticity:

$$E_u = \frac{\rho V_s^2 (3V_p^2 - 4V_s^2)}{V_p^2 - V_s^2} \qquad (1)$$

where E_u = dynamic Young's modulus of elasticity
V_p = compression wave velocity
V_s = shear wave velocity
ρ = bulk density

Dynamic shear modulus:

$$G_u = \rho V_s^2 \tag{2}$$

where G_u = dynamic shear modulus

Dynamic Poisson's ratio:

$$\nu_u = \frac{V_p^2 - 2V_s^2}{2(V_p^2 - V_s^2)} \tag{3}$$

where ν_u = dynamic Poisson's ratio

The p-wave velocity, s-wave velocity, dynamic Young's modulus, dynamic shear modulus and dynamic Poisson's ratio determined for each of the specimens are shown in Table 1. Their mean values and standard deviations (s.d.) can be summarized as follows:

p-wave velocity: 3.486 km/s (s.d. = 0.243 km/s)

s-wave velocity: 2.039 km/s (s.d. = 0.096 km/s)

dynamic Young's modulus: 26.97 GPa (s.d. = 2.51 GPa)

dynamic shear modulus: 10.95 GPa (s.d. = 1.04 GPa)

dynamic Poisson's ratio: 0.23 (s.d. = 0.05)

The p-wave and s-wave velocities for rock specimens from two boreholes at the 240 level were found to be in the ranges of 4.448 - 5.515 km/s and 2.615 - 2.949 km/s respectively (Lau and Gorski, 1989). The p-wave and s-wave velocities for specimens from Borehole 401-009-HF1 at the 420 level are lower than those obtained from the 240 level, indicating a higher degree of micro-cracking in these specimens. This suggests that at the 420 level, the in situ stress is higher and therefore the effect of stress relaxation is more prominent, resulting in higher crack porosity.

4. Test apparatus and procedure

The apparatus used to carry out the uniaxial and triaxial compression tests was a MTS 815 Rock Mechanics Test System. The MTS system is a servo-hydraulic press consisting of a 2.22 MN rated load cell, load frame, hydraulic power supply, triaxial cell, test controller, test processor, temperature controller and DEC micro PDP 11/73 computer. The triaxial cell is rated up to 200° C and equipped with a heater, heat shroud, thermocouples, three linear variable differential transducers (LVDTs) for the measurement of axial strain and an extensometer with a circumferential kit for the measurement of circumferential strain. For a detailed description of the MTS system and its operation, the reader is referred to the MTS Operation Manual (MTS Systems Corp., 1986) and CANMET Division Report MRL 87-33(INT) (Gorski, 1987).

The procedure used to conduct the uniaxial compression tests at room temperature conformed with the uniaxial compression test procedure described in the Pit Slope Manual Supplement 3-2 (Gyenge and Herget, 1977). The axial and circumferential strain gauges mounted on the specimen were connected to B & K type 1526 strain indicators in a half-bridge configuration. The indicators' output was monitored every second by the test processor in the MTS system. LVDTs in the triaxial cell were also used to measure axial displacement.

The procedure used to carry out the uniaxial compression tests at high temperature and the procedure used to conduct the triaxial compression tests were similar to the high temperature triaxial compression test procedure outlined in CANMET Division Report MRL 88-90(TR) (Lau et al., 1988a). The instrumented (LVDTs, extensometer and heater) rock specimen was placed in the triaxial cell which was then filled with Syltherm 800 heat transfer fluid. In the high temperature uniaxial compression test, no confining fluid pressure was applied to approximate a uniaxial testing condition. The hydrostatic pressure under this condition was very low (less than 3 kPa) and considered negligible. In the triaxial compression test, the confining fluid pressure and the axial load were raised simultaneously to the test level. In all high temperature tests, the confining fluid was heated at a rate of 1° C per minute until the test temperature was reached. A soak time of one hour was allowed to ensure even heat distribution throughout the specimen before testing.

The specimens were loaded at a constant rate of 1 kN per second under computer control. Signals from the load cell, LVDTs, extensometer and strain gauges were scanned by the computer every second. The signals were converted to engineering units and measurements from the LVDTs were corrected for end platen compression. The data

were stored on hard disk in the micro PDP 11/73 computer and later transferred to the VAX computer for data analysis and plotting.

5. Testing program

Testing took place at Canadian Mine Technology Laboratory, Mining Research Laboratories, CANMET, Energy, Mines and Resources Canada in Ottawa in September, 1989. The testing program consisted of twelve sets of tests. Four sets of tests at the confining pressures of 0.0, 3.5, 17.0 and 35.0 MPa were carried out at each of the following temperatures: 21°, 75° and 125° C. At least three tests were conducted in each set in order to obtain statistically significant mean values. A total of 39 tests were performed. The testing program is summarized in Table 2.

6. Results and discussion

6.1 Test results

Table 2 summarizes the axial strain at failure, failure deviator stress, tangent Young's modulus and pseudo Young's modulus at the stress level of 50% of the failure deviator stress, Poisson's ratio, failure angle θ and failure characteristics of each of the specimens. Note that axial strains were measured using LVDTs and circumferential strains were measured using an extensometer. In those instances (uniaxial compression tests at 21° C) where strain gauges were also used to measure the axial and circumferential strains, the values of the axial strain at failure, tangent Young's modulus, pseudo Young's modulus and Poisson's ratio determined from strain gauge measurements are also given in the table. Poisson's ratio was determined from the ratio of the circumferential to the axial tangent moduli at the stress level equivalent to 40% of the failure deviator stress. The effects of confining pressure and temperature on the strength and elastic properties of the rock samples will be discussed in the following subsections.

Stress versus axial strain and stress versus circumferential strain curves for all tests are presented in Appendix A. Note that the axial strain was determined from the average of the axial deformations obtained from the three LVDTs. These curves were plotted by the use of DATAPLOT curve fitting software. A cubic spline fit was used for this analysis which employed a third degree equation model of the form:

$$\sigma = a_0 + a_1\varepsilon + a_2\varepsilon^2 + a_3\varepsilon^3 \quad (4)$$

where σ = stress

ε = strain

and a_0, a_1, a_2 and a_3 are coefficients

6.2 Failure deviator stress

One of the main objectives of these tests is to study the effects of confining pressure and temperature on the strength of the rock specimens. The failure deviator stresses of the specimens obtained from these tests are shown in Table 2 and their mean values are presented in Table 3. Note that in Table 3, the standard deviations are given in brackets. The faliure deviator stresses are plotted against temperature in Figure 1. Figure 1 shows that the failure deviator stress increased as the confining pressure increased as expected, but decreased with increasing temperature at all confining pressures. As the temperature was raised from 21° to 75° and to 125° C, the mean failure deviator stress decreased from 171.7 to 169.3 and to 161.7 MPa under the unconfined condition; from 239.3 to 234.3 and to 229.7 MPa at the confining pressure of 3.5 MPa; and from 542.7 to 533.0 and to 523.0 MPa at the confining pressure of 35.0 MPa. At the confining pressure of 17.0 MPa, there was no change in the mean failure deviator stress when the temperature increased from 21° to 75° C. However, when the temperature was raised to 125° C, the mean failure deviator stress decreased from 407.0 to 388.3 MPa. This discrepancy is probably due to the inhomogeneity of the rock. The largest decrease in failure deviator stress with increasing temperature occurred in the unconfined condition. A reduction of 5.8% in the mean failure deviator stress was observed in the unconfined condition when the temperature increased from 21° to 125° C. Reductions of 4.0%, 4.5% and 3.6% were observed at the confining pressures of 3.5, 17.0 and 35.0 MPa respectively.

It should be pointed out that the uniaxial compressive strength (failure deviator stress at unconfined condition) of rock specimens from Borehole 401-009-HF1 at the 420 level in the URL is similar to that from Borehole 209-030-DIL1 at the 240 level at all test temperatures (Lau and Gorski, 1989), but lower than that from Borehole 209-021-SV1 also at the 240 level.

6.3 Axial strain at failure

The axial strain at failure increased as the confining pressure increased as expected, but decreased with increasing temperature as shown in Tables 2 and 3. As the temperature increased from 21° to 75° and to 125° C, the mean axial strain at failure decreased from 0.392 to 0.385 and to 0.365 % under the unconfined condition; from 0.543 to 0.526 and to 0.464 % at the confining pressure of 3.5 MPa; and from 0.720 to 0.703 and to 0.678 % at the confining pressure of 17.0 MPa. At the confining pressure of 35.0 MPa, the mean axial strain at failure decreased from 0.900 to 0.867 % when the temperature was raised from 21° to 75° C. However, little change was observed when the temperature increased from 75° to 125° C. The discrepancy is probably due to the inhomogeneity of the rock.

The axial strains at failure of rock specimens from Borehole 401-009-HF1 at the 420 level were found to be larger than those from Boreholes 209-021-SV1 and 209-030-DIL1 at the 240 level (Lau et al., 1988b; Lau and Gorski, 1989). At the 420 level, due to the higher in situ stress, the effect of stress relaxation on the rock specimens was more significant. As a result, more micro-cracks were present in these specimens and the specimens failed at larger axial strains.

6.4 Tangent Young's modulus

Tangent Young's moduli for each of the rock specimens were computed at nine stress levels corresponding to 10, 20, 30, 40, 50, 60, 70, 80 and 90 % of the failure deviator stress, $(\sigma_1 - \sigma_3)_f$, and are presented in Table 4. The tangent moduli were determined by using the following procedure. Firstly, the three equations (Equation 4) resulted from the cubic spline fit of the deviator stress and axial strain data were solved for the nine stress values (10 t0 90 % of the failure deviator stress). The nine axial strain values obtained from the solutions were then substituted into the derivatives of the equations to compute the nine modulus values.

The tangent Young's moduli are plotted against the normalized deviator stress at the three test temperatures of 21°, 75° and 125° C in Figures 2, 3 and 4 respectively. The normalized deviator stress is defined as the ratio of the deviator stress to the failure deviator stress. In the unconfined condition, the tangent modulus increased until the nomalized deviator stress reached approximately 0.6, and then decreased slowly until failure. At the confining pressures of 3.5 and 17.0 MPa, the tangent modulus behaved similarly. However, at 3.5 MPa, the maximum value of tangent modulus was reached at approximately $0.5(\sigma_1 - \sigma_3)_f$, and at the higher confining pressure of 17.0 MPa, the

maximum value was reached at approximately $0.3(\sigma_1 - \sigma_3)_f$. At the high confining pressure of 35.0 MPa, the tangent modulus decreased slowly with increasing deviator stress. In Figures 2 to 4, all modulus-stress curves merge at approximately $0.8(\sigma_1 - \sigma_3)_f$, indicating that the differences in moduli diminished. This implies that at stress levels above $0.8(\sigma_1 - \sigma_3)_f$, an increase in confining pressure had little effect on the tangent modulus . At stress levels below $0.8(\sigma_1 - \sigma_3)_f$, an increase in the confining pressure resulted in an increase in the tangent modulus, especially at low stress levels. The increase was particularly pronounced when the confining pressure was raised from 3.5 to 17.0 MPa, suggesting that some stress relaxation had occurred in these specimens, resulting in larger deformations and lower modulus values at low confining pressures. It should also be pointed out that the tangent moduli of these specimens at the confining pressures of 0.0 and 3.5 MPa are lower than those obtained at the 240 level of the URL (Lau et al., 1988b; Lau and Gorski, 1989), indicating again that the effect of stress relaxation is more prominent at the 420 level.

To study the effect of temperature on tangent Young's modulus, the tangent Young's moduli are plotted against the normalized deviator stress at the four confining pressures of 0.0, 3.5 17.0 and 35.0 MPa in Figures 5, 6, 7 and 8 respectively. These figures show that temperature had no effect on the tangent modulus at any of the four confining pressures tested. The mean tangent Young's moduli at $0.5(\sigma_1 - \sigma_3)_f$ at the temperatures of 21°, 75° and 125° C, namely $E_{21°}$, $E_{75°}$ and $E_{125°}$, were determined as follows:

$\sigma_3 = 0.0$ MPa $\quad E_{21°} = 58.27$ GPa (s.d. $= 1.23$) $\quad E_{75°} = 58.55$ GPa (s.d. $= 1.58$)
$E_{125°} = 57.63$ GPa (s.d. $= 1.93$)

$\sigma_3 = 3.5$ MPa $\quad E_{21°} = 61.41$ GPa (s.d. $= 0.90$) $\quad E_{75°} = 61.32$ GPa (s.d. $= 2.88$)
$E_{125°} = 64.96$ GPa (s.d. $= 2.32$)

$\sigma_3 = 17.0$ MPa $\quad E_{21°} = 69.06$ GPa (s.d. $= 1.50$) $\quad E_{75°} = 68.96$ GPa (s.d. $= 2.36$)
$E_{125°} = 69.20$ GPa (s.d. $= 2.20$)

$\sigma_3 = 35.0$ MPa $\quad E_{21°} = 69.68$ GPa (s.d. $= 1.18$) $\quad E_{75°} = 69.74$ GPa (s.d. $= 1.71$)
$E_{125°} = 69.01$ GPa (s.d. $= 0.53$)

In Figure 9, the tangent moduli at $0.5(\sigma_1 - \sigma_3)_f$ and their mean values are plotted versus temperature. No significant change in the mean values was observed at the confining pressures of 0.0, 17.0 and 35.0 MPa, when the temperature increased from 21° to 125° C. At the confining pressure of 3.5 MPa, an increase in the mean value was observed when

the temperature was raised from 75° to 125° C, probably due to the inhomogeneity of the rock.

It should be noted that the mean tangent Young's moduli at $0.5(\sigma_1 - \sigma_3)_f$ in the unconfined condition are approximately 2 and 7 GPa lower than those obtained from Boreholes 209-030-DIL1 and 209-021-SV1 respectively at the 240 level of the URL.

6.5 Pseudo Young's modulus

Actual stress versus axial strain curves for these specimens are nonlinear (see Appendix A). For modelling purposes, these nonlinear curves may be idealized as a series of straight lines joining points corresponding to stress levels of 0.0, 0.1, 0.2, 0.3, 0.4, 0.5, 0.6, 0.7, 0.8, 0.9 and 1.0 times the failure deviator stress. The slope of the linear stress-strain curve during each stress interval is defined as the pseudo Young's modulus. The pseudo Young's moduli of the rock specimens are presented in Table 5. In general, the pseudo moduli are lower than the tangent moduli at stress levels below $0.4(\sigma_1 - \sigma_3)_f$, but higher than the tangent moduli at stress levels above $0.6(\sigma_1 - \sigma_3)_f$. At stress levels between 0.4 and 0.6 times the failure deviator stress, the pseudo moduli are similar to the tangent moduli.

The plots of the pseudo Young's modulus against the normalized deviator stress at the test temperatures of 21°, 75° and 125° C are shown in Figures 10, 11 and 12 respectively. Their patterns are similar to those of the tangent modulus-stress curves (Figs. 2 to 4). The pseudo modulus increased until the normalized deviator stress reached approximately 0.7, 0.6, 0.3 and 0.2 at the confining pressures of 0.0, 3.5, 17.0 and 35.0 MPa respectively, and then decreased slowly until failure. The pseudo modulus-stress curves also merge at approximately $0.8(\sigma_1 - \sigma_3)_f$.

The pseudo Young's moduli are plotted versus the normalized deviator stress at the confining pressures of 0.0, 3.5, 17.0 and 35.0 MPa in Figures 13, 14 ,15 and 16 respectively to study the effect of temperature. They show that temperature also had no effect on the pseudo modulus at any stress level at all four confining pressures. The mean pseudo Young's moduli at $0.5(\sigma_1 - \sigma_3)_f$ at the temperatures of 21°, 75° and 125° C, namely $E_{p21°}$, $E_{p75°}$ and $E_{p125°}$, were found to be:

$\sigma_3 = 0.0$ MPa $\quad E_{p21°} = 57.05$ GPa (s.d. $= 1.25$) $\quad E_{p75°} = 57.31$ GPa (s.d. $= 1.61$)
$E_{p125°} = 56.37$ GPa (s.d. $= 1.93$)

$\sigma_3 = 3.5$ MPa $\quad E_{p21°} = 60.96$ GPa (s.d. $= 1.01$) $\quad E_{p75°} = 60.57$ GPa (s.d. $= 3.21$)
$E_{p125°} = 64.54$ GPa (s.d. $= 2.35$)

$\sigma_3 = 17.0$ MPa $\quad E_{p21°} = 69.93$ GPa (s.d. $= 1.48$) $\quad E_{p75°} = 69.83$ GPa (s.d. $= 2.47$)
$E_{p125°} = 70.09$ GPa (s.d. $= 2.36$)

$\sigma_3 = 35.0$ MPa $\quad E_{p21°} = 71.17$ GPa (s.d. $= 1.18$) $\quad E_{p75°} = 71.07$ GPa (s.d. $= 1.82$)
$E_{p125°} = 70.43$ GPa (s.d. $= 0.55$)

The pseudo moduli at $0.5(\sigma_1 - \sigma_3)_f$ and their mean values are plotted against temperature in Figure 17. They show the same patterns as displayed by the tangent moduli, including the discrepancy at the confining pressure of 3.5 MPa. In general, temperature had no significant effect on the pseudo modulus at $0.5(\sigma_1 - \sigma_3)_f$.

It should also be pointed out that the mean pseudo Young's moduli at $0.5(\sigma_1 - \sigma_3)_f$ in the unconfined condition are similar to those obtained from Borehole 209-030-DIL1 and approximately 5 GPa lower than those obtained from Borehole 209-021-SV1 at the 240 level.

6.6 Poisson's ratio

The Poisson's ratios determined in these tests are presented in Table 2 and their mean values are given in Table 3. The Poisson's ratios are also plotted with their mean values versus temperature in Figure 18. The plots show that the mean Poisson's ratio increased with increasing confining pressure, but decreased with increasing temperature. As the temperature increased from 21° to 75° and to 125° C, the mean Poisson's ratio decreased from 0.360 to 0.313 and to 0.283 at the confining pressure of 3.5 MPa; from 0.398 to 0.370 and to 0.350 at the confining pressure of 17.0 MPa; and from 0.390 to 0.373 and to 0.35 at the confining pressure of 35.0 MPa. In the unconfined condition, the mean Poisson's ratio decreased from 0.357 to 0.230 when the temperature increased from 21° to 75° C, and then increased slightly to 0.243 when the temperature was raised to 125° C. This discrepancy is probably due to the inhomogeneity of the rock.

6.7 Strength properties of intact rock material

The strength properties of intact rock material can be expressed in terms of the Hoek and Brown failure criterion. The empirical relationship developed by Hoek and Brown (1980) between the principal stresses associated with the failure of a rock is given as follows:

$$\sigma_1 = \sigma_3 + \sqrt{m\sigma_c\sigma_3 + s\sigma_c{}^2} \qquad (5)$$

where σ_1 = major principal stress at failure
σ_3 = minor principal stress applied to the rock sample
σ_c = uniaxial compressive strength of the intact rock material in the specimen
m and s are constants

The values of m and s depend on the properties of the rock and the extent to which the rock has been broken before being subjected to the principal stresses σ_1 and σ_3. For an intact rock, $s = 1$, and the uniaxial compressive strength σ_c and the material constant m can be computed by using the following equations:

$$\sigma_c^2 = \frac{\sum y_i}{n} - \left[\frac{\sum x_i y_i - \frac{\sum x_i \sum y_i}{n}}{\sum x_i^2 - \frac{(\sum x_i)^2}{n}}\right]\frac{\sum x_i}{n} \tag{6}$$

$$m = \frac{1}{\sigma_c}\left[\frac{\sum x_i y_i - \frac{\sum x_i \sum y_i}{n}}{\sum x_i^2 - \frac{(\sum x_i)^2}{n}}\right] \tag{7}$$

where $x = \sigma_3$
$y = (\sigma_1 - \sigma_3)^2$
n = total number of data pairs x_i and y_i

The coefficient of determination r^2 is given by:

$$r^2 = \frac{\left[\sum x_i y_i - \frac{\sum x_i \sum y_i}{n}\right]^2}{\left[\sum x_i^2 - \frac{(\sum x_i)^2}{n}\right]\left[\sum y_i^2 - \frac{(\sum y_i)^2}{n}\right]} \tag{8}$$

The closer the value of r^2 is to 1.00, the better the fit between Equation 5 and the test data is.

The Hoek and Brown failure envelopes generated by using Equation 5 for tests conducted at the temperatures of 21°, 75° and 125° C are shown in Figures 19, 20 and 21 respectively. The values of σ_c, m and r^2 computed by using Equations 6, 7 and 8

are presented in Table 6. The coefficient of determination, r^2, was found to range from 0.9919 to 0.9961, indicating that the fit of Equation 5 to the data was good. From Table 6, it can be seen that there was little change in the predicted value of σ_c (from 178 to 179 MPa) when the temperature increased from 21° to 75° C. However, when the temperature was raised to 125° C, σ_c decreased to 168 MPa. Temperature appeared to have no effect on the m value. The m value changed from 42.60 to 41.08 and to 42.17 as the temperature increased from 21° to 75° and to 125° C.

It should be noted that a comparison of the results obtained from Borehole 401-009-HF1 with those obtained from Boreholes 209-021-SV1 and 209-030-DIL1 (Lau et al., 1988b; Lau and Gorski, 1989) shows that the values of σ_c are in general lower, but the values of m are higher at the 420 level than at the 240 level of the URL.

Hoek and Brown also suggest that the relationship between the normal and shear stresses (σ and τ) and the principal stresses at failure can be expressed as follows:

$$\sigma = \sigma_3 + \frac{\tau_m^2}{\tau_m + m\sigma_c/8} \tag{9}$$

$$\tau = (\sigma - \sigma_3)\sqrt{1 + m\sigma_c/4\tau_m} \tag{10}$$

where $\tau_m = \frac{1}{2}(\sigma_1 - \sigma_3)$

By substituting successive pairs of σ_1 and σ_3 into Equations 9 and 10, a Mohr failure envelope can be generated.

The Mohr failure envelopes and the Mohr circles for tests conducted at the temperatures of 21°, 75° and 125° C are plotted in Figures 22, 23 and 24 respectively. Note that only the mean values of σ_1 and σ_3 are used to plot the Mohr circles. From these plots, it can be seen that the Mohr failure envelopes generated by using Equations 9 and 10 provide a good fit to the Mohr circles. The angle of internal friction and the cohesive strength, measured from the tangent to the failure envelope at the point of intersection of the failure envelope and the Mohr circle, of each set of tests, are shown in Table 7. The angle of internal friction was found to decrease, but the cohesive strength to increase with increasing confining pressure at all test temperatures as expected. No significant change in the angle of internal friction with increasing temperature was observed. The cohesive strength appeared to decrease with increasing temperature.

7. Conclusions

The results of these tests have provided some thermo-mechanical data as well as some insight into the behaviour of the grey granite at the 420 level of the URL. It has also been found that the effect of stress relaxation on the rock specimens is higher at the 420 level than at the 240 level, resulting in higher crack porosity, lower p-wave and s-wave velocities, larger deformations and lower Young's modulus values. This suggests that the in situ stress is higher at the 420 level than at the 240 level. From the results, the following conclusions can be made.

The failure deviator stress increased as the confining pressure increased, but decreased as the temperature increased. The largest decrease occurred in the unconfined condition where a reduction of 5.8% in the mean failure deviator stress (unconfined compressive strength) was observed.

The axial strain at failure increased with increasing confining pressure, but decreased with increasing temperature.

At stress levels below the normalized deviator stress of 0.8, the tangent Young's modulus and the pseudo Young's modulus increased as the confining pressure increased. The increase was particularly pronounced at low confining pressures and at low stress levels. At stress levels above 0.8 times the failure deviator stress, the confining pressure had little effect on the moduli. Temperature was found to have no effect on both the tangent Young's modulus and the pseudo Young's modulus.

The Poisson's ratio increased with increasing confining pressure, but decreased with increasing temperature.

The strength properties of the intact rock material are expressed in terms of the Hoek and Brown failure criterion. Little change in the predicted uniaxial compressive strength of the intact rock material σ_c was observed when the temperature increased from 21° to 75° C. However, σ_c was found to decrease when the temperature was raised from 75° to 125° C. Temperature appeared to have no effect on the material constant m.

Mohr failure envelopes were generated by using equations suggested by Hoek and Brown. Angles of internal friction and cohesive strengths of the rock samples were measured from the plots of Mohr failure envelopes and Mohr circles. The cohesive strength appeared to decrease with increasing temperature, but the angle of internal friction was insensitive to the increase in temperature.

8. Recommendations

This is the first time in AECL's laboratory rock testing program that a complete series of uniaxial compression and triaxial compression tests at the confining pressures of 0.0, 3.5, 17.0 and 35.0 MPa and at the test temperatures of 21°, 75° and 125° C were conducted on selected rock samples all from the same location at the URL. The results are promising and many discrepancies observed in the results of previous incomplete test series were not found here. This uniaxial compression and triaxial compression testing program is recommended for the URL characterization program during the operating phase of the URL and for future site selection program if the disposal concept is deemed acceptable. Ambient temperature and high temperature tension tests should also be included in the testing program in order to obtain more accurate values of σ_c and m.

It is also recommended that additional tests to be carried out on samples from Boreholes 209-021-SV1, 209-030-DIL1 and URL-5 to complete the series of unaxial compression and triaxial compression tests at the four confining pressures and three test temperatures as recommended above for each of those boreholes.

Although results obtained from this testing program have shed some light on the thermo-mechanical properties of the URL rock samples, questions remain to be answered. What are the scale effects on the thermo-mechanical properties of the URL rock samples? What are the effects of moisture on the thermo-mechanical properties? Will the rock behave the same way at very high confining pressure? These questions should be addressed to in the future.

Acknowledgements

The authors wish to express their thanks to R. Jackson of CANMET for reviewing this report and making several helpful suggestions. Gratitude is expressed to J. Folta of CANMET, and D. Stebner, G.P. Hunter and P.A. Tibble, co-op students from the University of Waterloo, for the preparation of specimens and for carrying out the compression wave and shear wave velocities measurements.

References

Annor, A. and Jackson, R. (1985), "Mechanical properties of rock samples from the Lac du Bonnet Batholith, Manitoba", Division Report M&ET/MRL 85-41(TR), CANMET, Energy, Mines and Resources Canada, 101 p.

Annor, A. and Jackson, R. (1987), "Mechanical, thermomechanical and joint properties of rock samples from the Lac du Bonnet Batholith, Manitoba", in Geotechnical studies at Whiteshell Research Area (RA-3) (edited by Katsube, T.J. and Hume, J.P.), Divisional Report MRL 87-52(TR), CANMET, Energy, Mines and Resources Canada, p. 49-110.

Brown, E.T. (1981), "Rock characterization testing and monitoring, ISRM suggested methods", International Society for Rock Mechanics, the Commission on Testing Methods, Pergamon, 211 p.

Gorski, B. (1987), "Post-failure uniaxial strength determinations using a servo-hydraulic test system", Division Report MRL 87-33(INT), CANMET, Energy, Mines and Resources Canada, 77 p.

Gyenge, M. and Herget, G. (1977), "Pit slope manual supplement 3-2 - laboratory tests for design parameters", CANMET, Report 77-26, 74 p.

Gyenge, M. and Ladanyi, B. (1977), "Pit slope manual supplement 3-5 - sampling and specimen preparation", CANMET, Report 77-29, 30 p.

Hoek, E. and Brown, E.T. (1980), "Underground excavations in rock", The institution of Mining and Metallurgy, London, 527 p.

Jackson, R. (1984), "Summary of mechanical properties of Lac du Bonnet and Eye-Dashwa specimens", Division Report MRP/MRL 84-85(TR), CANMET, Energy, Mines and Resources Canada, 48 p.

Lau, J.S.O., Jackson, R. and Gorski, B. (1988a), "High temperature triaxial tests on rock samples from Borehole URL-5, Lac du Bonnet, Manitoba", Division Report MRL 88-90(TR), CANMET, Energy, Mines and Resources Canada, 86 p.

Lau, J.S.O., Jackson, R. and Gorski, B. (1988b), "High temperature triaxial tests on rock samples from Boreholes 209-021-SV1 and 209-030-DIL1, Lac du Bonnet, Manitoba", Division Report MRL 88-112(TR), CANMET, Energy, Mines and Resources Canada, 57 p.

Lau, J.S.O. and Gorski, B. (1989), "High temperature uniaxial compression tests on URL rock samples from Boreholes 209-021-SV1 and 209-030-DIL1", Divisional Report MRL 89-90(TR), CANMET, Energy, Mines and Resources Canada, 68 p.

MTS Systems Corporation (1986), "Operation manual for 815 rock mechanics test systems", MTS Systems Corp., Minneapolis, Minnesota, U.S.A.

Simmons, G.R. and Soonawala, N.M. (1982), "Underground research laboratory experimental program", Atomic Energy of Canada Limited Technical Record, TR-153, 126 p.

Terrametrics (1980), "Instruction manual - sonic velocity equipment", Terrametrics, Inc., Golden, Colorado, U.S.A., 17 p.

Table 1. Dimensions, densities and dynamic elastic properties of rock specimens.

Specimen Identification	Length (mm)	Diameter (mm)	Bulk Density (Mg/m^3)	P-wave Velocity (km/s)	S-wave Velocity (km/s)	Dynamic Young's Modulus (GPa)	Dynamic Shear Modulus (GPa)	Dynamic Poisson's Ratio
401-009-HF1-32.100	110.72	44.90	2.63	3.386	2.039	26.58	10.93	0.22
401-009-HF1-32.216	110.62	44.93	2.63	3.292	2.000	25.41	10.52	0.21
401-009-HF1-32.398	107.30	44.93	2.62	3.232	1.913	23.59	9.58	0.23
401-009-HF1-33.151	105.97	44.95	2.63	3.282	2.159	27.42	12.26	0.12
401-009-HF1-33.266	108.14	44.95	2.63	3.618	2.113	29.14	11.74	0.24
401-009-HF1-33.383	106.70	44.95	2.62	3.799	2.109	29.77	11.65	0.28
401-009-HF1-34.812	105.74	44.90	2.63	3.401	1.899	24.15	9.48	0.27
401-009-HF1-35.063	105.25	44.93	2.63	3.787	2.009	27.69	10.61	0.30
401-009-HF1-35.177	107.81	44.93	2.63	3.852	2.157	31.11	12.23	0.27
401-009-HF1-35.291	108.23	44.93	2.63	3.573	2.066	28.04	11.22	0.25
401-009-HF1-35.408	107.70	44.91	2.63	3.521	1.987	26.31	10.39	0.27
401-009-HF1-35.642	107.82	44.96	2.63	3.391	2.031	26.47	10.84	0.22
401-009-HF1-35.757	107.94	44.98	2.63	3.322	1.974	25.15	10.24	0.23
401-009-HF1-35.874	106.96	44.97	2.63	3.333	2.030	26.12	10.84	0.21
401-009-HF1-36.041	107.09	44.96	2.62	3.633	2.125	29.33	11.83	0.24
401-009-HF1-36.156	108.09	44.96	2.63	3.646	2.157	30.13	12.24	0.23
401-009-HF1-36.272	107.08	44.96	2.63	3.300	1.998	25.42	10.50	0.21
401-009-HF1-36.385	106.78	44.96	2.63	3.518	2.065	27.76	11.22	0.24
401-009-HF1-37.041	105.73	44.94	2.62	3.189	1.902	23.20	9.47	0.22
401-009-HF1-37.156	110.60	44.94	2.63	3.129	1.868	22.45	9.18	0.22
401-009-HF1-37.300	108.05	44.96	2.63	3.719	2.102	29.41	11.62	0.27
401-009-HF1-37.415	108.72	44.97	2.62	3.265	1.988	24.96	10.35	0.21
401-009-HF1-37.652	108.60	44.97	2.64	3.194	2.015	25.07	10.72	0.17
401-009-HF1-37.767	109.36	44.97	2.65	3.682	2.178	30.96	12.58	0.23
401-009-HF1-37.884	105.28	44.97	2.63	3.353	2.171	28.23	12.39	0.14
401-009-HF1-38.080	111.21	44.92	2.63	3.884	2.168	31.49	12.36	0.27
401-009-HF1-38.194	107.42	44.97	2.63	3.275	1.967	24.79	10.18	0.22
401-009-HF1-38.308	111.11	44.96	2.64	3.494	2.129	28.82	11.96	0.20
401-009-HF1-38.424	109.01	44.96	2.63	3.412	2.008	26.19	10.60	0.24
401-009-HF1-38.585	108.10	44.94	2.62	3.106	1.991	23.91	10.38	0.15
401-009-HF1-38.700	106.78	44.94	2.62	3.521	1.774	21.92	8.24	0.33
401-009-HF1-38.817	108.14	44.94	2.63	3.691	2.272	32.44	13.57	0.19
401-009-HF1-39.459	108.51	44.98	2.63	3.735	2.028	27.93	10.82	0.29
401-009-HF1-39.574	108.00	45.00	2.62	3.429	2.077	27.35	11.30	0.21
401-009-HF1-40.177	106.70	44.93	2.61	3.268	1.961	24.47	10.04	0.22
401-009-HF1-40.289	105.15	44.92	2.62	3.540	2.011	26.73	10.59	0.26
401-009-HF1-40.427	109.37	44.94	2.61	4.058	2.028	28.63	10.73	0.33
401-009-HF1-40.541	105.56	44.94	2.62	3.209	2.058	25.53	11.09	0.15
401-009-HF1-40.655	107.83	44.94	2.63	3.457	2.016	26.56	10.69	0.24
Mean			2.63	3.486	2.039	26.97	10.95	0.23
Standard deviation			0.01	0.243	0.096	2.51	1.04	0.05

Table 2. Results of ambient temperature and high temperature uniaxial and triaxial compression tests.

Specimen Identification	Confining Pressure (MPa)	Temp. (deg C.)	Total Axial Strain (%)	Failure Deviator Stress (MPa)	Tangent Young's Modulus (GPa)	Pseudo Young's Modulus (GPa)	Poisson's Ratio	θ (deg.)	Failure characteristics
401-009-HF1-35.291	0.0	21	0.380	168	57.92	56.72	0.33		multiple cracks
			0.373*		54.05*	53.20*	0.31*		
401-009-HF1-38.194	0.0	21	0.393	176	59.64	58.43	0.39		multiple cracks
			0.380*		55.18*	54.29*	0.37*		
401-009-HF1-38.700	0.0	21	0.403	171	57.26	55.99	0.35		multiple cracks
			0.368*		56.39*	55.37*	0.34*		
401-009-HF1-35.408	0.0	75	0.406	175	59.54	58.33	0.24		multiple cracks
401-009-HF1-37.884	0.0	75	0.365	166	59.37	58.15	0.22		multiple cracks
401-009-HF1-39.459	0.0	75	0.384	167	56.73	55.46	0.23		multiple cracks
401-009-HF1-35.642	0.0	125	0.368	160	56.98	55.67	0.23		multiple cracks
401-009-HF1-38.308	0.0	125	0.349	161	59.81	58.56	0.24		multiple cracks
401-009-HF1-40.177	0.0	125	0.378	164	56.11	54.89	0.26		multiple cracks
401-009-HF1-33.151	3.5	21	0.513	234	60.91	60.34	0.35	70	2 fragments, curved fracture
401-009-HF1-36.272	3.5	21	0.577	239	60.86	60.42	0.38		multiple cracks
401-009-HF1-37.415	3.5	21	0.540	245	62.45	62.13	0.35		3 fragments, conical bottom end
401-009-HF1-33.266	3.5	75	0.534	229	59.44	58.08	0.30	72	2 fragments, curved fracture
401-009-HF1-36.041	3.5	75	0.529	232	59.88	59.43	0.33		2 fragments, curved fracture
401-009-HF1-37.652	3.5	75	0.515	242	64.63	64.19	0.31		multiple cracks
401-009-HF1-33.383	3.5	125	0.466	234	65.25	64.89	0.27		multiple cracks
401-009-HF1-36.156	3.5	125	0.481	222	62.51	62.03	0.29		multiple cracks,wedge-shaped bottom end
401-009-HF1-37.767	3.5	125	0.445	233	67.13	66.69	0.29		multiple cracks

*computed from strain gauge measurements

Table 2 - (Cont'd)

Specimen Identification	Confining Pressure (MPa)	Temp. (deg C.)	Total Axial Strain (%)	Failure Deviator Stress (MPa)	Tangent Young's Modulus (GPa)	Pseudo Young's Modulus (GPa)	Poisson's Ratio	θ (deg.)	Failure characteristics
401-009-HF1-32.100	17.0	21	0.726	417	70.47	71.47	0.41	68	2 fragments, planar fracture
401-009-HF1-34.812	17.0	21	0.714	407	68.73	69.66	0.39	69	2 fragments, planar fracture
401-009-HF1-36.385	17.0	21	0.744	404	67.10	68.01	0.39		4 fragments, 3 fractures
401-009-HF1-38.585	17.0	21	0.697	399	69.95	70.57	0.40	72	2 fragments, curved fracture
401-009-HF1-32.216	17.0	75	0.671	404	70.53	71.46	0.38	70	2 fragmnets, planar fracture
401-009-HF1-35.063	17.0	75	0.712	412	69.81	70.76	0.38	68	2 fragments, planar fracture
401-009-HF1-37.041	17.0	75	0.729	399	65.45	66.14	0.35	65	2 fragments, curved fracture
401-009-HF1-38.817	17.0	75	0.700	413	70.04	70.94	0.37		2 fragments, wedge-shaped bottom end
401-009-HF1-32.398	17.0	125	0.674	403	70.96	71.94	0.37	70	2 fragments, curved fracture
401-009-HF1-35.177	17.0	125	0.650	381	70.21	71.19	0.36	70	2 fragments, curved fracture
401-009-HF1-37.156	17.0	125	0.693	361	66.00	66.65	0.31	73	2 fragments, curved fracture
401-009-HF1-39.574	17.0	125	0.693	408	69.63	70.59	0.36	67	2 fragments, planar fracture
401-009-HF1-35.757	35.0	21	0.869	531	71.00	72.52	0.38	64	2 fragments, curved fracture
401-009-HF1-37.300	35.0	21	0.928	546	68.74	70.35	0.40		3 fragments, vertical fracture wedge-shaped top end
401-009-HF1-40.289	35.0	21	0.903	551	69.29	70.63	0.39	72	2 fragments, irregular fracture
401-009-HF1-35.874	35.0	75	0.870	537	70.46	71.83	0.37	69	2 fragments, planar fracture
401-009-HF1-38.080	35.0	75	0.859	539	70.97	72.39	0.36	67	2 fragments, curved fracture
401-009-HF1-40.427	35.0	75	0.873	523	67.78	69.00	0.39	66	2 fragments, planar fracture
401-009-HF1-38.424	35.0	125	0.891	523	68.73	70.11	0.35	63	2 fragments, curved fracture
401-009-HF1-40.541	35.0	125	0.866	526	69.63	71.07	0.35	70	2 fragments, planar fracture
401-009-HF1-40.655	35.0	125	0.853	520	68.68	70.12	0.35	70	2 fragments, planar fracture

Table 3. Mean failure deviator stresses, mean axial strains at failure and mean Poisson's ratios.

σ_3 (MPa)	Mean failure deviator (MPa)			Mean axial strain at failure (%)			Mean Poisson's ratio		
	21° C	75° C	125° C	21° C	75° C	125° C	21° C	75° C	125° C
0.0	171.7 (4.0)	169.3 (4.9)	161.7 (2.1)	0.392 (0.012)	0.385 (0.021)	0.365 (0.015)	0.357 (0.031)	0.230 (0.010)	0.243 (0.015)
3.5	239.3 (5.5)	234.3 (6.8)	229.7 (6.7)	0.543 (0.032)	0.526 (0.010)	0.464 (0.018)	0.360 (0.017)	0.313 (0.015)	0.283 (0.012)
17.0	406.8 (7.6)	407.0 (6.7)	388.3 (21.6)	0.720 (0.020)	0.703 (0.024)	0.678 (0.020)	0.398 (0.010)	0.370 (0.014)	0.350 (0.027)
35.0	542.7 (10.4)	533.0 (8.7)	523.0 (3.0)	0.900 (0.030)	0.867 (0.007)	0.870 (0.019)	0.390 (0.010)	0.373 (0.015)	0.350 (0.000)

Table 4. Tangent Young's moduli at stress levels ranging from 10% to 90% of the failure deviator stress.

Specimen Identification	σ_3 (MPa)	Temp. (deg C.)	Tangent Young's Modulus (GPa)								
			10%	20%	30%	40%	50%	60%	70%	80%	90%
401-009-HF1-35.291	0.0	21	30.63	42.85	50.49	55.23	57.92	58.90	58.30	55.94	47.12
401-009-HF1-35.291*			29.84	41.21	48.04	52.06	54.05	54.28	52.80	49.57	49.61
401-009-HF1-38.194	0.0	21	30.30	43.41	51.82	56.89	59.64	60.48	59.51	56.60	47.99
401-009-HF1-38.194*			30.10	41.95	48.96	53.11	55.18	55.49	54.06	50.75	59.00
401-009-HF1-38.700	0.0	21	28.33	40.98	49.32	54.41	57.26	58.30	57.64	55.16	46.38
401-009-HF1-38.700*			28.18	40.89	49.17	54.00	56.39	56.76	55.15	51.94	67.92
401-009-HF1-35.408	0.0	75	30.45	43.46	51.79	56.80	59.54	60.39	59.48	56.67	48.84
401-009-HF1-37.884	0.0	75	30.63	43.59	51.71	56.64	59.37	60.28	59.48	56.89	49.35
401-009-HF1-39.459	0.0	75	28.05	40.65	48.89	53.90	56.73	57.80	57.24	54.98	47.75
401-009-HF1-35.642	0.0	125	28.68	40.61	48.96	54.06	56.98	58.15	57.70	55.58	47.33
401-009-HF1-38.308	0.0	125	30.61	43.42	51.89	57.00	59.81	60.71	59.82	57.04	49.21
401-009-HF1-40.177	0.0	125	29.13	40.87	48.63	53.40	56.11	57.13	56.60	54.45	46.84
401-009-HF1-33.151	3.5	21	37.93	49.45	55.85	59.45	60.91	60.40	57.88	52.96	44.16
401-009-HF1-36.272	3.5	21	39.55	50.86	56.52	59.68	60.86	60.19	57.61	52.42	41.62
401-009-HF1-37.415	3.5	21	43.42	53.85	58.79	61.53	62.45	61.66	59.06	53.92	42.69
401-009-HF1-33.266	3.5	75	29.90	41.80	50.92	56.40	59.44	60.51	59.75	56.18	46.02
401-009-HF1-36.041	3.5	75	39.60	50.10	55.59	58.69	59.88	59.31	56.91	51.86	40.98
401-009-HF1-37.652	3.5	75	43.29	54.61	60.27	63.45	64.63	63.95	61.35	56.05	44.54
401-009-HF1-33.383	3.5	125	44.77	55.71	61.19	64.21	65.25	64.41	61.59	56.01	44.64
401-009-HF1-36.156	3.5	125	41.33	52.40	58.06	61.25	62.51	62.00	59.65	54.43	43.00
401-009-HF1-37.767	3.5	125	46.66	57.52	62.90	65.97	67.13	66.51	64.05	58.80	47.23

*computed from strain gauge measurements

Table 4 - (Cont'd)

Specimen Identification	σ_3 (MPa)	Temp. (deg C.)	Tangent Young's Modulus (GPa)								
			10%	20%	30%	40%	50%	60%	70%	80%	90%
401-009-HF1-32.100	17.0	21	69.10	72.80	73.06	72.29	70.47	67.47	63.06	56.83	46.76
401-009-HF1-34.812	17.0	21	66.31	70.49	70.97	70.40	68.73	65.86	61.57	55.41	45.57
401-009-HF1-36.385	17.0	21	65.72	69.14	69.42	68.75	67.10	64.37	60.37	54.72	45.41
401-009-HF1-38.585	17.0	21	64.10	69.51	70.84	70.99	69.95	67.65	63.92	58.39	48.95
401-009-HF1-32.216	17.0	75	68.63	72.27	72.77	72.21	70.53	67.64	63.31	57.11	47.27
401-009-HF1-35.063	17.0	75	68.04	71.62	72.11	71.52	69.81	66.87	62.47	56.17	46.10
401-009-HF1-37.041	17.0	75	62.72	66.00	66.84	66.66	65.45	63.12	59.50	54.25	45.39
401-009-HF1-38.817	17.0	75	69.05	71.56	72.16	71.66	70.04	67.18	62.87	56.67	47.01
401-009-HF1-32.398	17.0	125	69.26	73.06	73.43	72.74	70.96	67.97	63.55	57.25	47.22
401-009-HF1-35.177	17.0	125	69.51	72.04	72.57	71.98	70.21	67.14	62.52	55.84	45.78
401-009-HF1-37.156	17.0	125	60.66	64.70	66.63	67.05	66.00	63.37	58.88	51.89	40.64
401-009-HF1-39.574	17.0	125	70.55	71.91	72.13	71.38	69.63	66.77	62.59	56.72	47.76
401-009-HF1-35.757	35.0	21	77.74	77.96	76.25	73.95	71.00	67.27	62.60	56.69	47.97
401-009-HF1-37.300	35.0	21	77.91	77.33	74.78	71.93	68.74	65.13	61.04	56.32	49.31
401-009-HF1-40.289	35.0	21	75.47	75.34	73.88	71.88	69.29	66.02	61.93	56.79	49.07
401-009-HF1-35.874	35.0	75	76.30	76.42	75.06	73.09	70.46	67.06	62.72	57.18	48.76
401-009-HF1-38.080	35.0	75	77.76	77.37	75.82	73.71	70.97	67.52	63.20	57.76	49.53
401-009-HF1-40.427	35.0	75	72.89	72.75	71.75	70.11	67.78	64.66	60.60	55.32	47.67
401-009-HF1-38.424	35.0	125	75.60	75.00	73.47	71.40	68.73	65.36	61.13	55.81	47.63
401-009-HF1-40.541	35.0	125	77.16	76.40	74.66	72.42	69.63	66.19	61.97	56.75	48.79
401-009-HF1-40.655	35.0	125	76.04	75.56	73.75	71.48	68.68	65.26	61.11	55.99	48.17

Table 5. Pseudo Young's moduli at stress levels ranging from 10% to 90% of the failure deviator stress.

Specimen Identification	σ_3 (MPa)	Temp. (deg C.)	Pseudo Young's Modulus (GPa)								
			10%	20%	30%	40%	50%	60%	70%	80%	90%
401-009-HF1-35.291	0.0	21	20.19	36.95	46.85	53.02	56.72	58.54	58.73	57.31	52.22
401-009-HF1-35.291*			20.11	35.77	44.82	50.21	53.20	54.30	53.69	51.27	49.10
401-009-HF1-38.194	0.0	21	18.90	37.00	47.84	54.54	58.43	60.21	60.14	58.22	52.97
401-009-HF1-38.194*			19.15	36.29	45.66	51.20	54.29	55.48	54.92	52.55	53.02
401-009-HF1-38.700	0.0	21	17.55	34.77	45.35	52.04	55.99	57.92	58.11	56.57	51.48
401-009-HF1-38.700*			17.47	34.64	45.24	51.78	55.37	56.74	56.12	53.46	57.54
401-009-HF1-35.408	0.0	75	21.89	36.97	47.86	54.48	58.33	60.11	60.08	58.23	53.59
401-009-HF1-37.884	0.0	75	21.83	37.17	47.87	54.35	58.15	59.96	60.02	58.34	54.02
401-009-HF1-39.459	0.0	75	19.54	34.35	44.99	51.56	55.46	57.40	57.66	56.26	52.17
401-009-HF1-35.642	0.0	125	21.81	34.59	45.01	51.68	55.67	57.70	58.06	56.78	52.37
401-009-HF1-38.308	0.0	125	23.81	36.89	47.87	54.63	58.56	60.41	60.42	58.59	53.98
401-009-HF1-40.177	0.0	125	21.37	35.04	44.96	51.18	54.89	56.75	57.00	55.66	51.52
401-009-HF1-33.151	3.5	21	23.92	44.06	52.86	57.83	60.34	60.82	59.31	55.61	48.96
401-009-HF1-36.272	3.5	21	23.10	45.72	53.89	58.27	60.42	60.68	59.06	55.29	47.46
401-009-HF1-37.415	3.5	21	28.80	49.22	56.49	60.31	62.13	62.20	60.51	56.78	48.80
401-009-HF1-33.266	3.5	75	22.81	35.67	46.58	53.85	58.08	60.13	60.28	58.35	51.66
401-009-HF1-36.041	3.5	75	28.19	45.26	53.04	57.30	59.43	59.74	58.26	54.68	46.88
401-009-HF1-37.652	3.5	75	29.36	49.49	57.63	62.02	64.19	64.44	62.81	59.00	50.79
401-009-HF1-33.383	3.5	125	32.89	50.74	58.65	62.87	64.89	64.98	63.16	59.10	50.77
401-009-HF1-36.156	3.5	125	28.60	47.32	55.44	59.81	62.03	62.40	60.98	57.38	49.20
401-009-HF1-37.767	3.5	125	34.28	52.65	60.39	64.59	66.69	66.97	65.44	61.76	53.51

*computed from strain gauge measurements

Table 5 - (Cont'd)

Specimen Identification	σ_3 (MPa)	Temp. (deg C.)	Pseudo Young's Modulus (GPa)								
			10%	20%	30%	40%	50%	60%	70%	80%	90%
401-009-HF1-32.100	17.0	21	55.90	71.86	73.01	72.76	71.47	69.06	65.37	60.07	52.30
401-009-HF1-34.812	17.0	21	53.44	69.35	70.82	70.77	69.66	67.39	63.82	58.62	50.94
401-009-HF1-36.385	17.0	21	55.54	68.23	69.36	69.16	68.01	65.82	62.47	57.66	50.60
401-009-HF1-38.585	17.0	21	49.49	67.79	70.27	71.01	70.57	68.91	65.90	61.29	54.25
401-009-HF1-32.216	17.0	75	59.62	71.20	72.61	72.58	71.46	69.19	65.59	60.34	52.61
401-009-HF1-35.063	17.0	75	58.08	70.59	71.95	71.90	70.76	68.44	64.79	59.45	51.58
401-009-HF1-37.041	17.0	75	56.51	64.88	66.51	66.84	66.14	64.38	61.41	56.99	50.36
401-009-HF1-38.817	17.0	75	62.78	70.71	71.95	72.00	70.94	68.71	65.14	59.90	52.24
401-009-HF1-32.398	17.0	125	59.61	72.01	73.33	73.17	71.94	69.56	65.87	60.52	52.68
401-009-HF1-35.177	17.0	125	55.70	71.22	72.40	72.37	71.19	68.78	64.94	59.32	51.08
401-009-HF1-37.156	17.0	125	54.26	62.98	65.79	66.97	66.65	64.81	61.27	55.56	46.57
401-009-HF1-39.574	17.0	125	68.46	71.37	72.10	71.84	70.59	68.29	64.78	59.77	52.62
401-009-HF1-35.757	35.0	21	71.76	78.39	77.15	75.14	72.52	69.19	65.00	59.72	52.77
401-009-HF1-37.300	35.0	21	70.27	78.27	76.07	73.37	70.35	66.96	63.11	58.71	53.36
401-009-HF1-40.289	35.0	21	71.42	75.76	74.65	72.92	70.63	67.71	64.03	59.43	53.41
401-009-HF1-35.874	35.0	75	72.40	76.74	75.79	74.12	71.83	68.81	64.95	60.02	53.45
401-009-HF1-38.080	35.0	75	75.19	77.84	76.64	74.81	72.39	69.30	65.42	60.55	54.14
401-009-HF1-40.427	35.0	75	71.12	72.98	72.30	70.98	69.00	66.28	62.70	58.04	51.85
401-009-HF1-38.424	35.0	125	74.31	75.49	74.28	72.48	70.11	67.09	63.30	58.53	52.24
401-009-HF1-40.541	35.0	125	75.58	77.00	75.57	73.58	71.07	67.96	64.13	59.42	53.30
401-009-HF1-40.655	35.0	125	73.24	76.14	74.69	72.65	70.12	67.01	63.23	58.60	52.59

Table 6. Values of σ_c, m, s and r^2 derived from the Hoek and Brown failure criterion.

Test Temperature (°C.)	Number of Samples n	Uniaxial Compressive Strength of Intact Material σ_c (MPa)	m	s	r^2
21	13	178	42.60	1.00	0.9961
75	13	179	41.08	1.00	0.9941
125	13	168	42.17	1.00	0.9919

Table 7. Angles of internal friction and coehesive strengths measured from Mohr failure emvelopes.

Confining pressure (MPa)	Test temperature (°C)	Number of samples	Angle of internal friction	Cohesive strength (MPa)
0.0	21	3	65°	21
	75	3	65°	19
	125	3	65°	18
3.5	21	3	63°	22
	75	3	64°	21
	125	3	63°	22
17.0	21	4	56°	39
	75	4	56°	39
	125	4	56°	35
35.0	21	3	48°	67
	75	3	49°	61
	125	3	49°	59

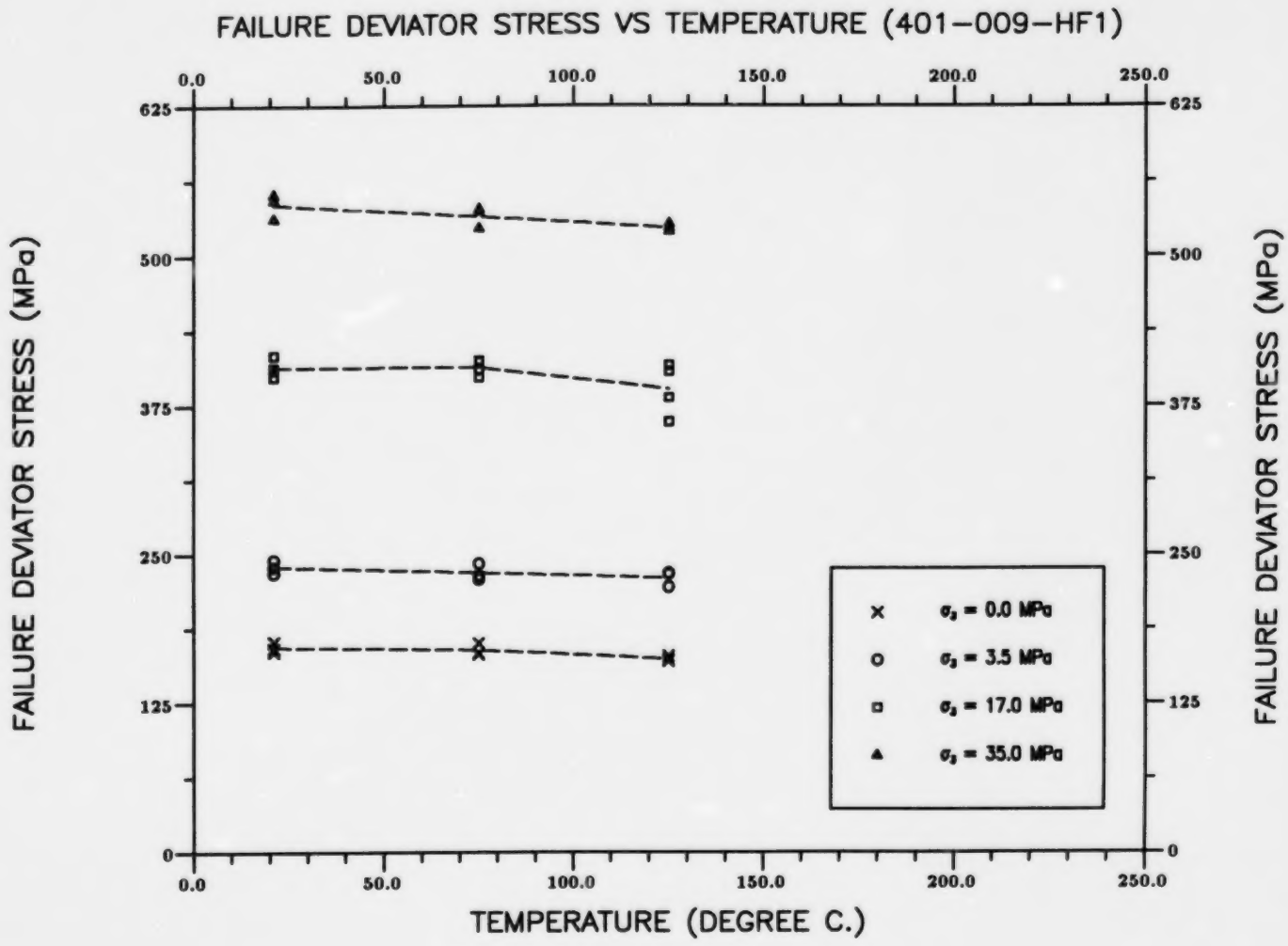

Figure 1. Plots of failure deviator stress versus temperature.

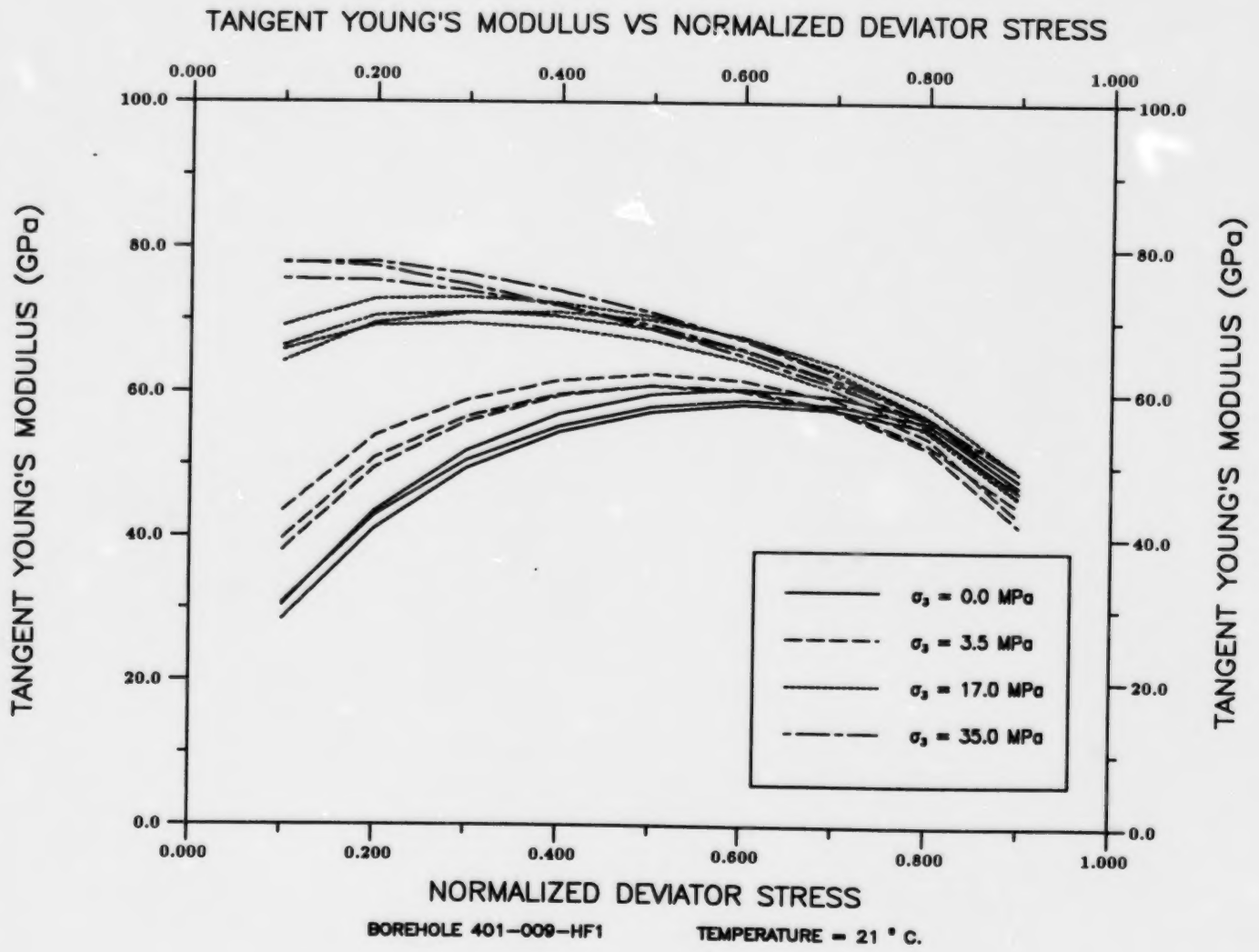

Figure 2. Plots of tangent Young's modulus versus normalized deviator stress at 21° C.

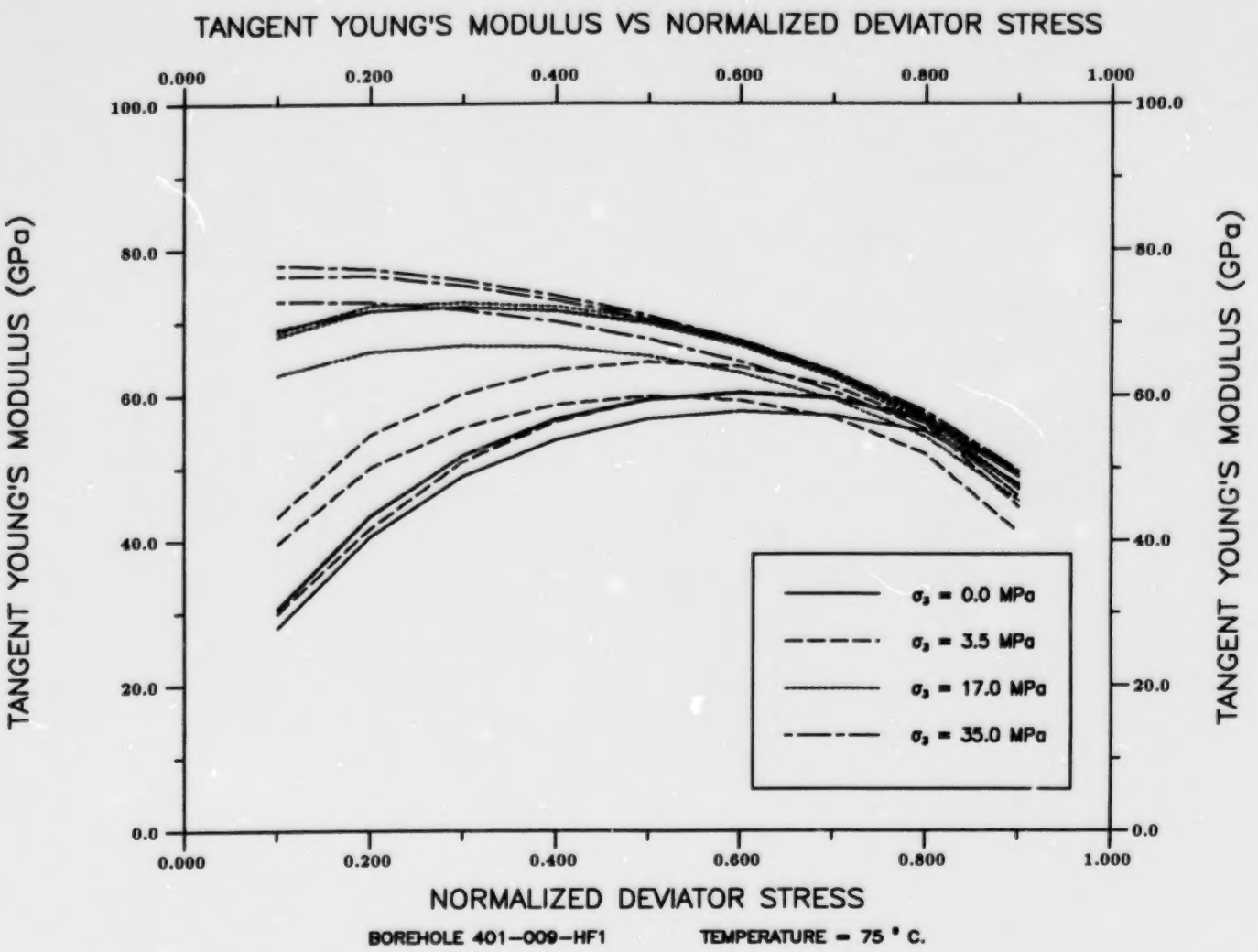

Figure 3. Plots of tangent Young's modulus versus normalized deviator stress at 75° C.

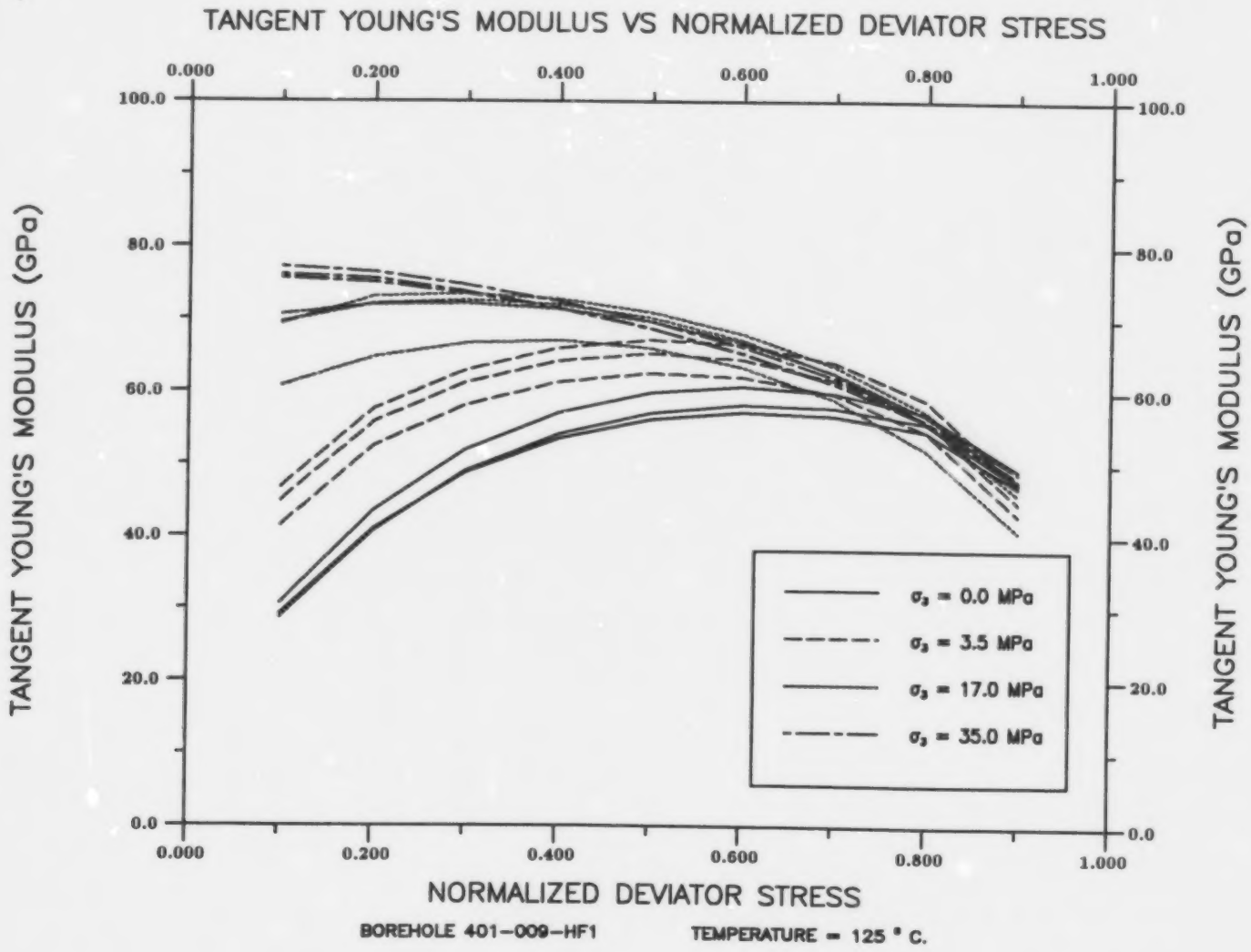

Figure 4. Plots of tangent Young's modulus versus normalized deviator stress at 125° C.

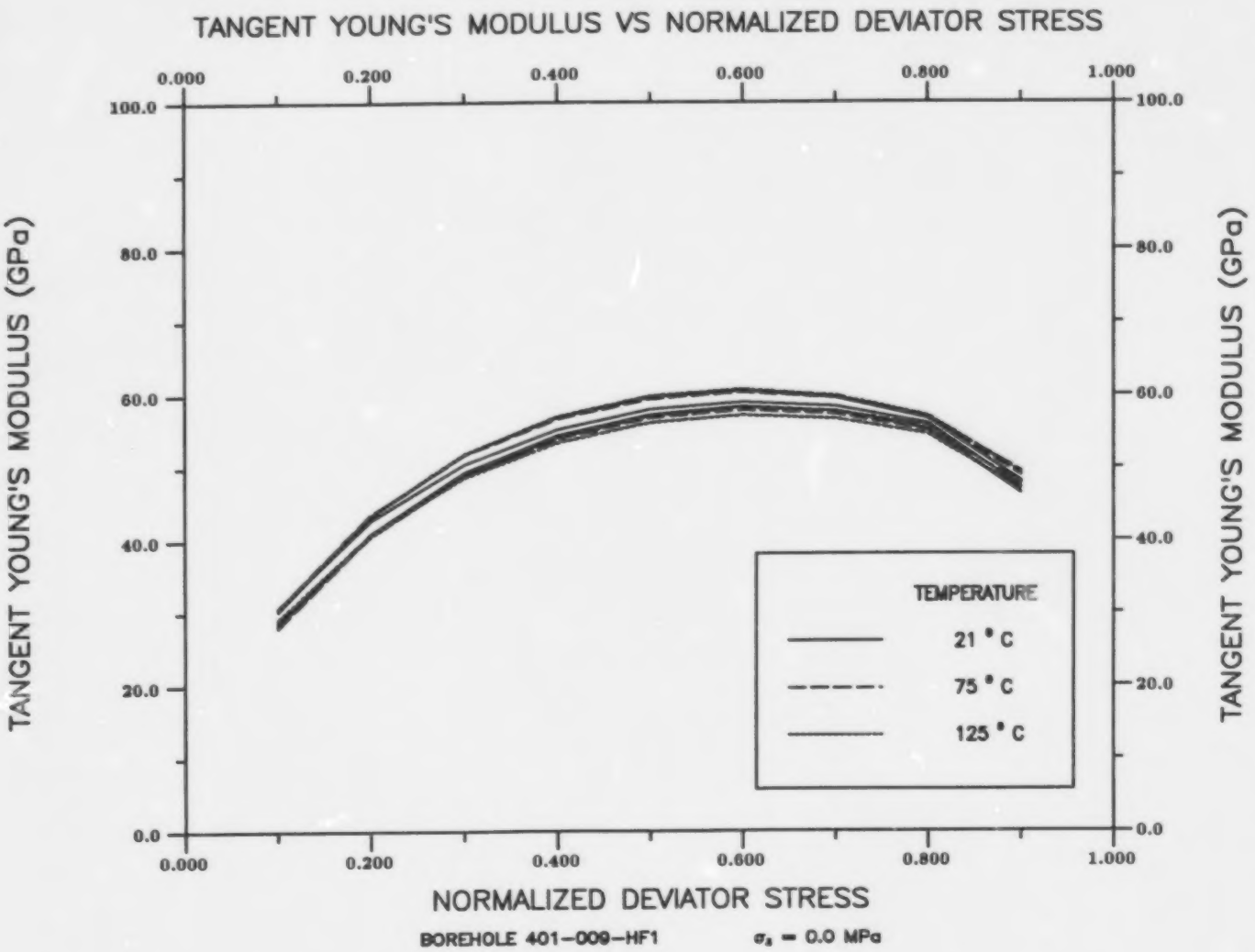

Figure 5. Plots of tangent Young's modulus versus normalized deviator stress at the unconfined condition.

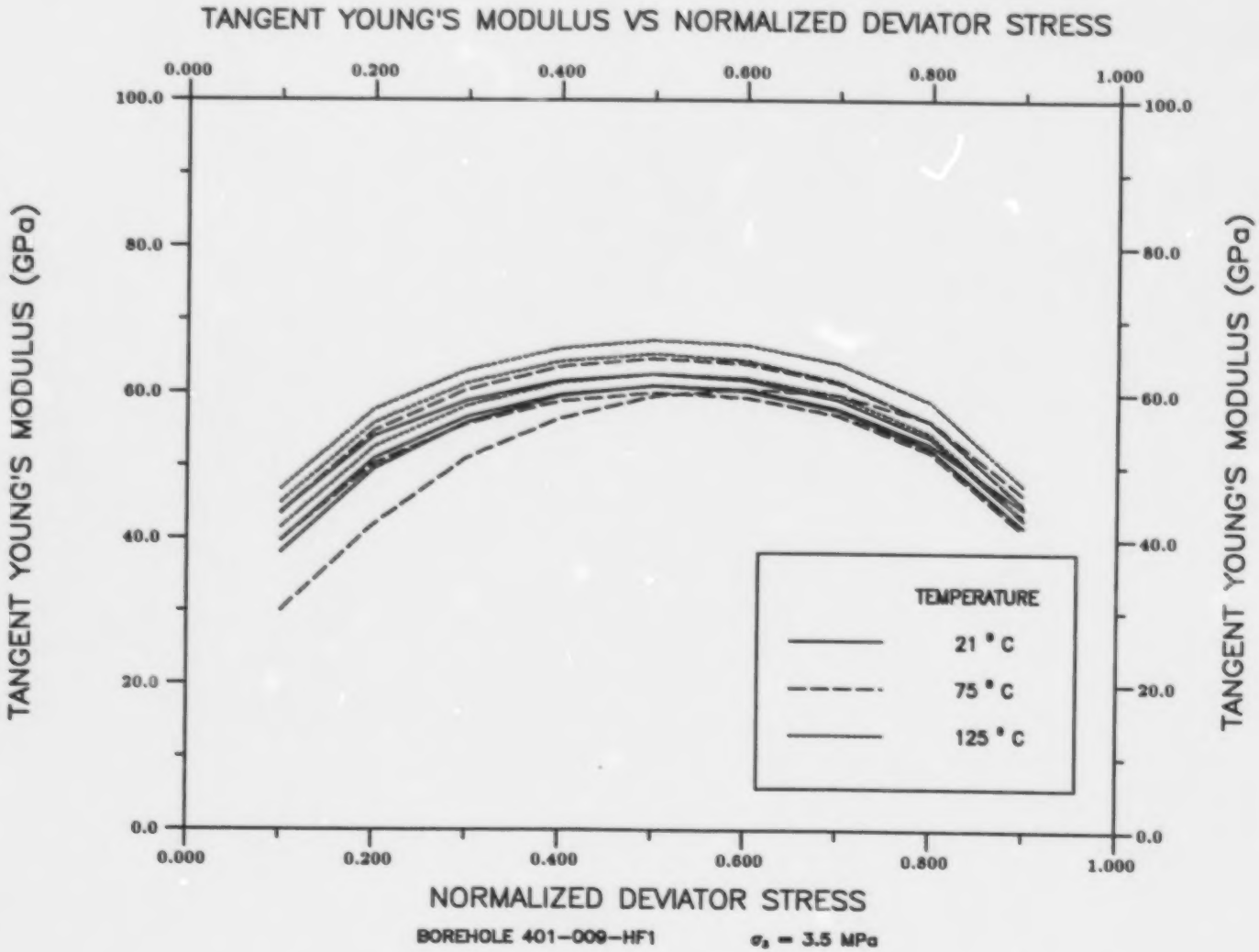

Figure 6. Plots of tangent Young's modulus versus normalized deviator stress at the confining pressure of 3.5 MPa.

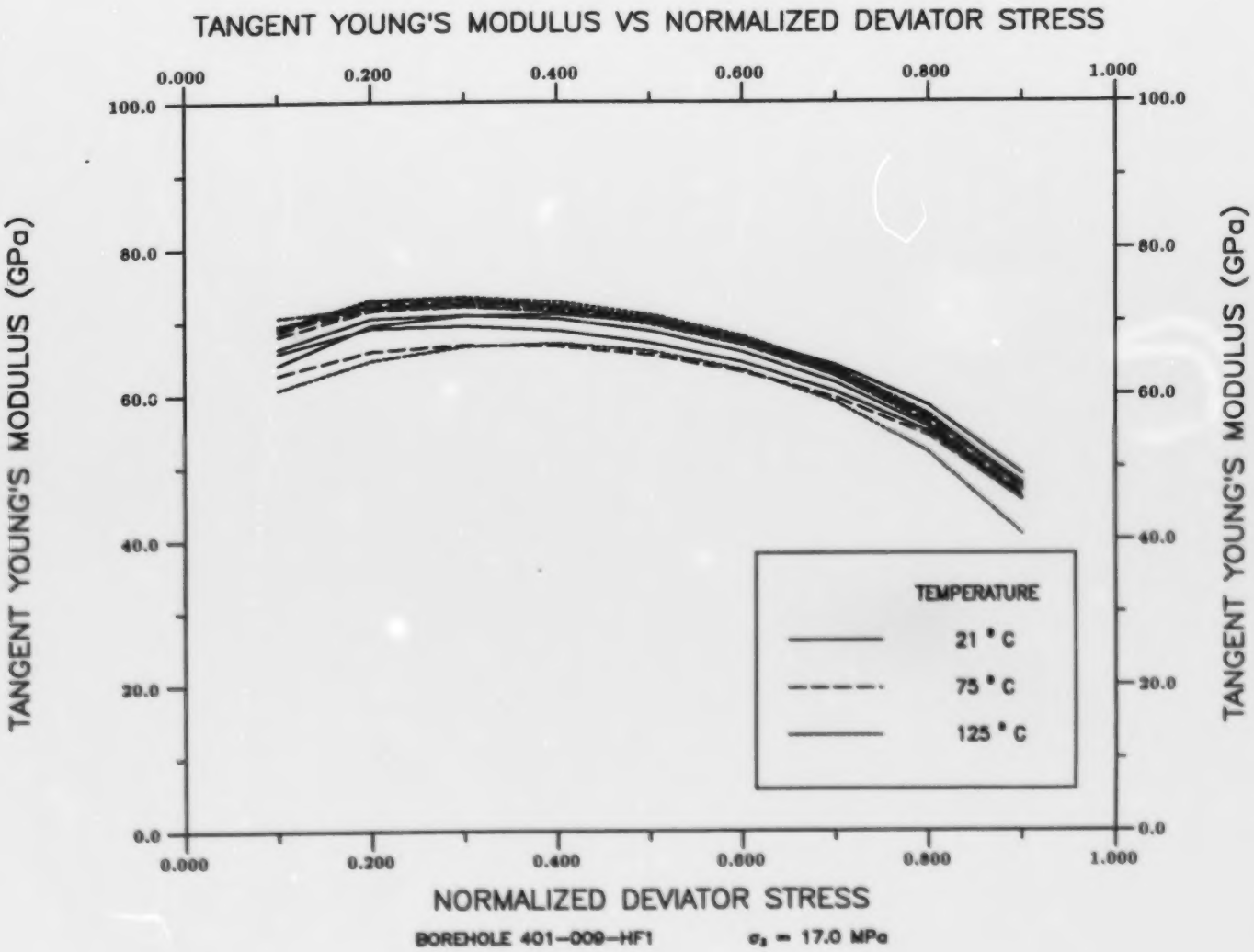

Figure 7. Plots of tangent Young's modulus versus normalized deviator stress at the confining pressure of 17.0 MPa.

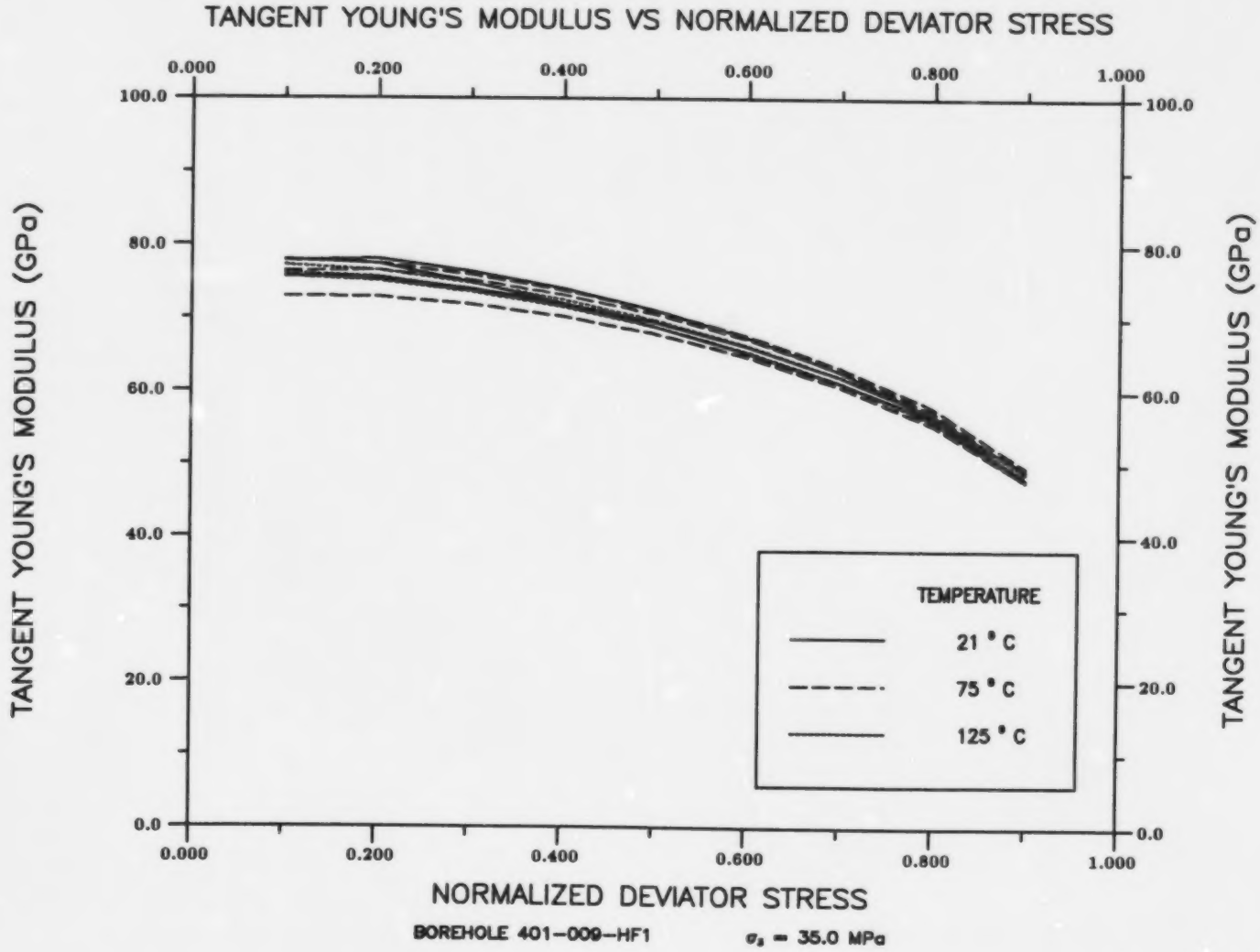

Figure 8. Plots of tangent Young's modulus versus normalized deviator stress at the confining pressure of 35.0 MPa.

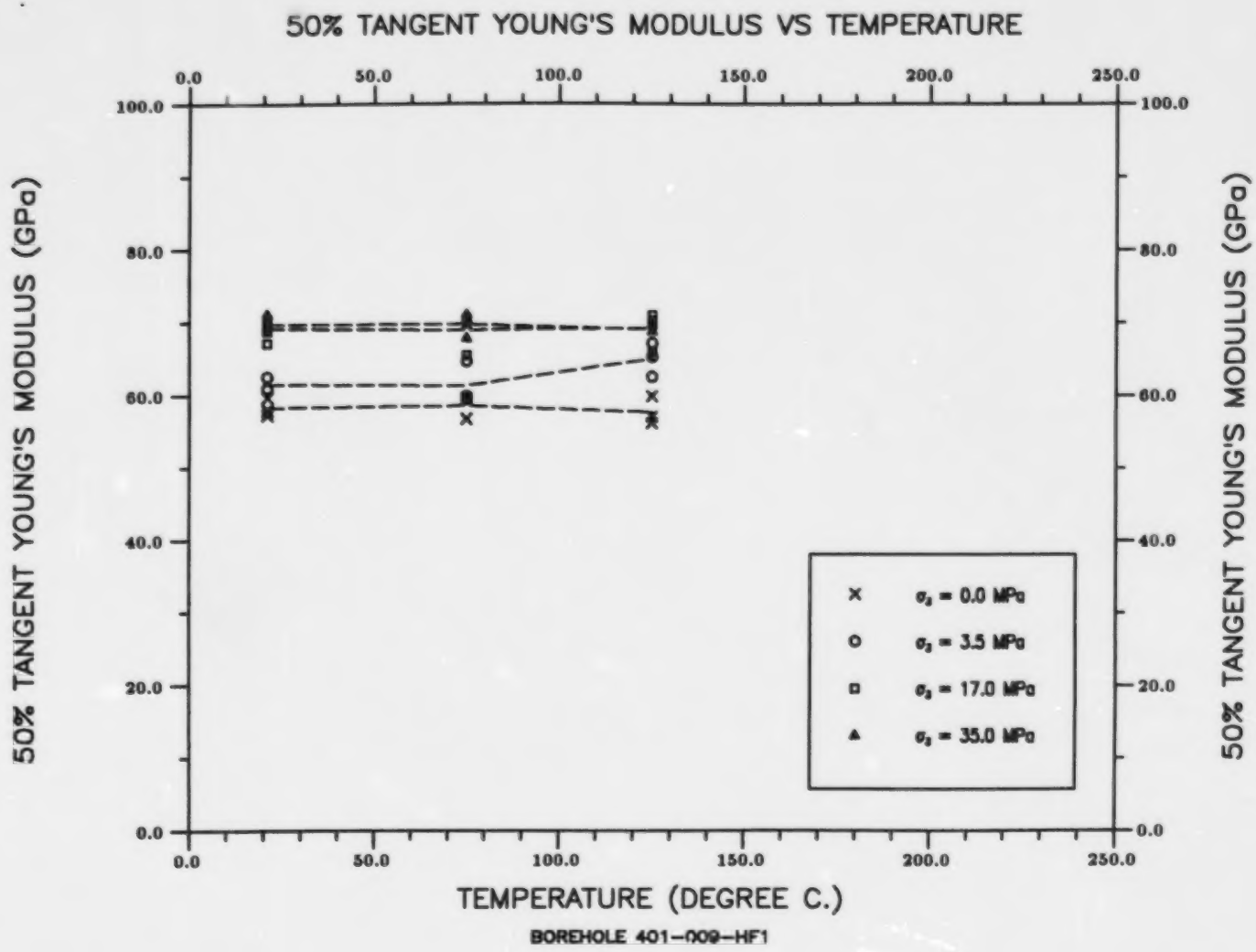

Figure 9. Plots of tangent Young's modulus at $0.5(\sigma_1 - \sigma_3)_f$ versus temperature.

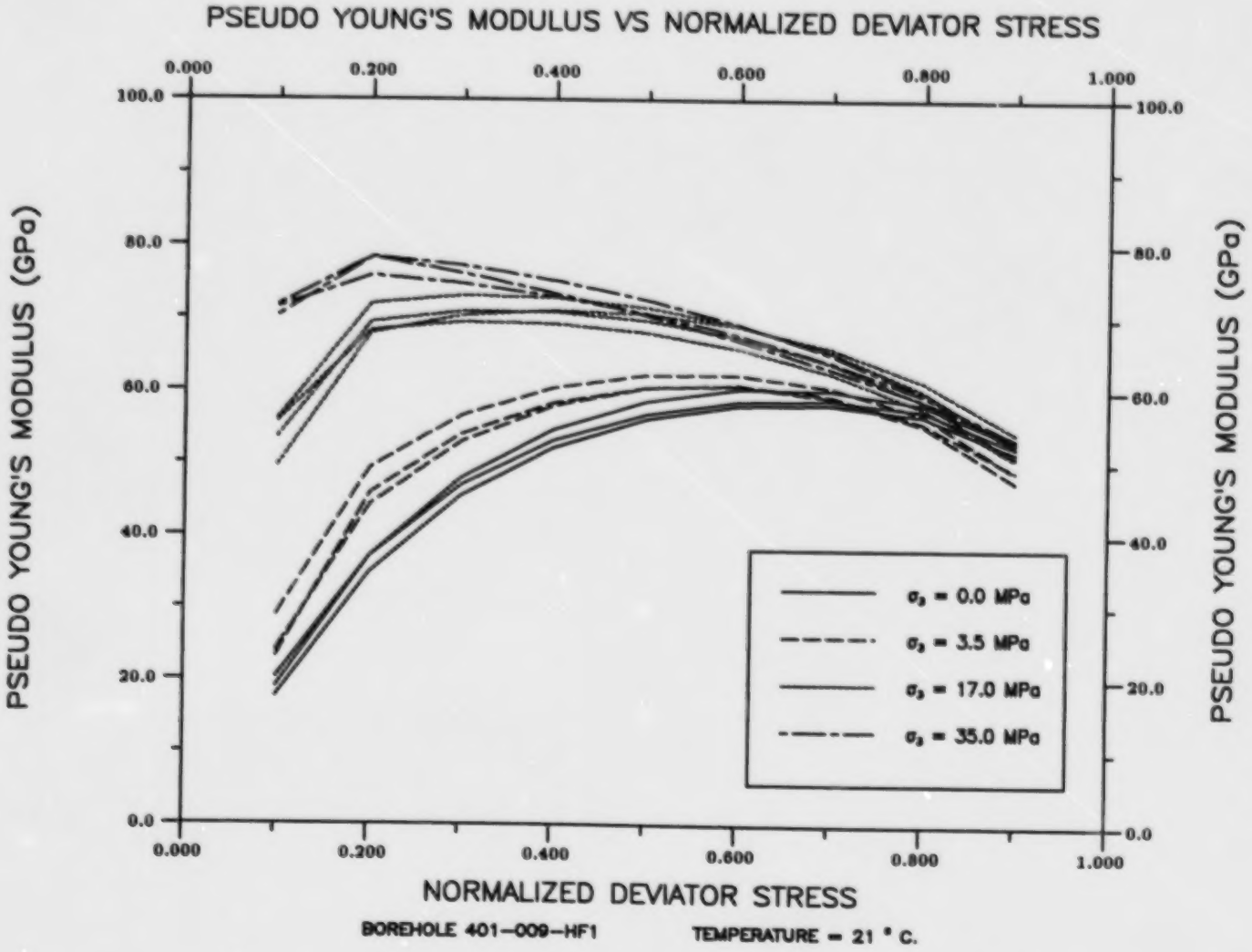

Figure 10. Plots of pseudo Young's modulus versus normalized deviator stress at 21° C.

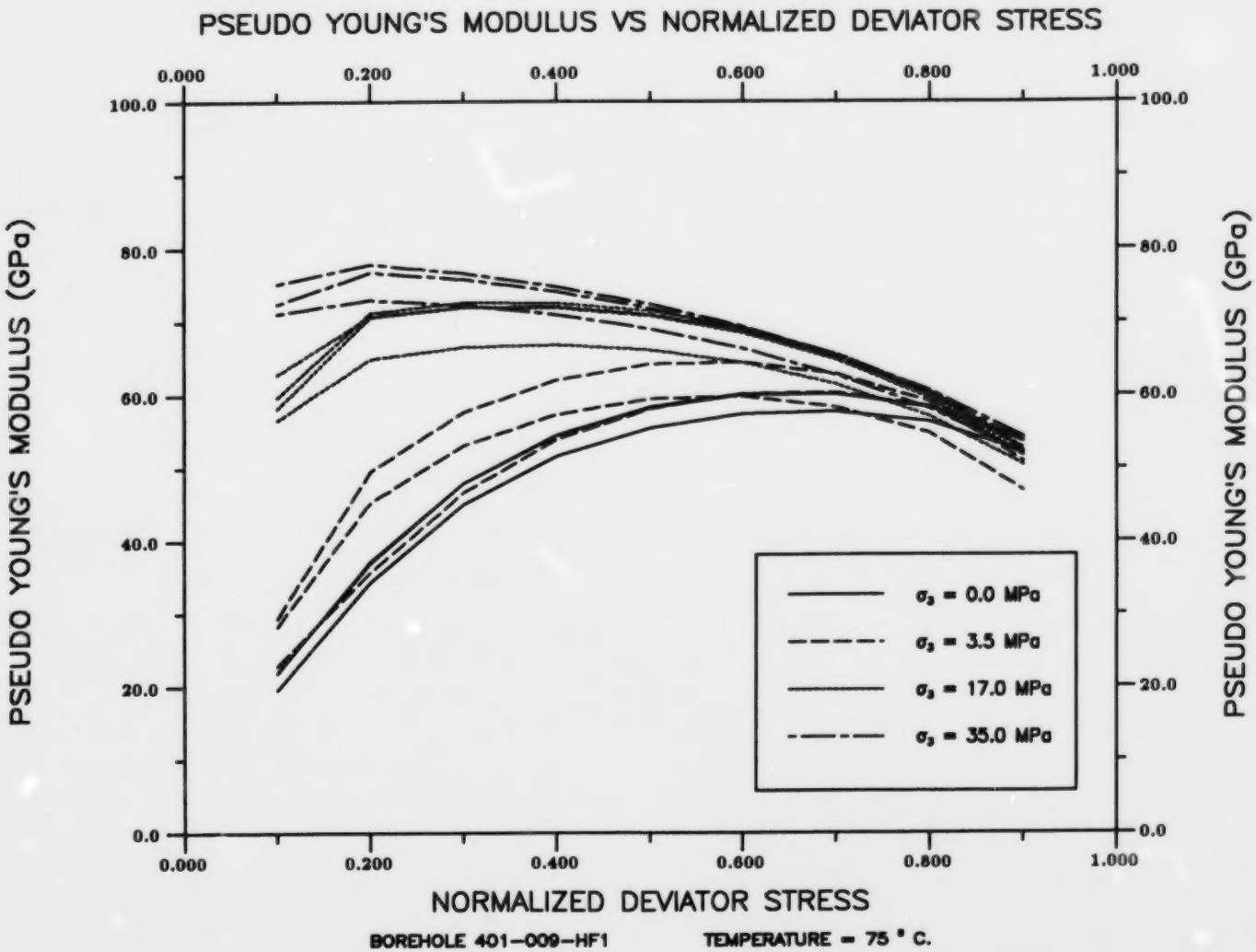

Figure 11. Plots of pseudo Young's modulus versus normalized deviator stress at 75° C.

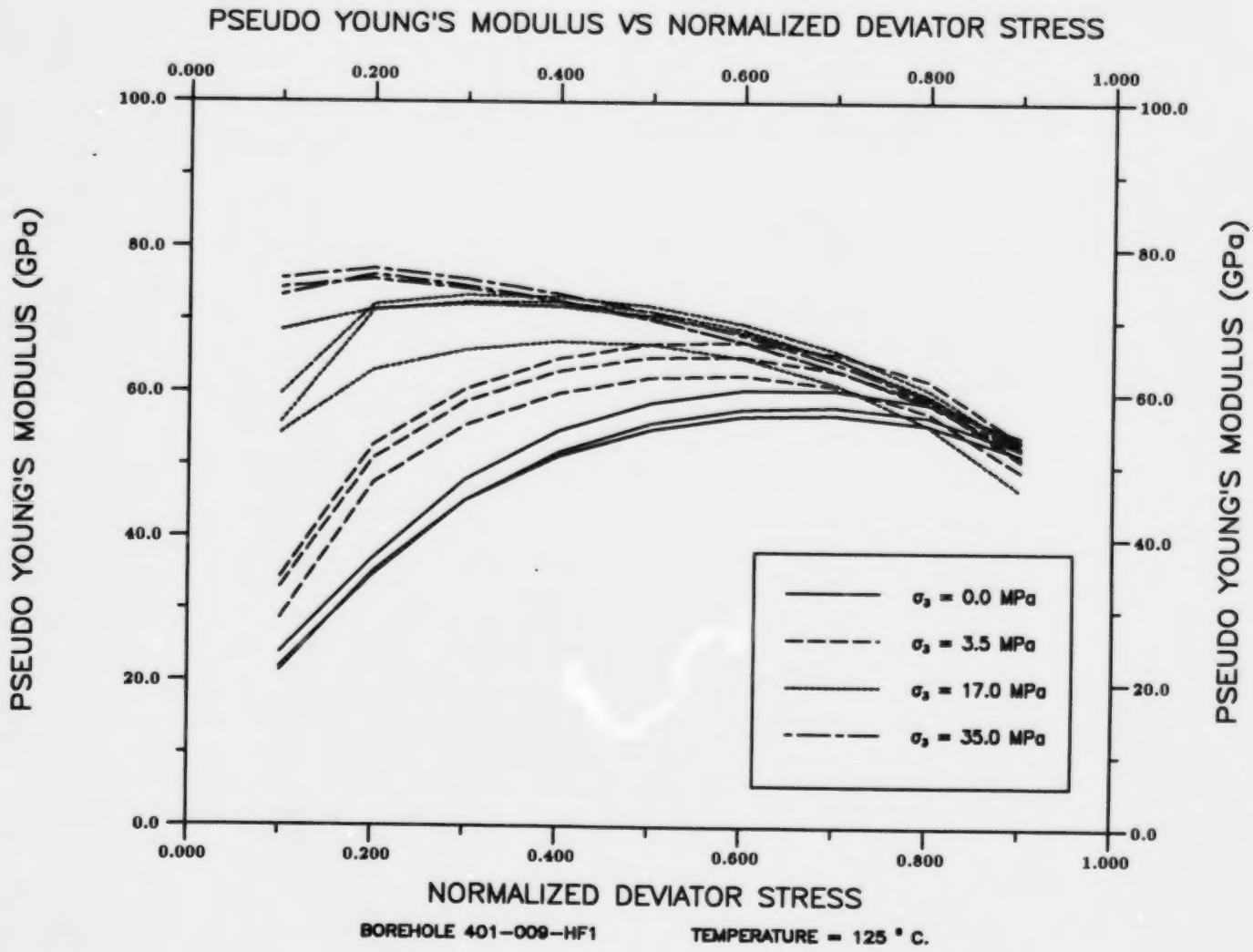

Figure 12. Plots of pseudo Young's modulus versus normalized deviator stress at 125° C.

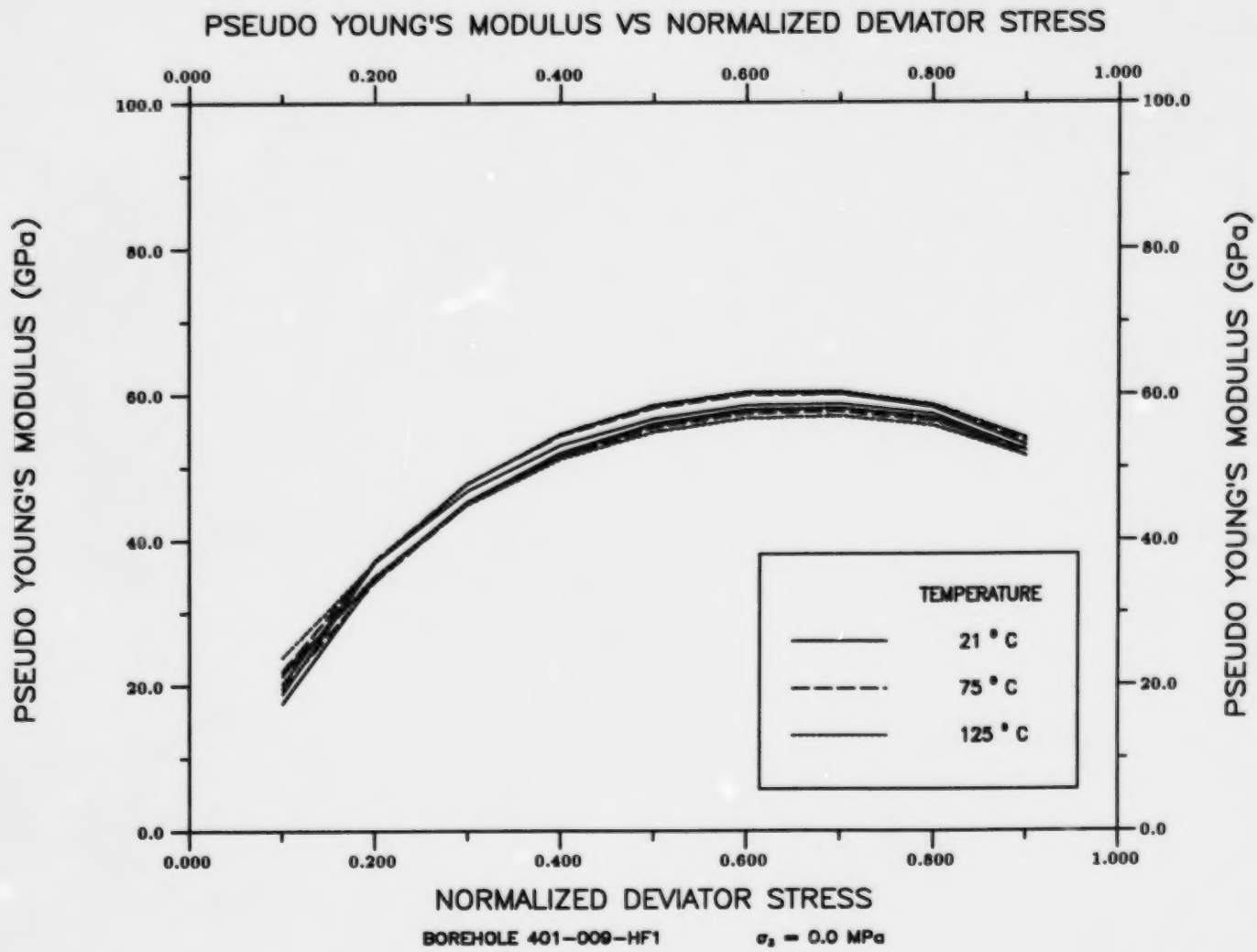

Figure 13. Plots of pseudo Young's modulus versus normalized deviator stress at the unconfined condition.

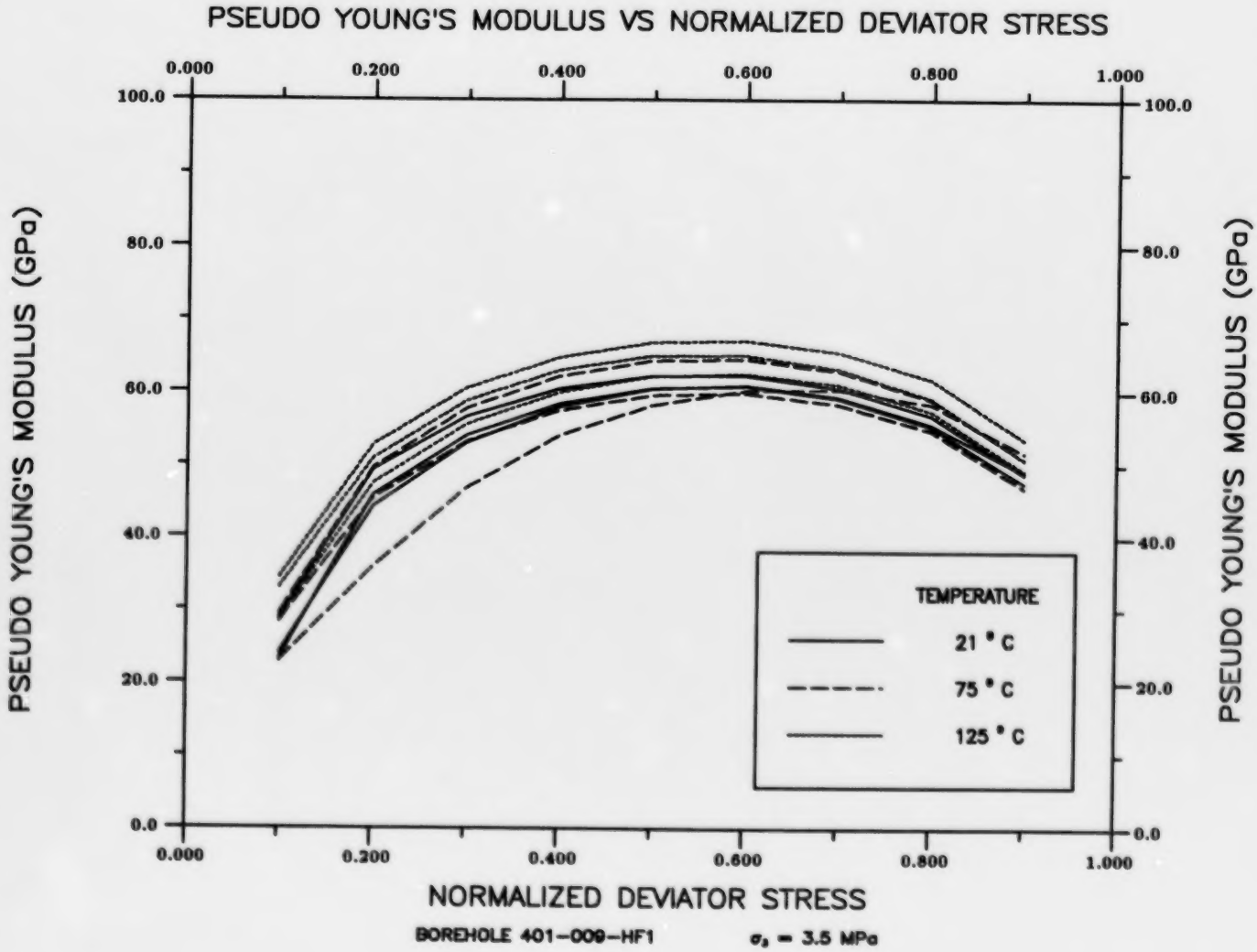

Figure 14. Plots of pseudo Young's modulus versus normalized deviator stress at the confining pressure of 3.5 MPa.

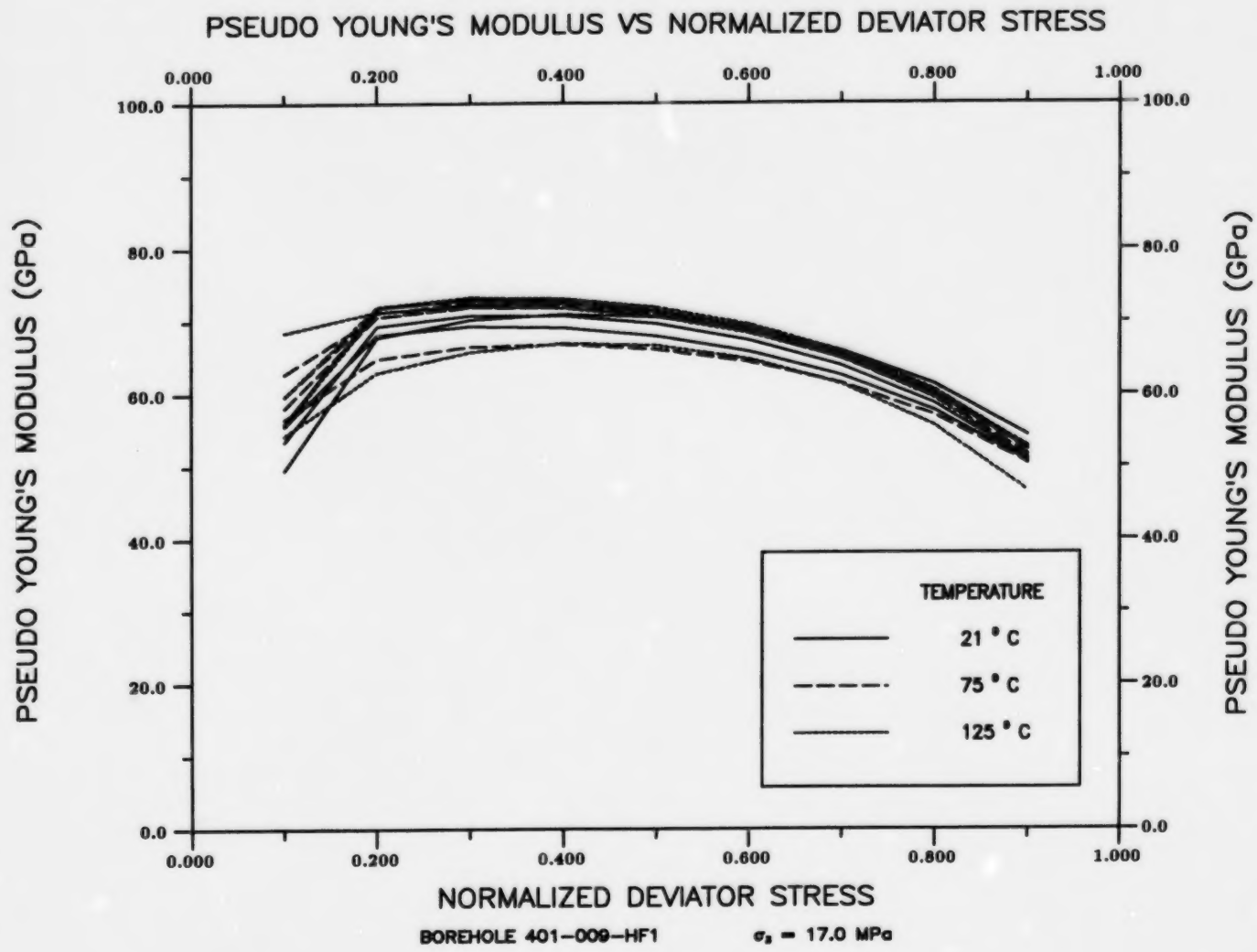

Figure 15. Plots of pseudo Young's modulus versus normalized deviator stress at the confining pressure of 17.0 MPa.

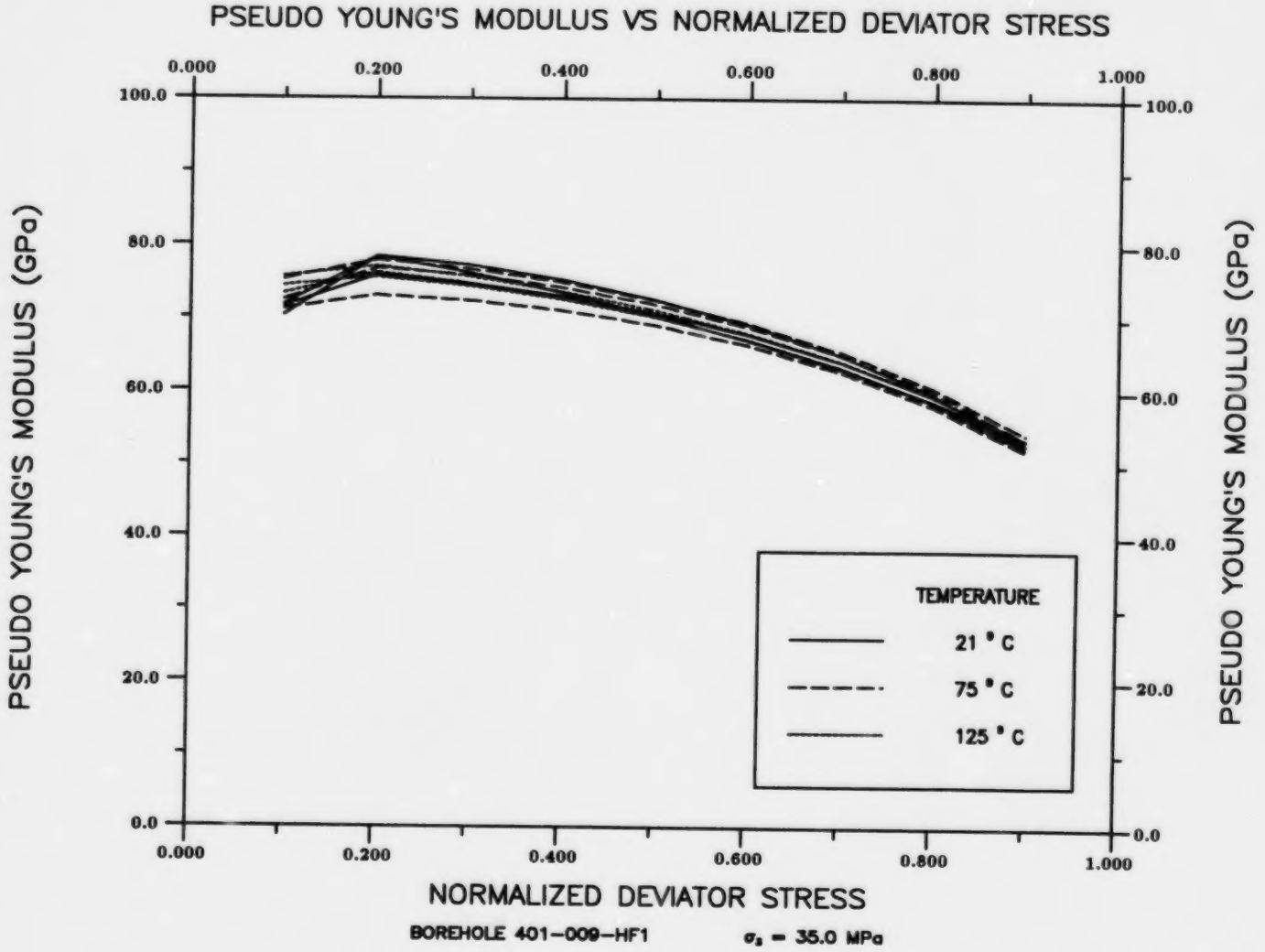

Figure 16. Plots of pseudo Young's modulus versus normalized deviator stress at the confining pressure of 35.0 MPa.

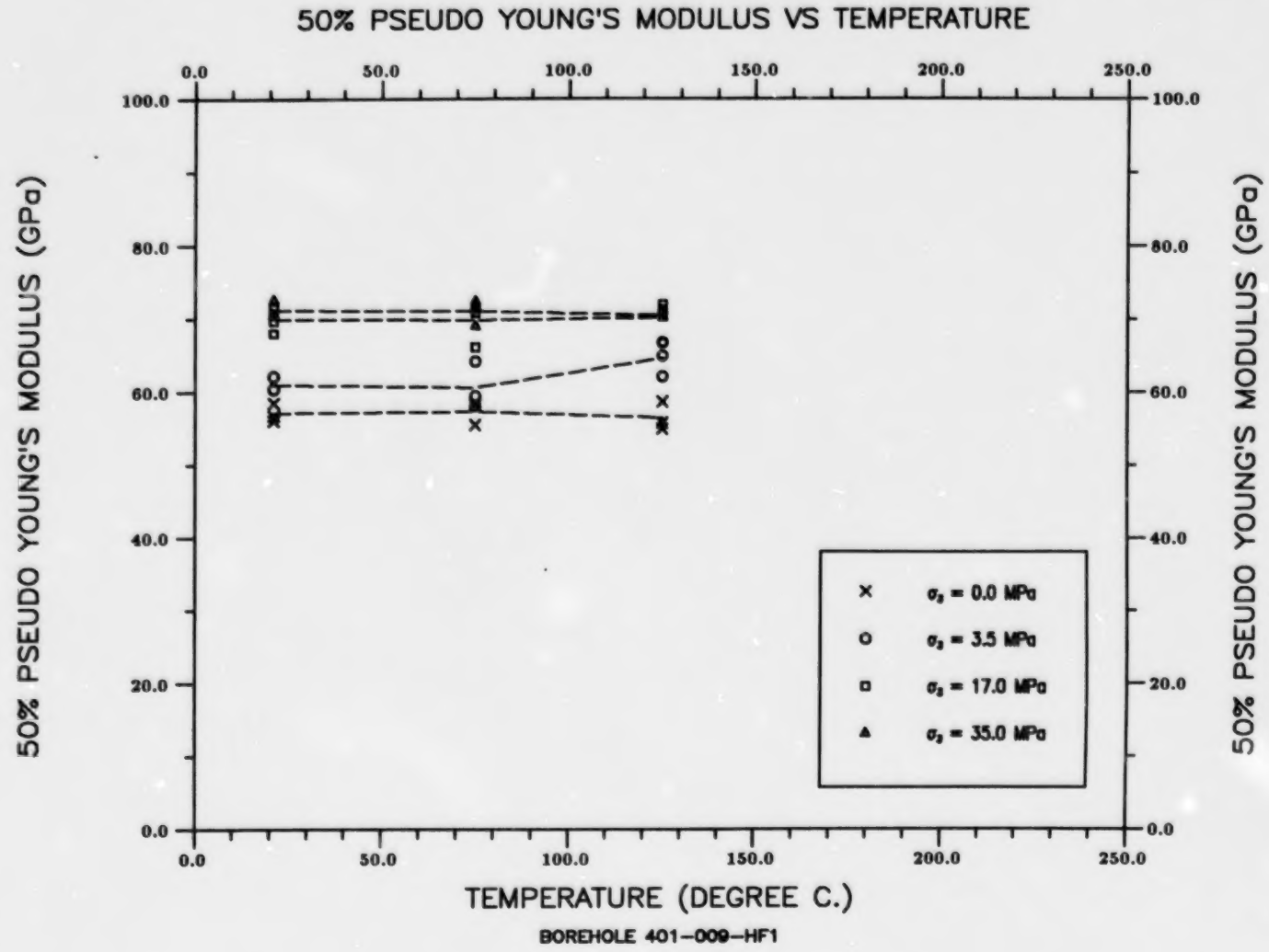

Figure 17. Plots of pseudo Young's modulus at $0.5(\sigma_1 - \sigma_3)_f$ versus temperature.

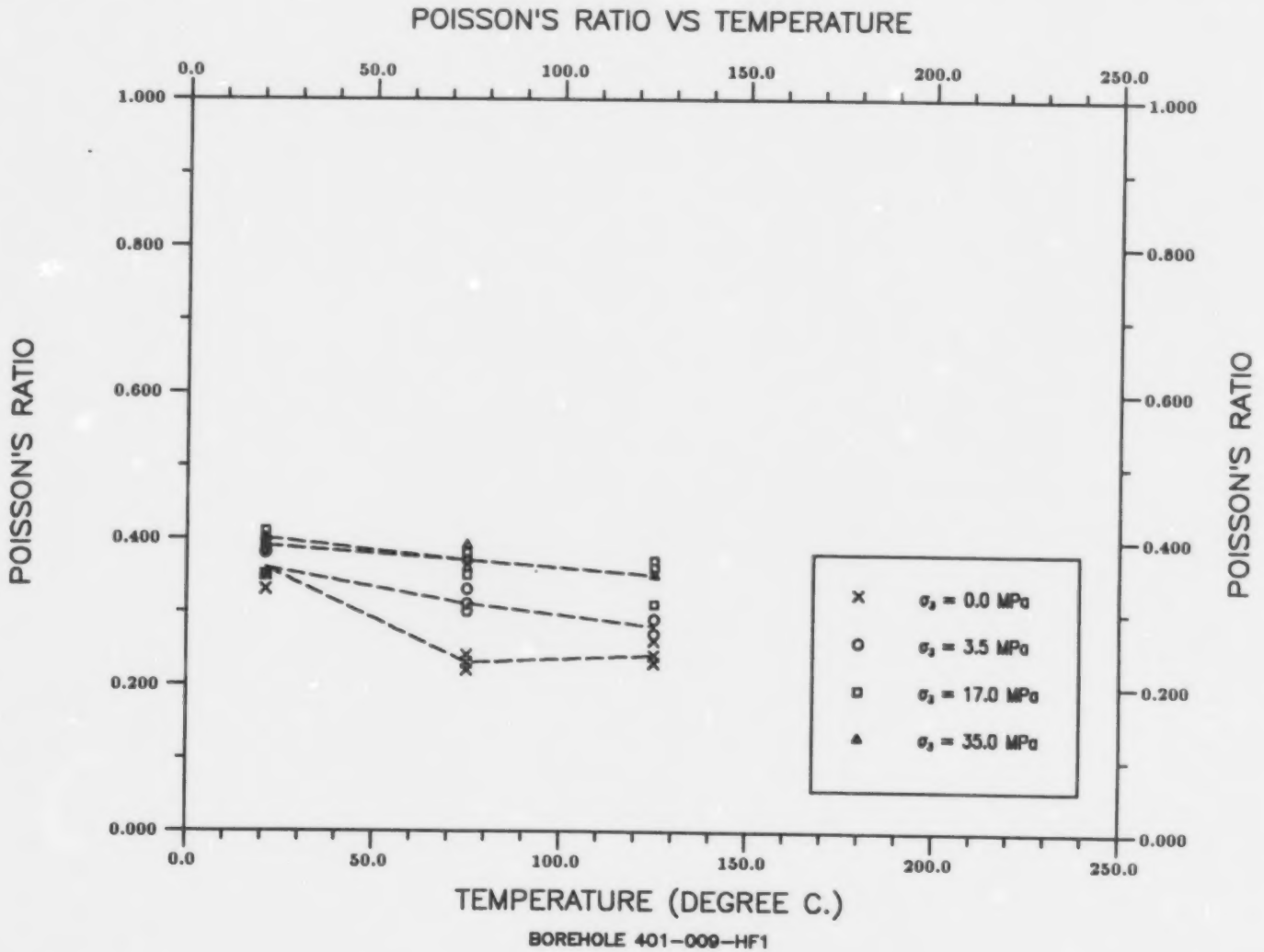

Figure 18. Plots of Poisson's ratio at $0.4(\sigma_1 - \sigma_3)_f$ versus temperature.

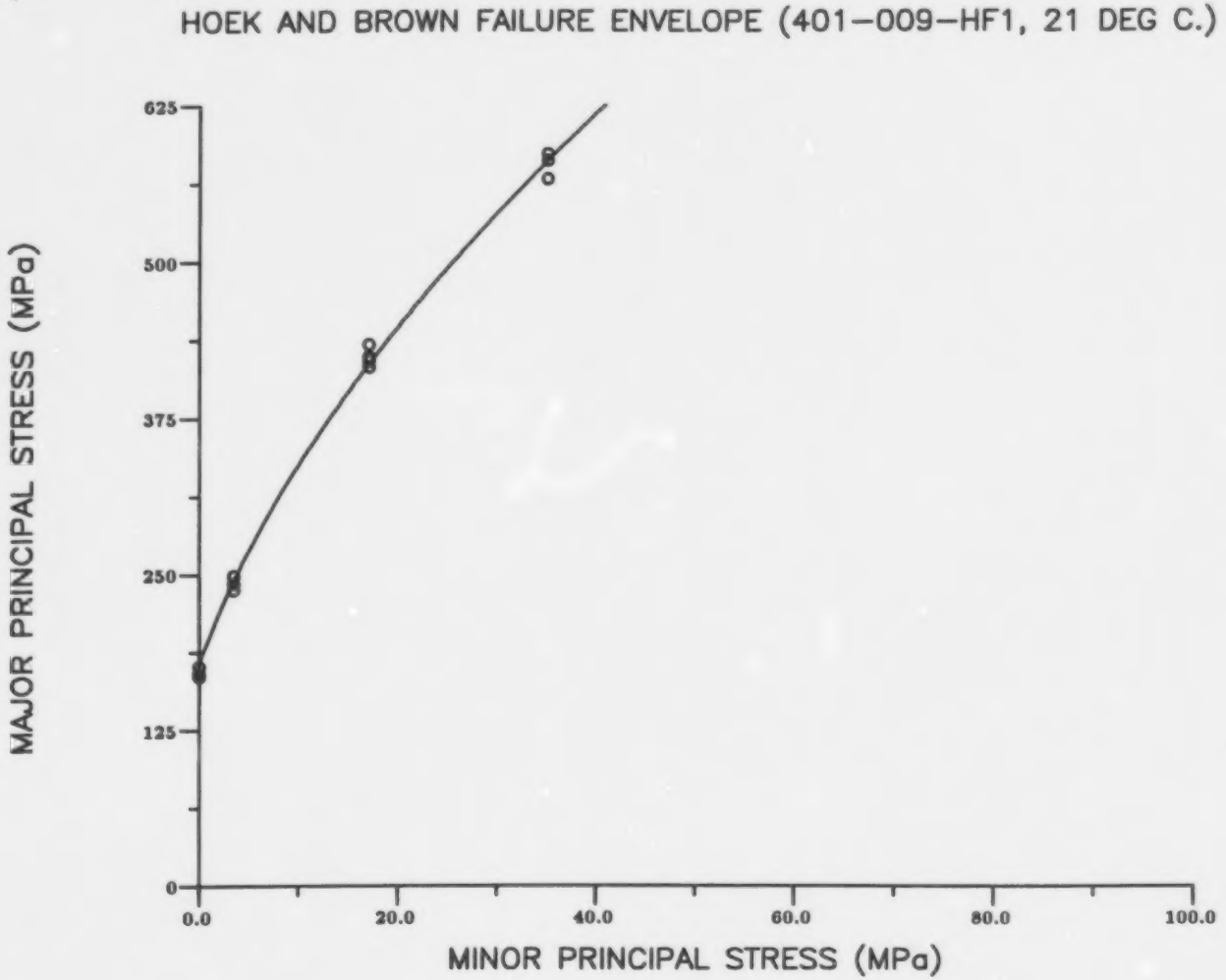

Figure 19. Hoek and Brown failure envelope at 21° C.

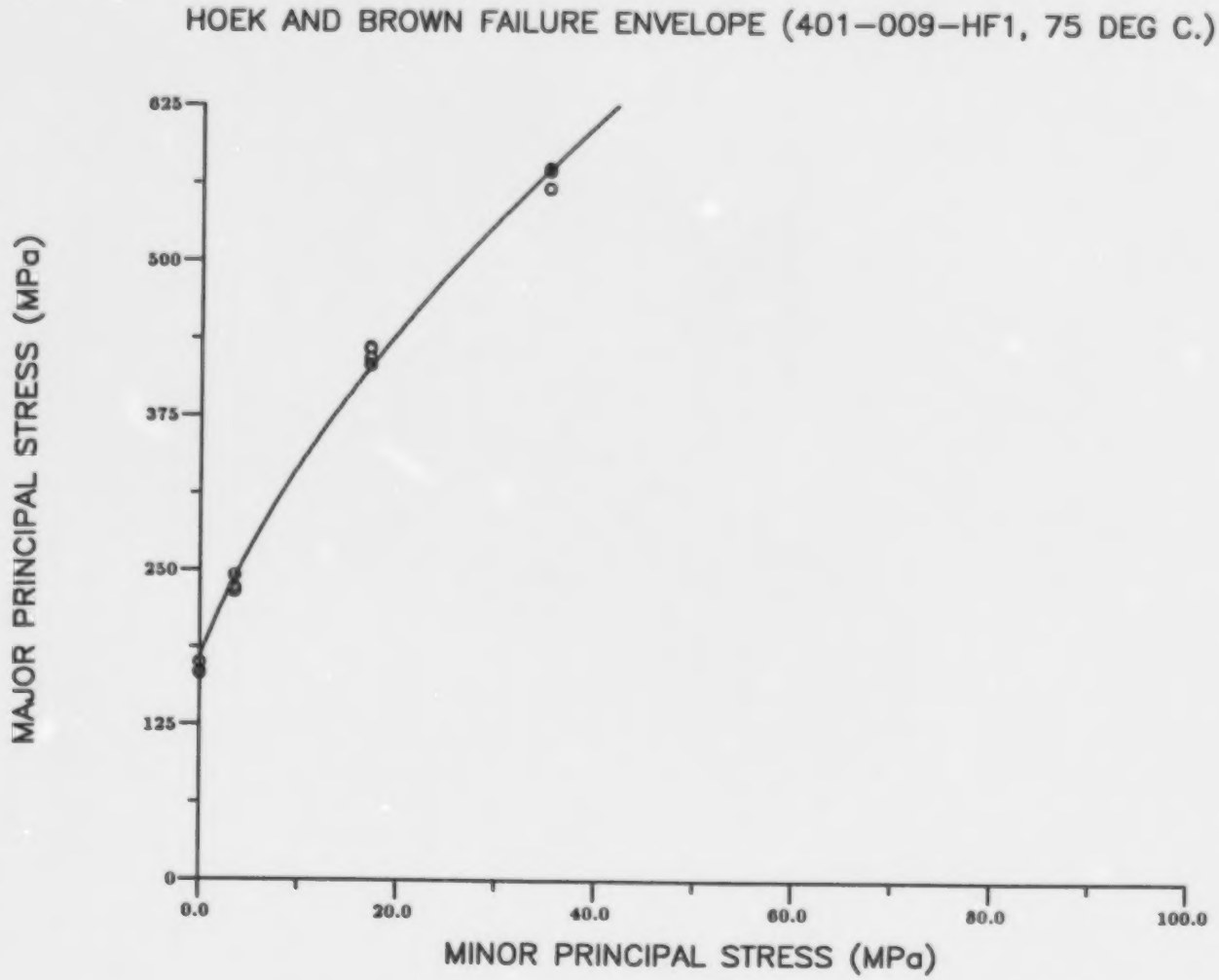

Figure 20. Hoek and Brown failure envelope at 75° C.

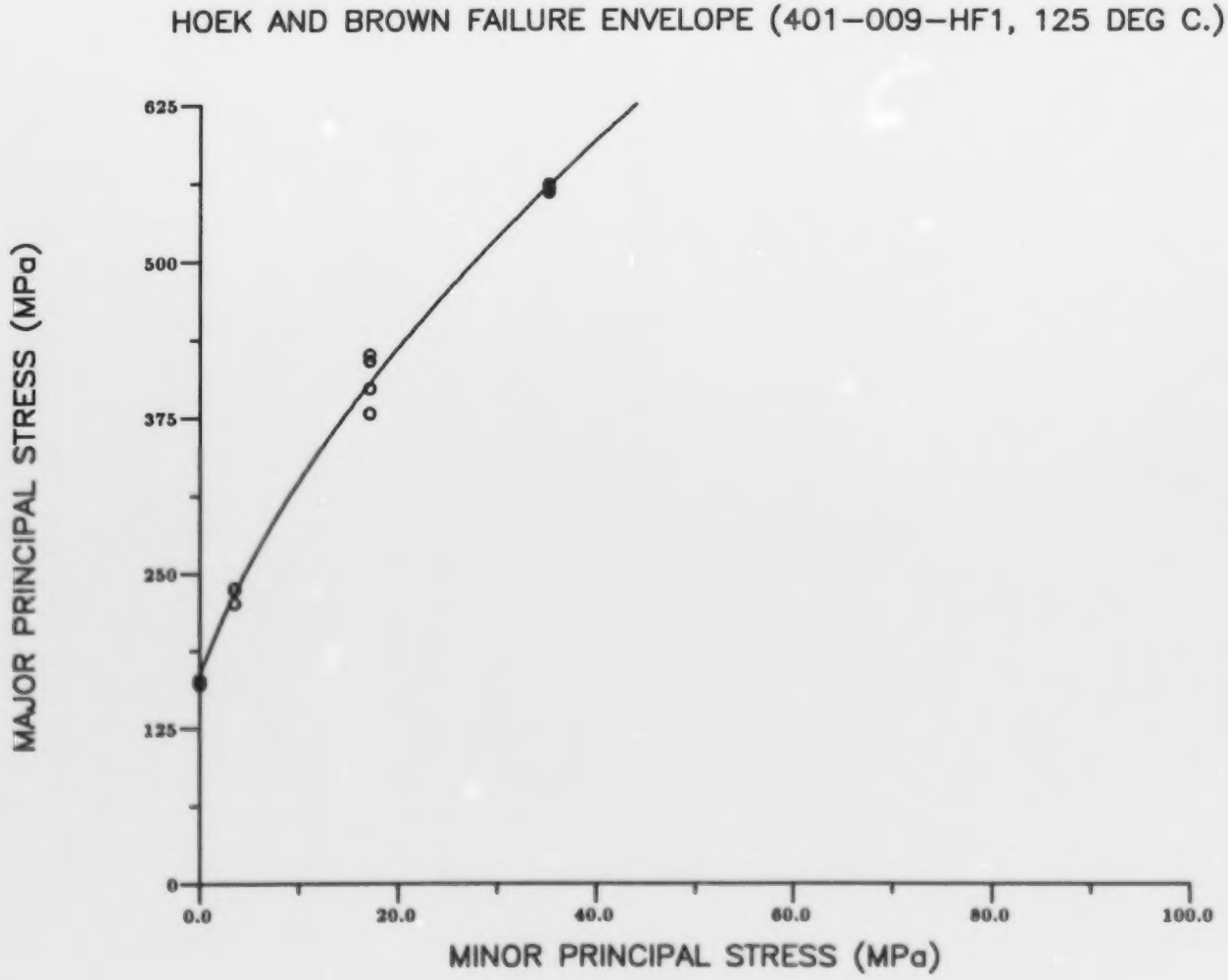

Figure 21. Hoek and Brown failure envelope at 125° C.

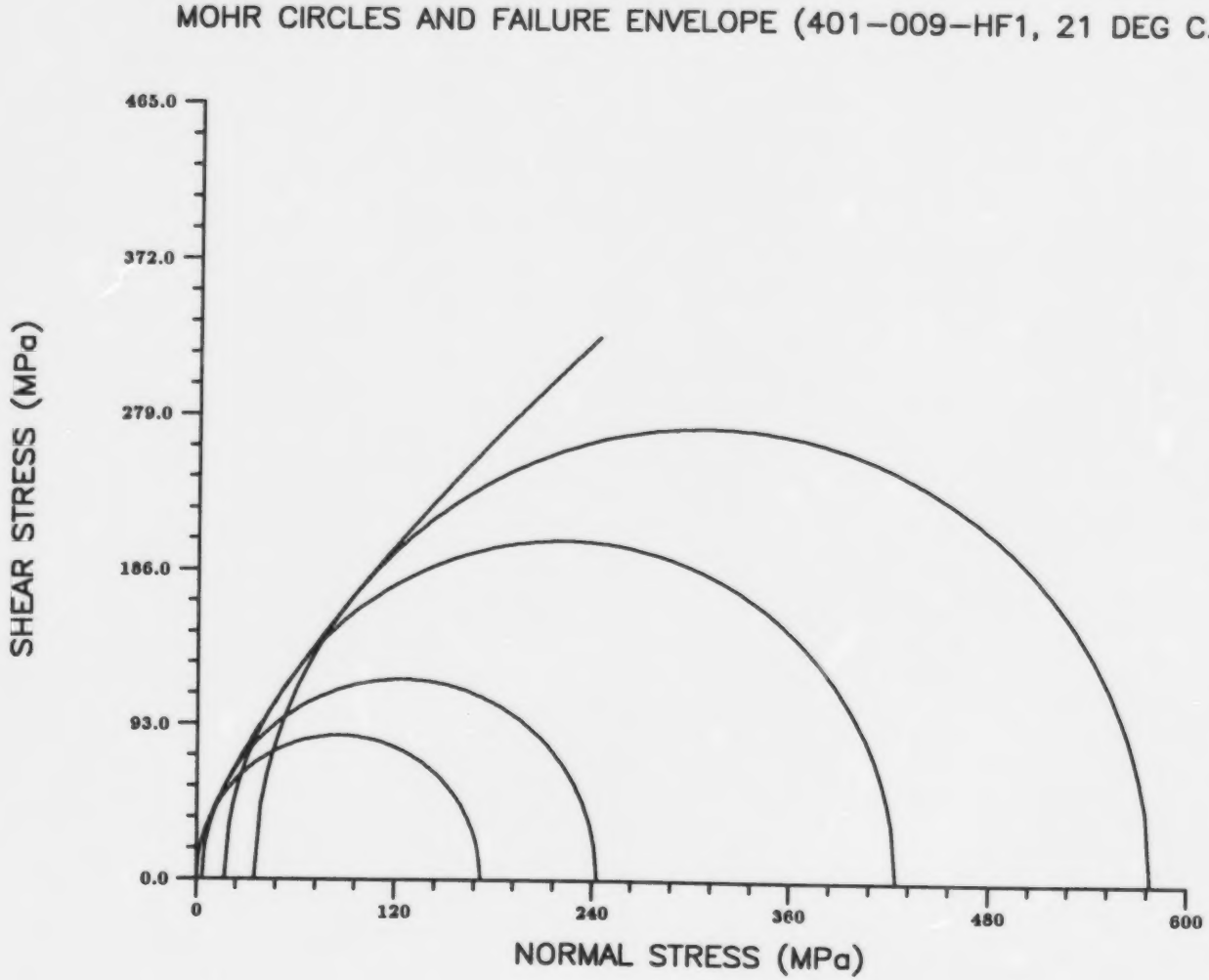

Figure 22. Mohr circles and failure envelope at 21° C.

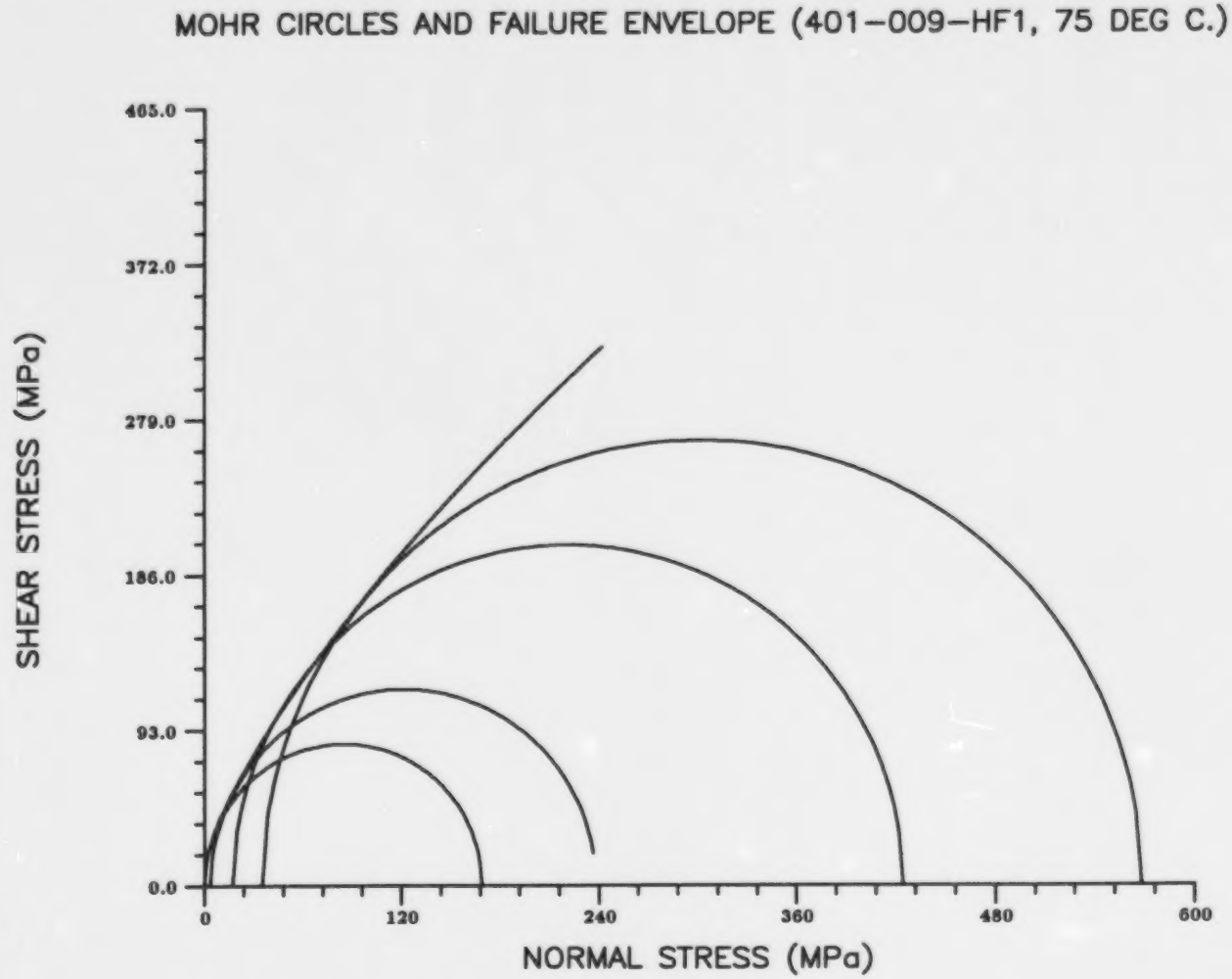

Figure 23. Mohr circles and failure envelope at 75° C.

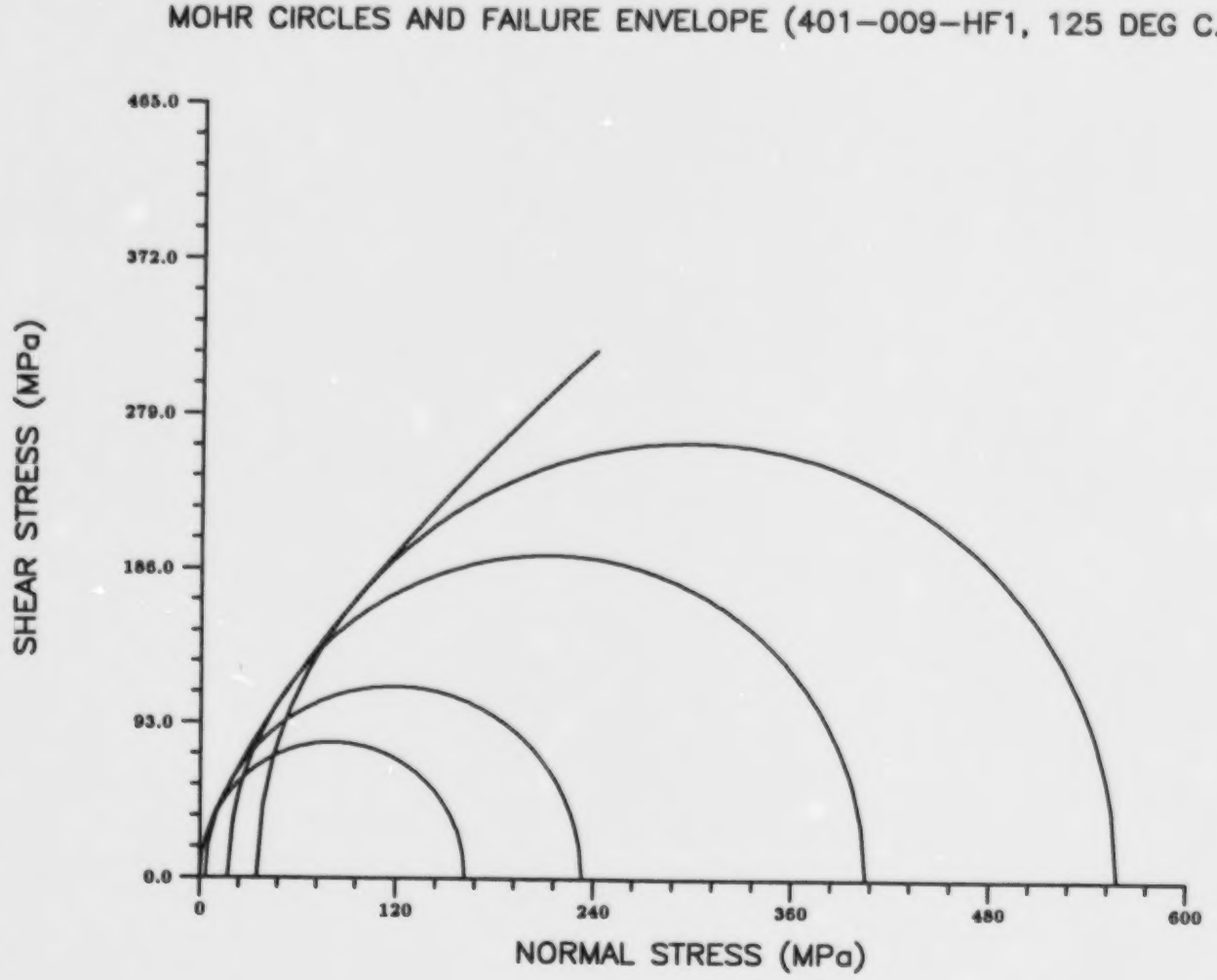

Figure 24. Mohr circles and failure envelope at 125° C.

Appendix A

Stress-strain curves for specimens from Borehole 401-009-HF1

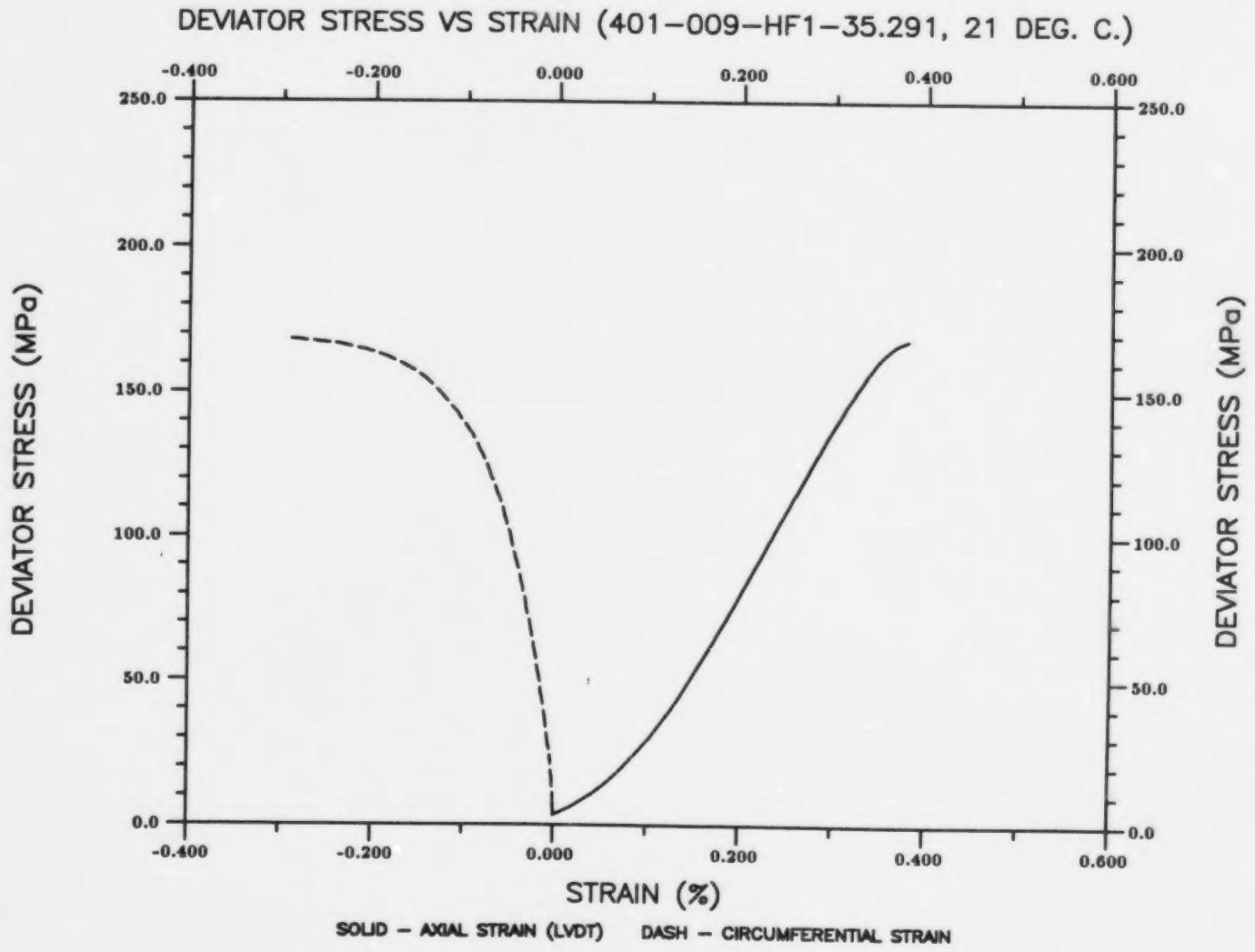

Figure A1. Stress-strain curves for Specimen 401-009-HF1-35.291 tested at 21° C and at the unconfined condition.

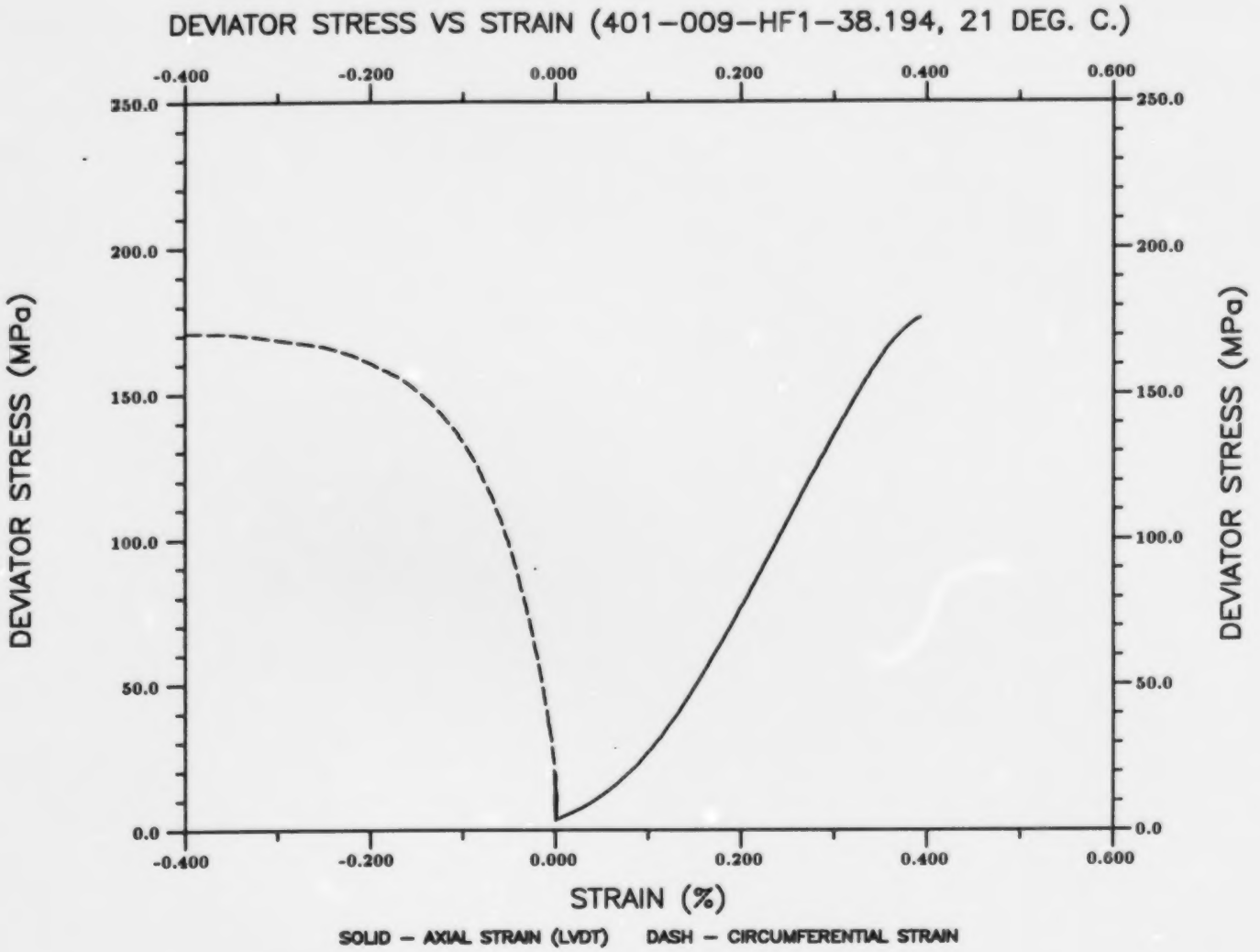

Figure A2. Stress-strain curves for Specimen 401-009-HF1-38.194 tested at 21° C and at the unconfined condition.

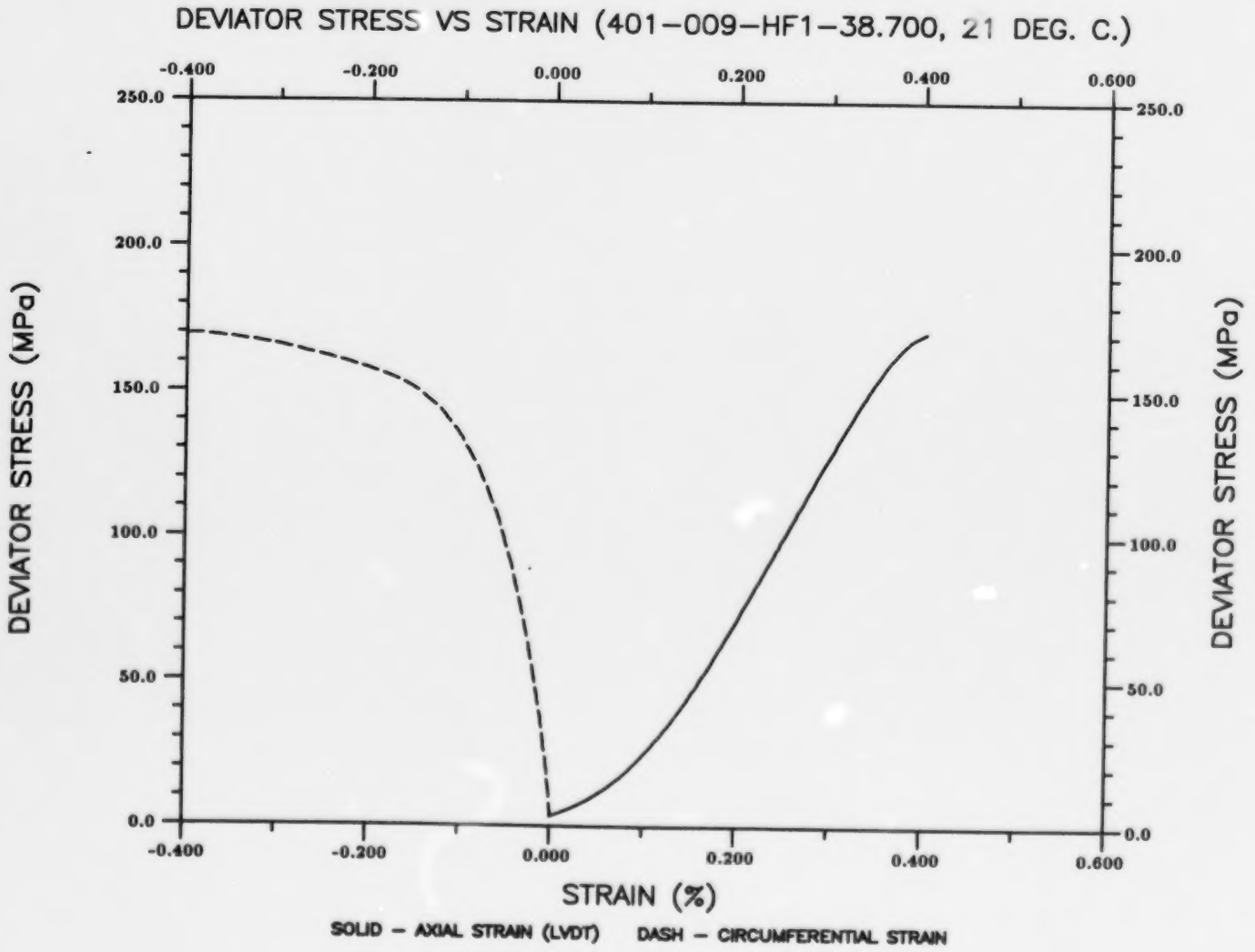

Figure A3. Stress-strain curves for Specimen 401-009-HF1-38.700 tested at 21° C and at the unconfined condition.

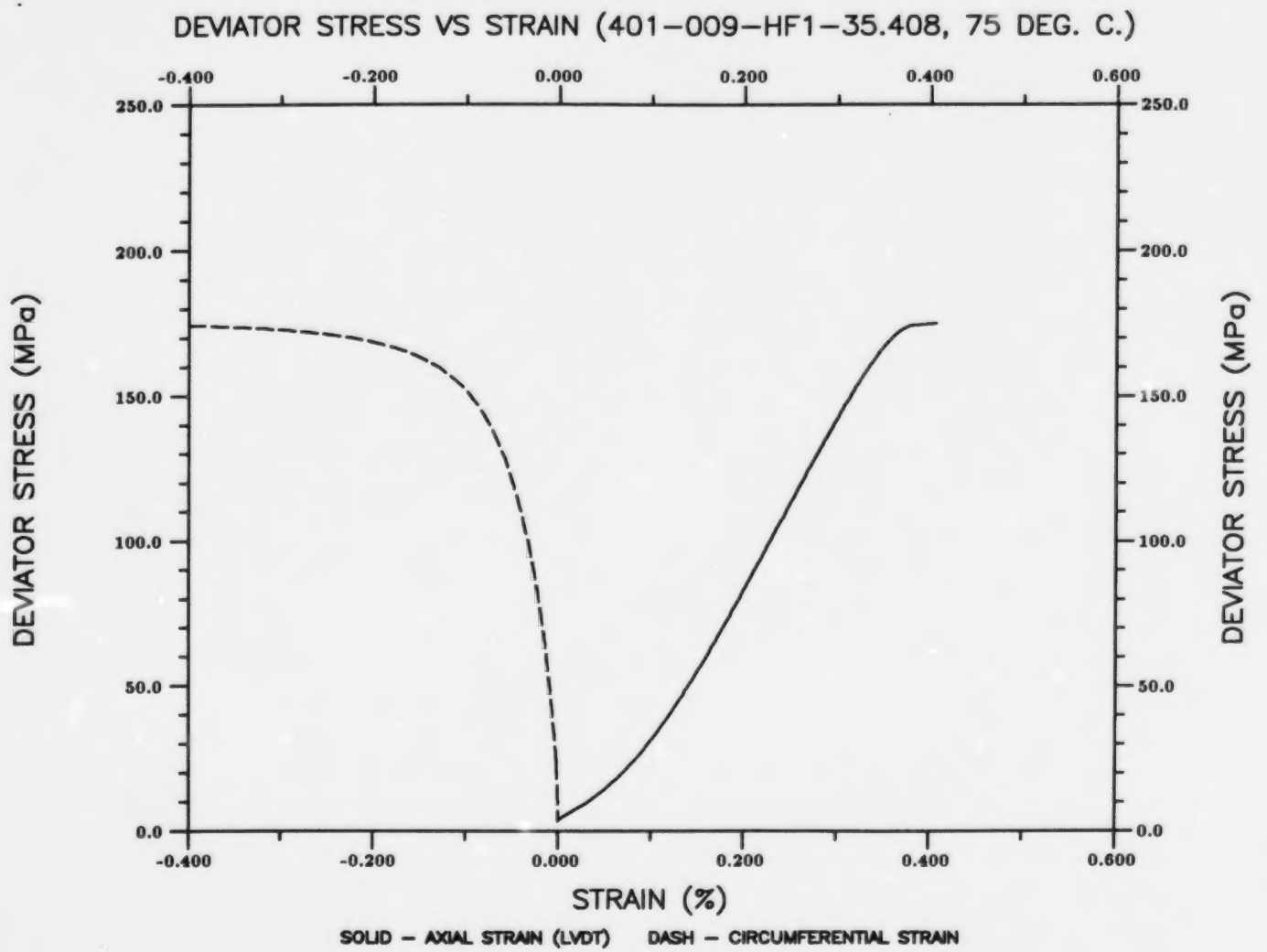

Figure A4. Stress-strain curves for Specimen 401-009-HF1-35.408 tested at 75° C and at the unconfined condition.

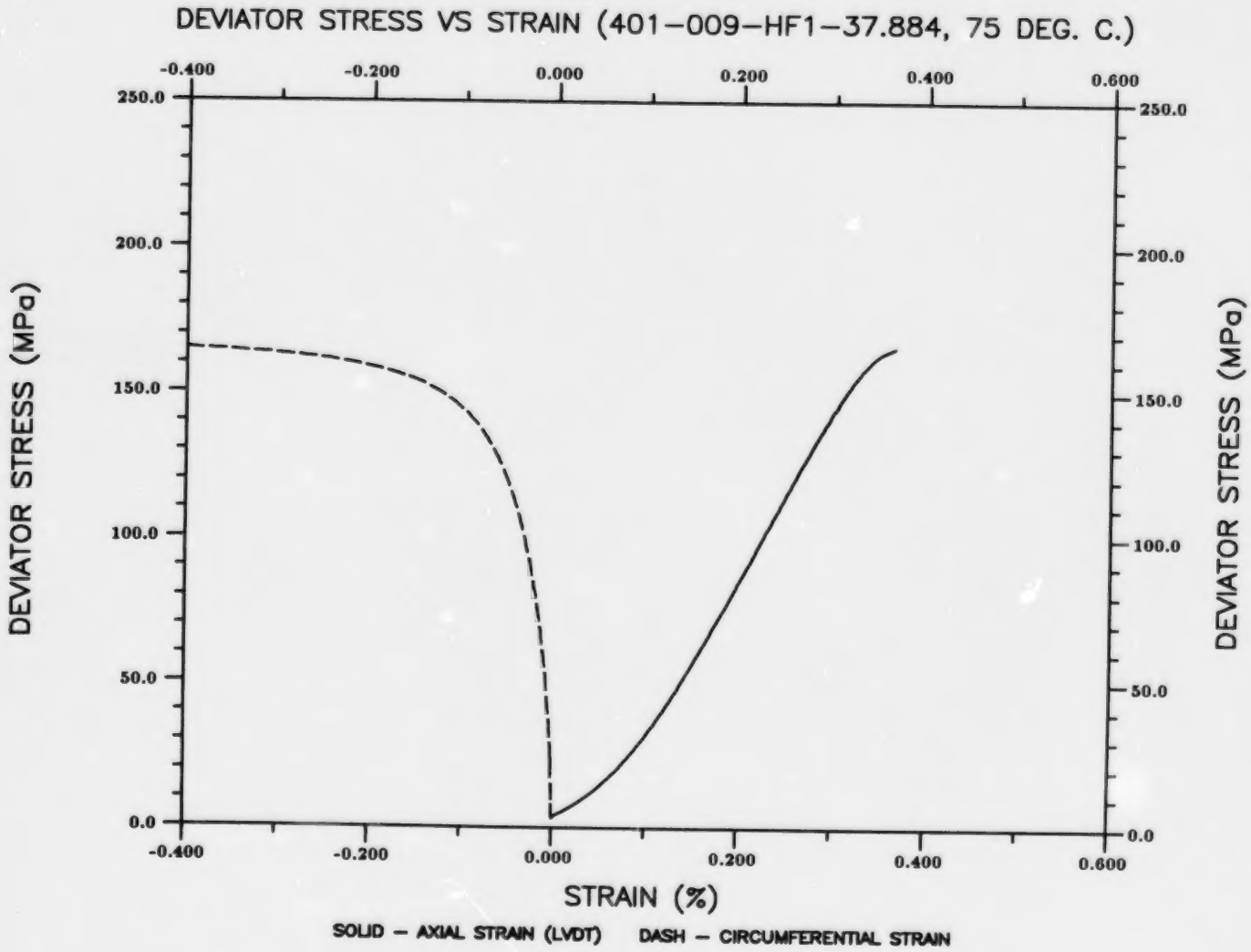

Figure A5. Stress-strain curves for Specimen 401-009-HF1-37.884 tested at 75° C and at the unconfined condition.

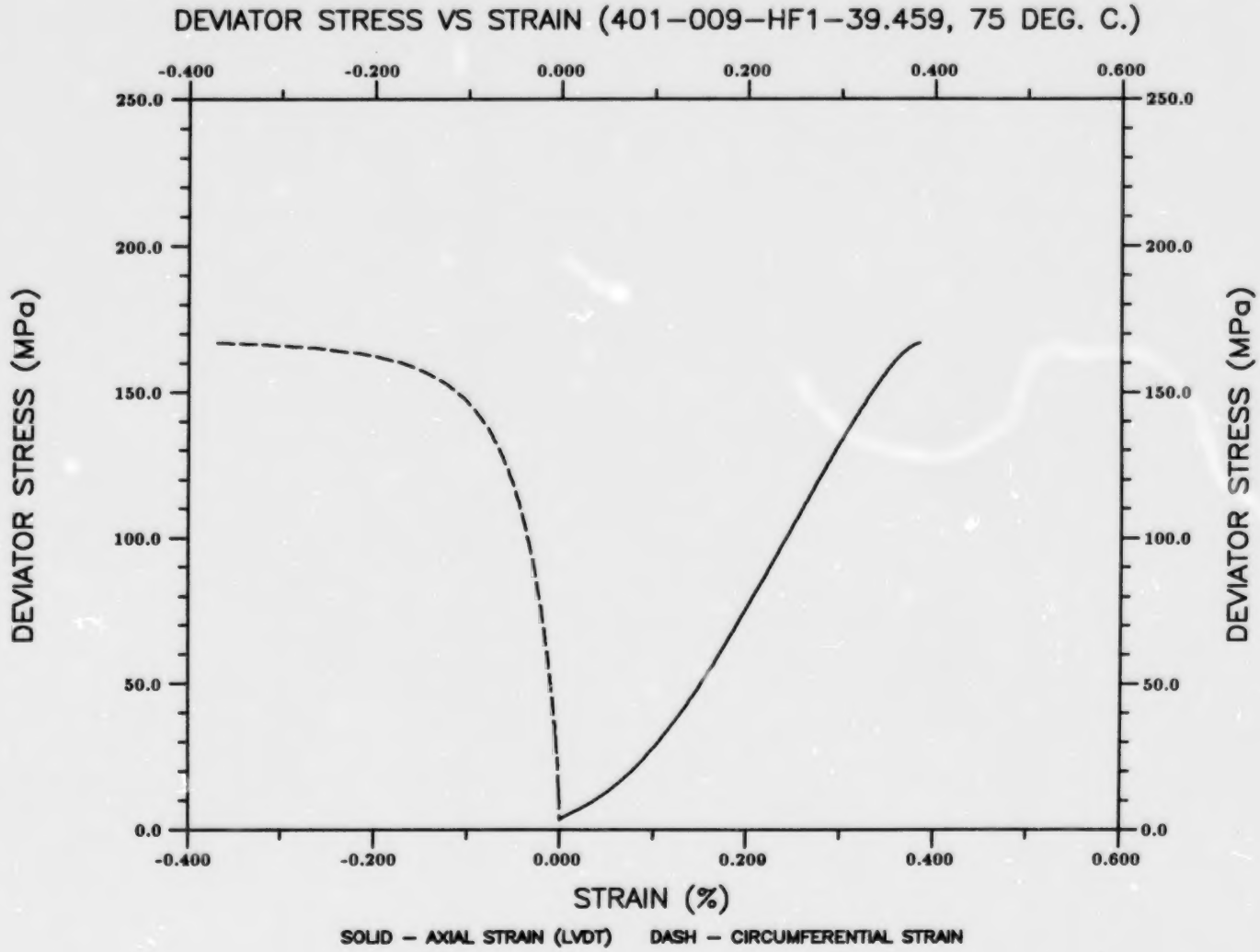

Figure A6. Stress-strain curves for Specimen 401-009-HF1-39.459 tested at 75° C and at the unconfined condition.

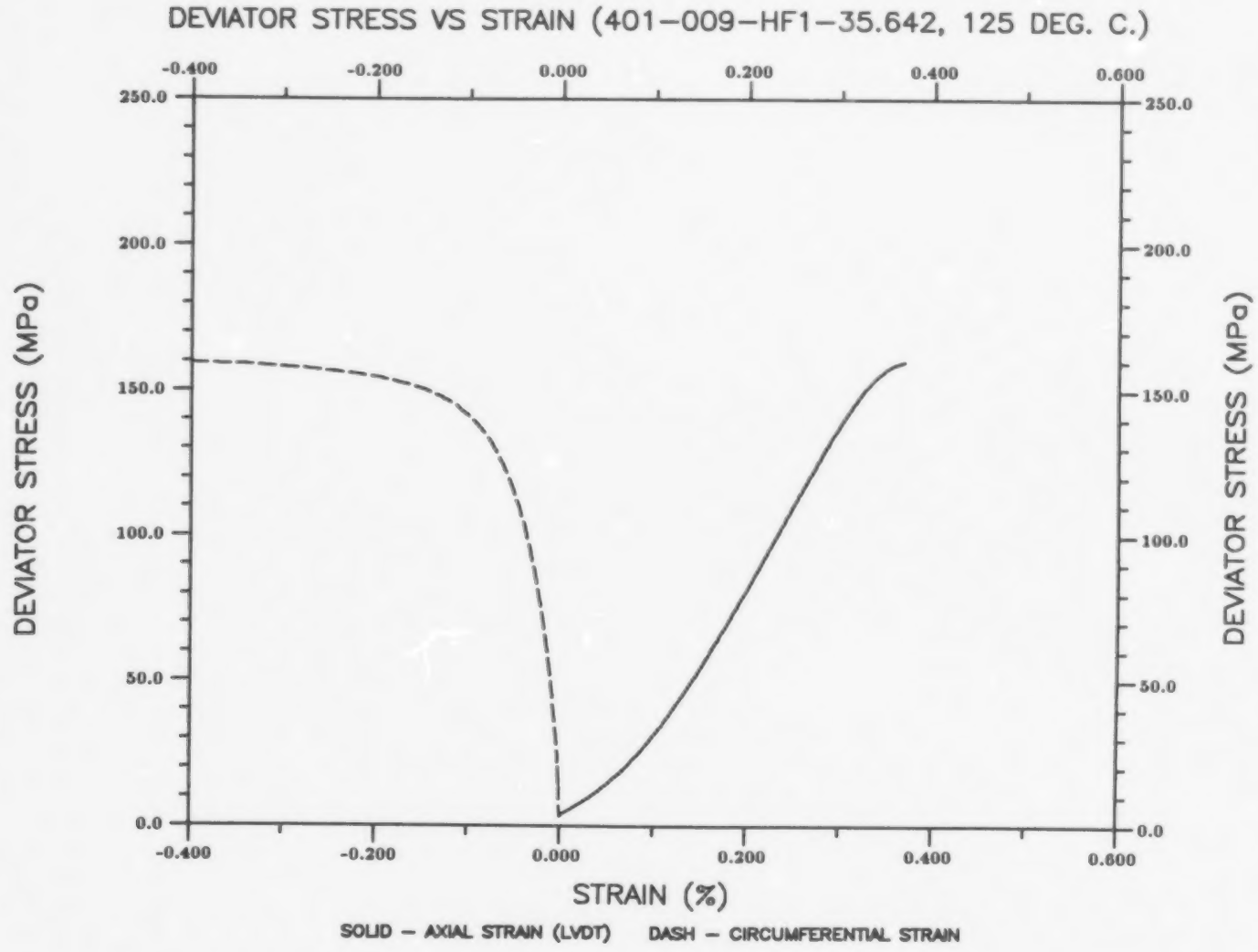

Figure A7. Stress-strain curves for Specimen 401-009-HF1-35.642 tested at 125° C and at the unconfined condition.

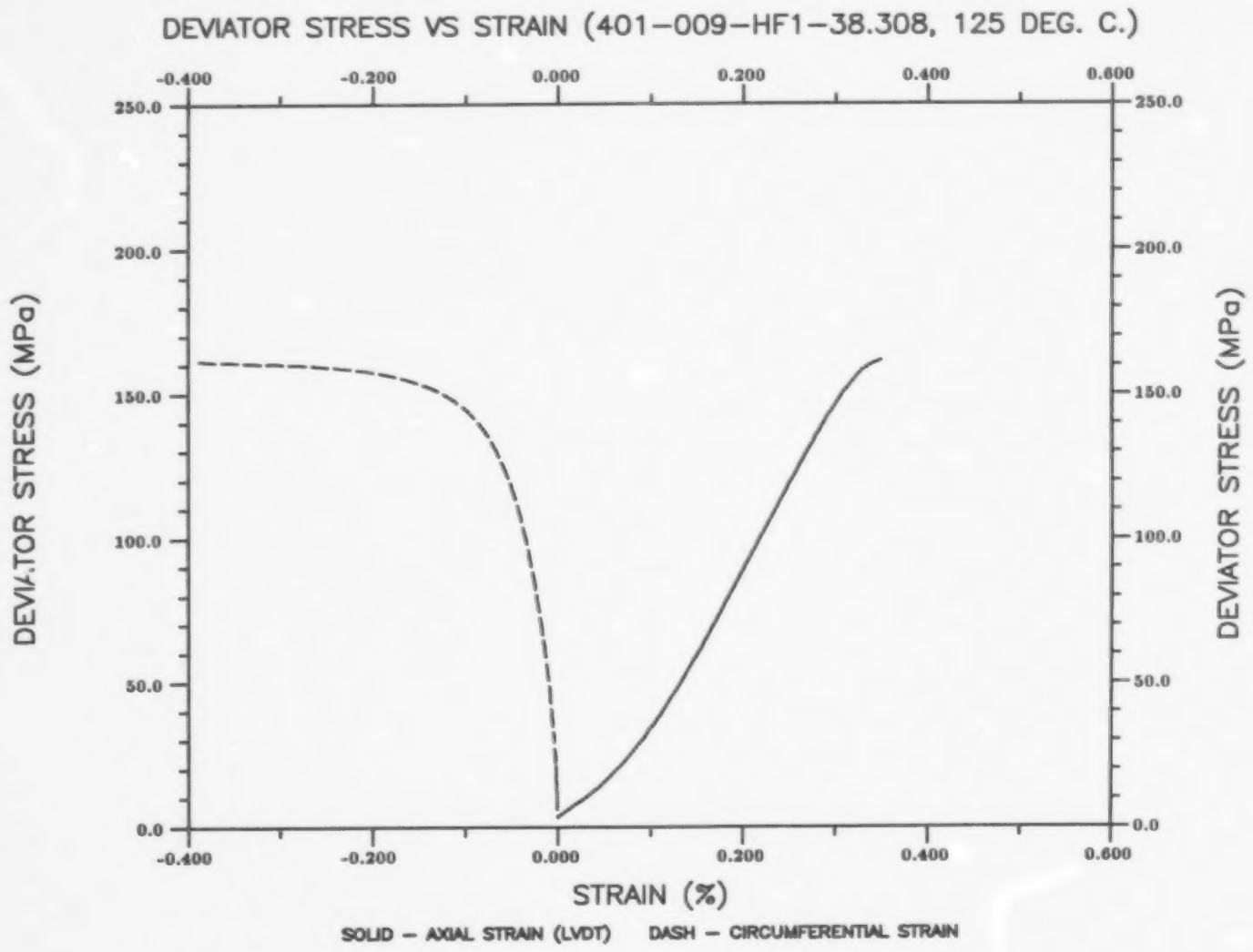

Figure A8. Stress-strain curves for Specimen 401-009-HF1-38.308 tested at 125° C and at the unconfined condition.

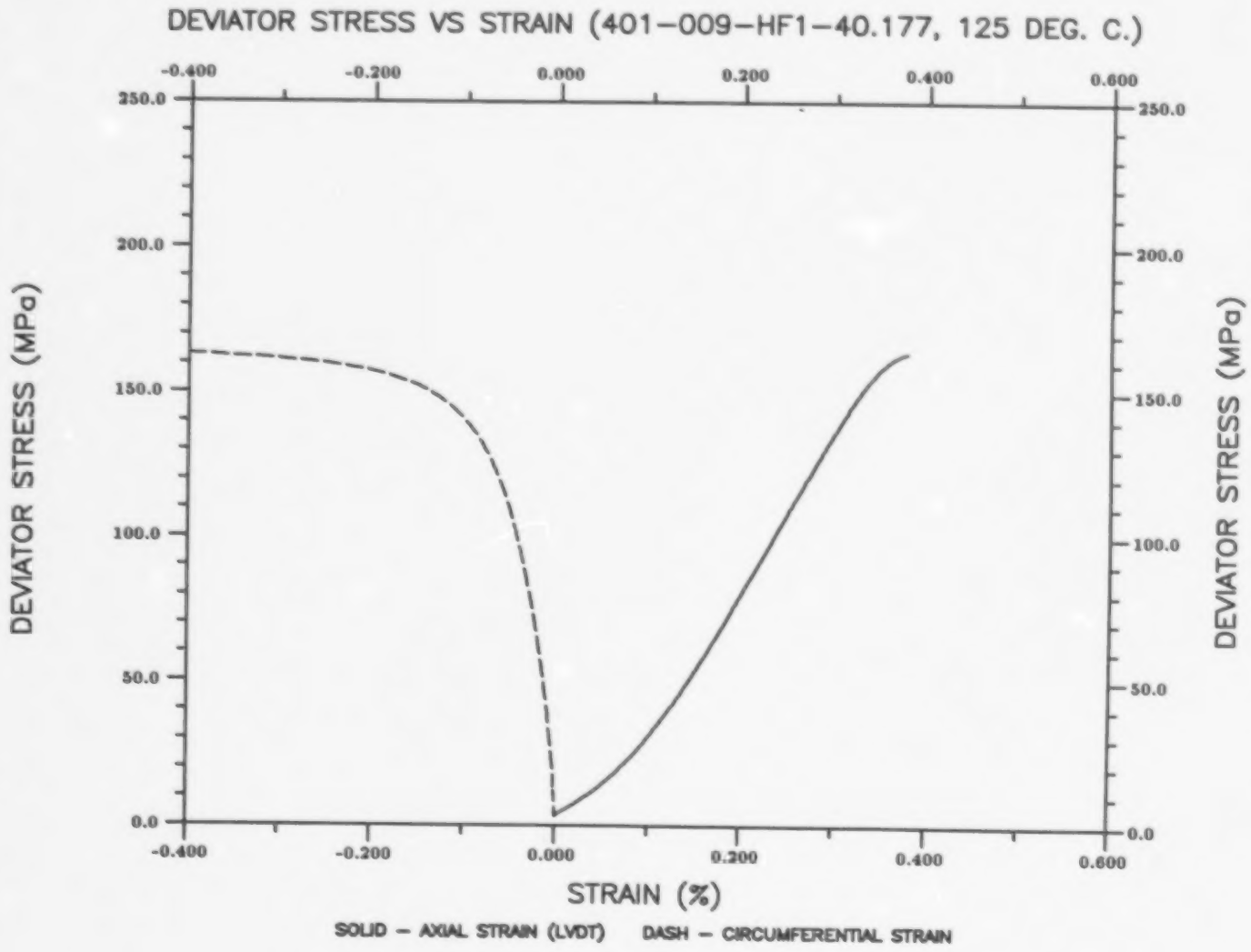

Figure A9. Stress-strain curves for Specimen 401-009-HF1-40.177 tested at 125° C and at the unconfined condition.

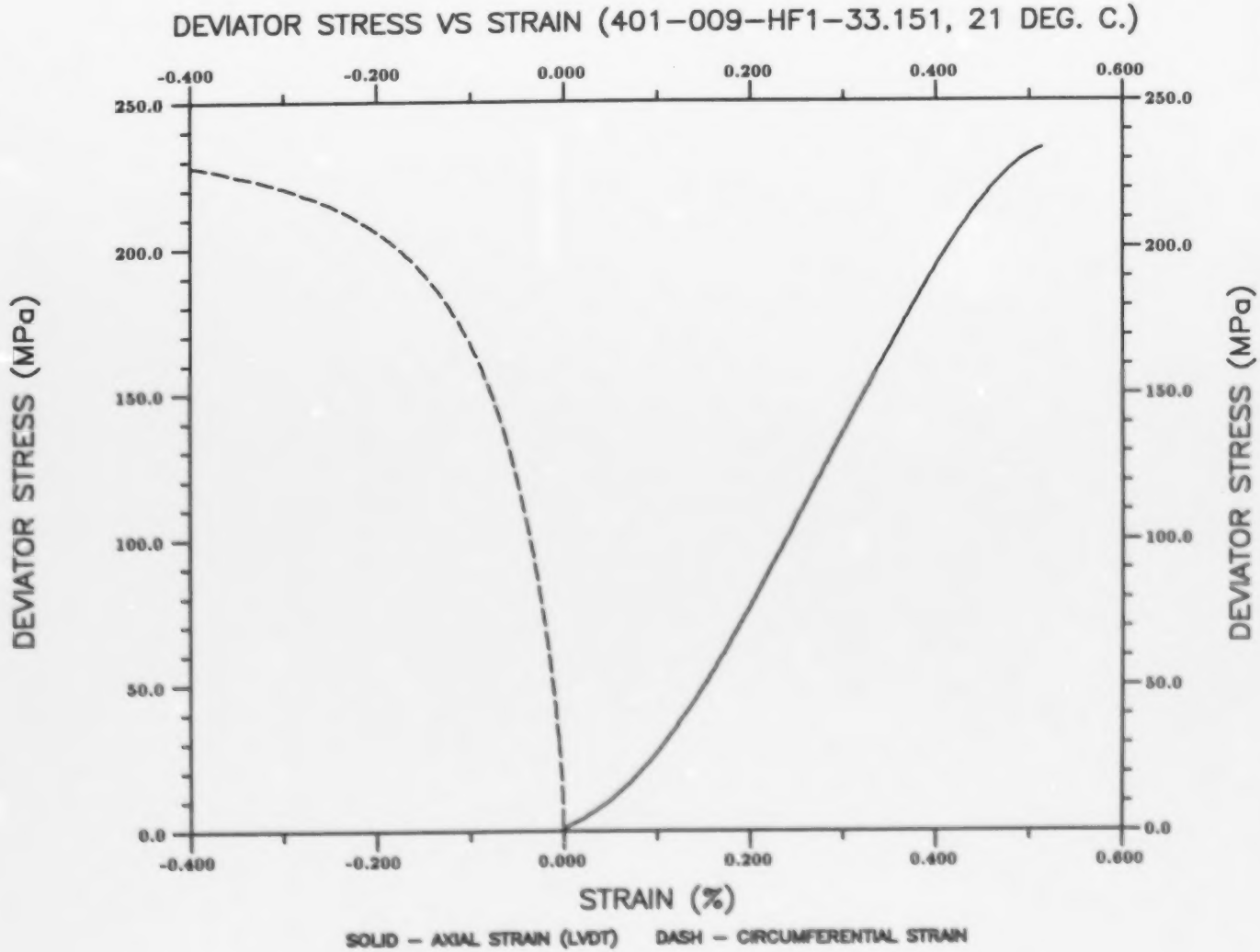

Figure A10. Stress-strain curves for Specimen 401-009-HF1-33.151 tested at 21° C and at $\sigma_3 = 3.5$ MPa.

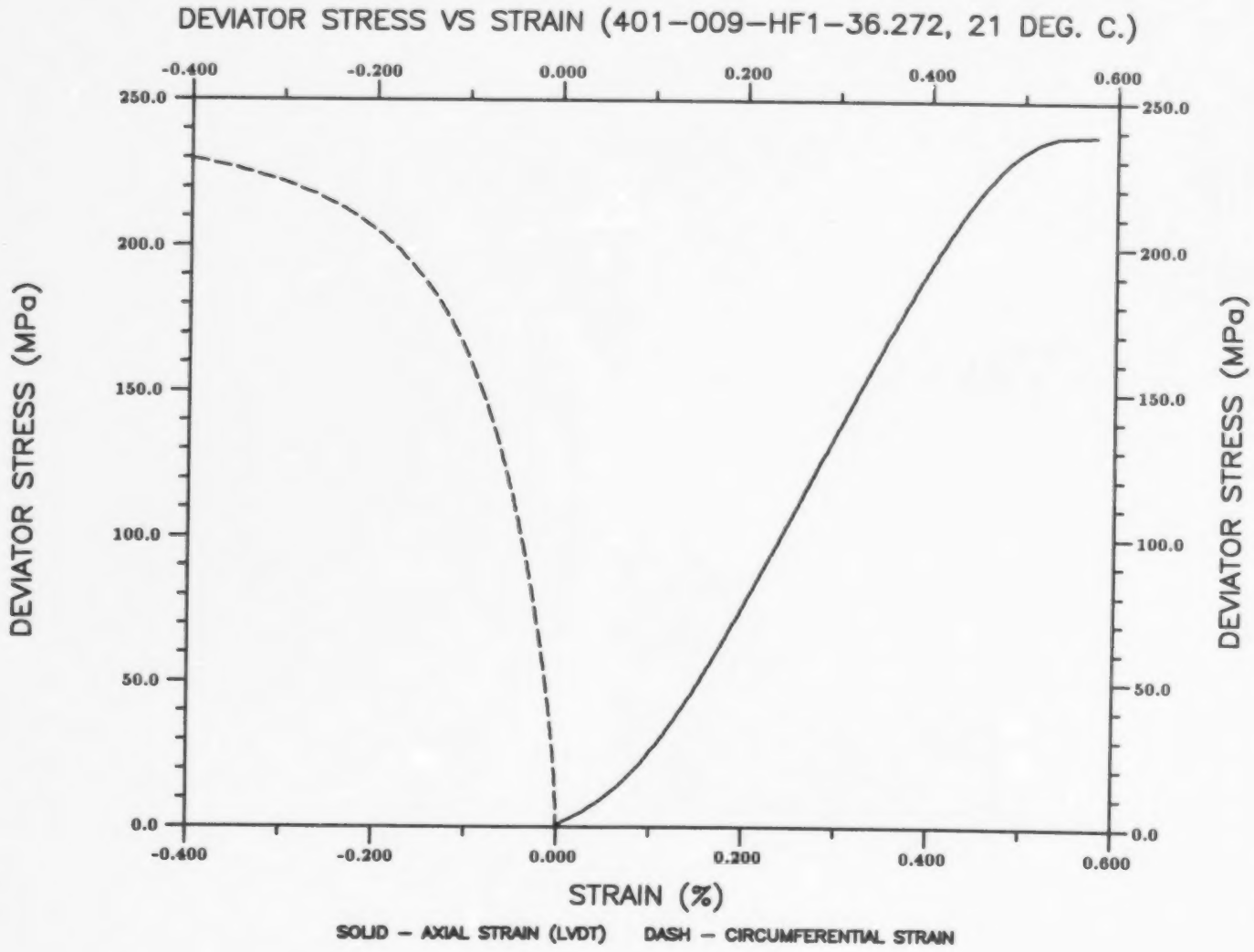

Figure A11. Stress-strain curves for Specimen 401-009-HF1-36.272 tested at 21° C and at $\sigma_3 = 3.5$ MPa.

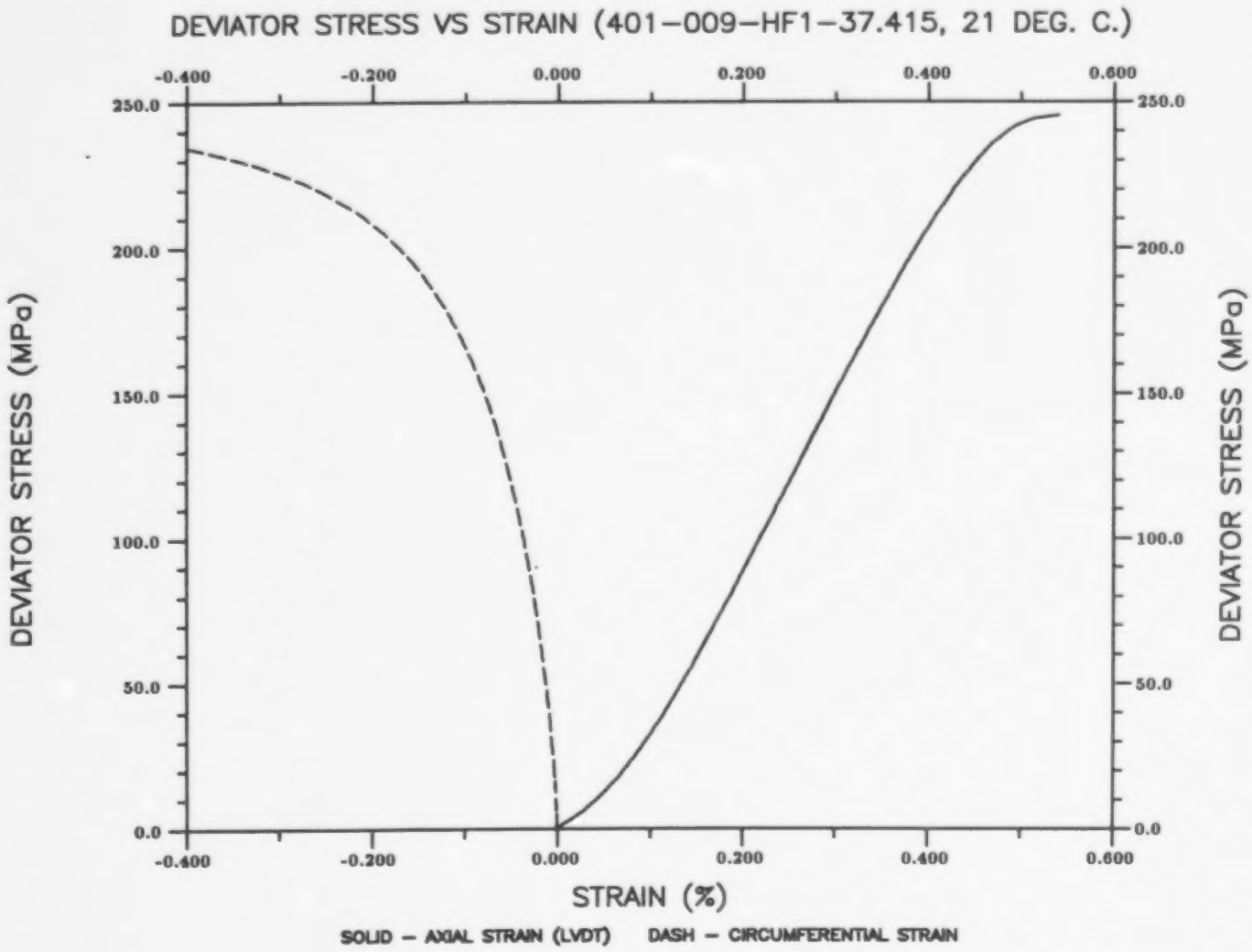

Figure A12. Stress-strain curves for Specimen 401-009-HF1-37.415 tested at 21° C and at $\sigma_3 = 3.5$ MPa.

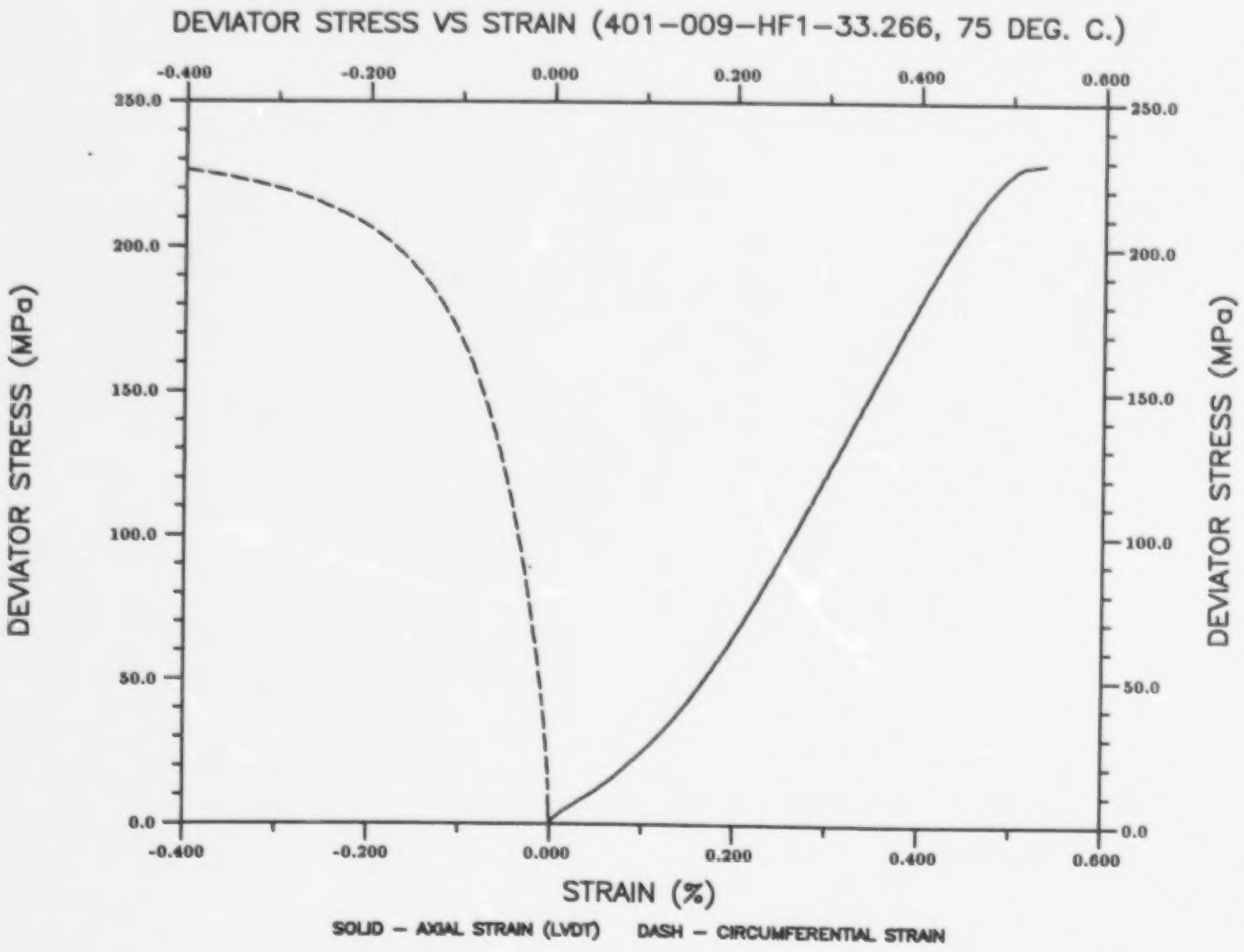

Figure A13. Stress-strain curves for Specimen 401-009-HF1-33.266 tested at 75° C and at $\sigma_3 = 3.5$ MPa.

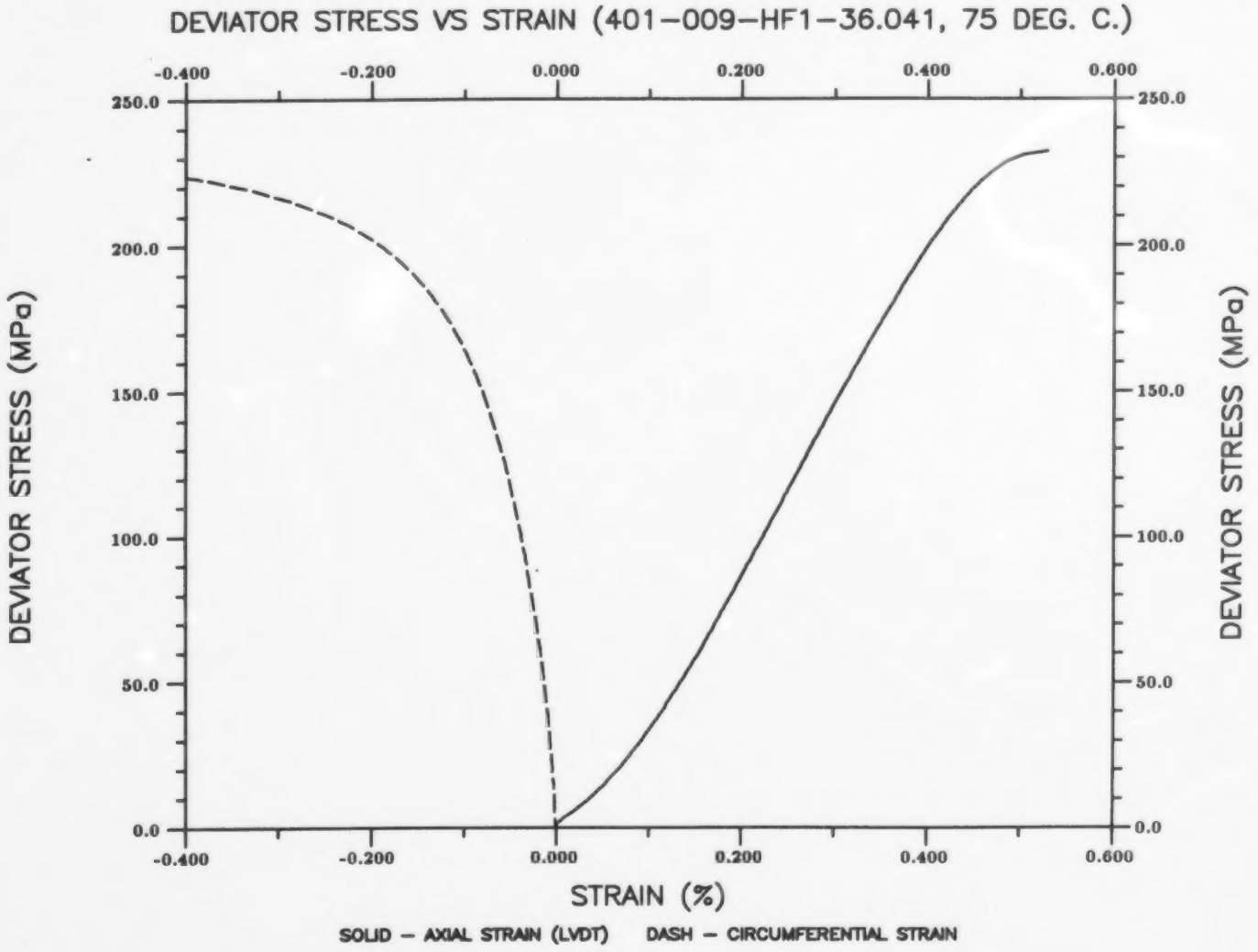

Figure A14. Stress-strain curves for Specimen 401-009-HF1-36.041 tested at 75° C and at $\sigma_3 = 3.5$ MPa.

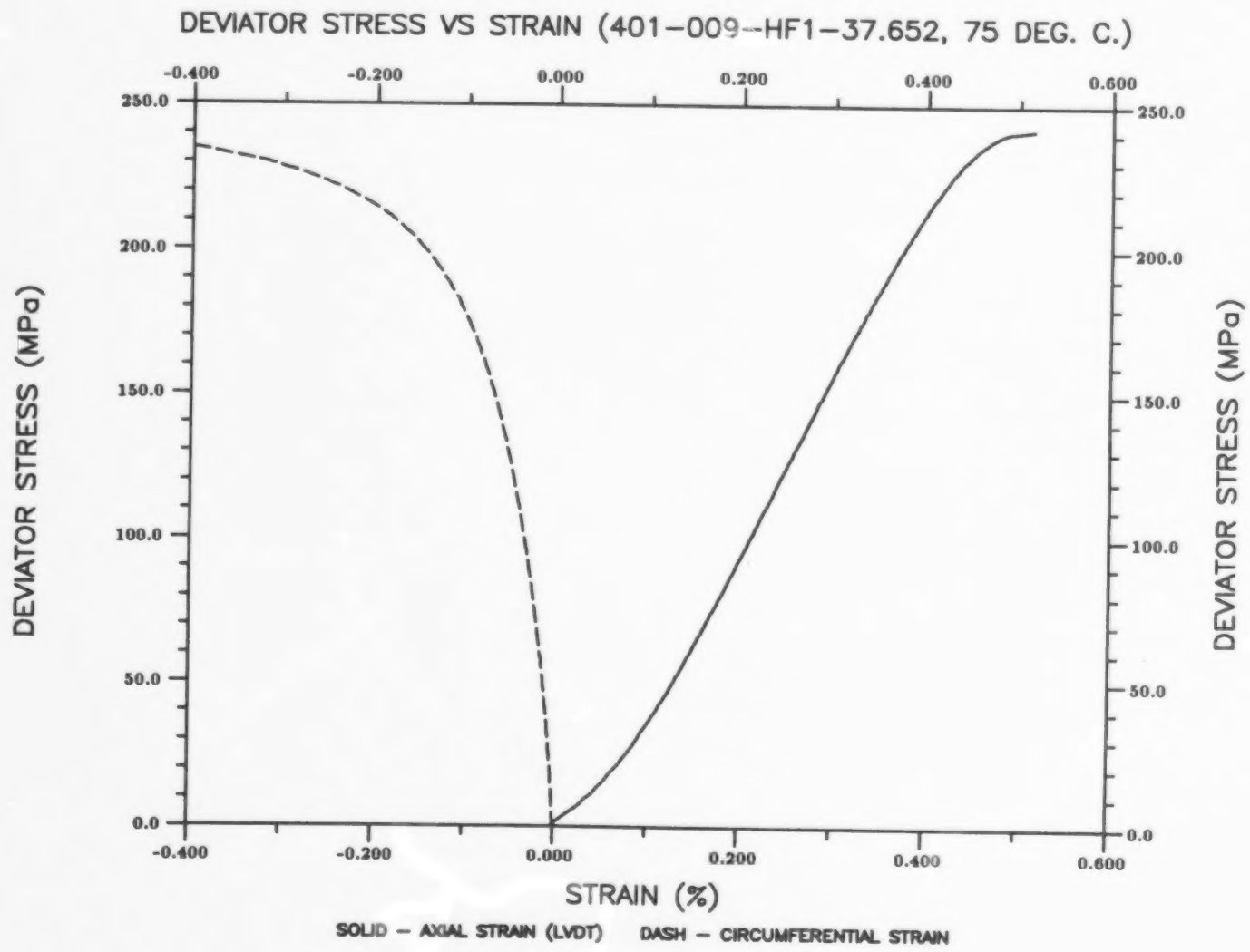

Figure A15. Stress-strain curves for Specimen 401-009-HF1-37.652 tested at 75° C and at $\sigma_3 = 3.5$ MPa.

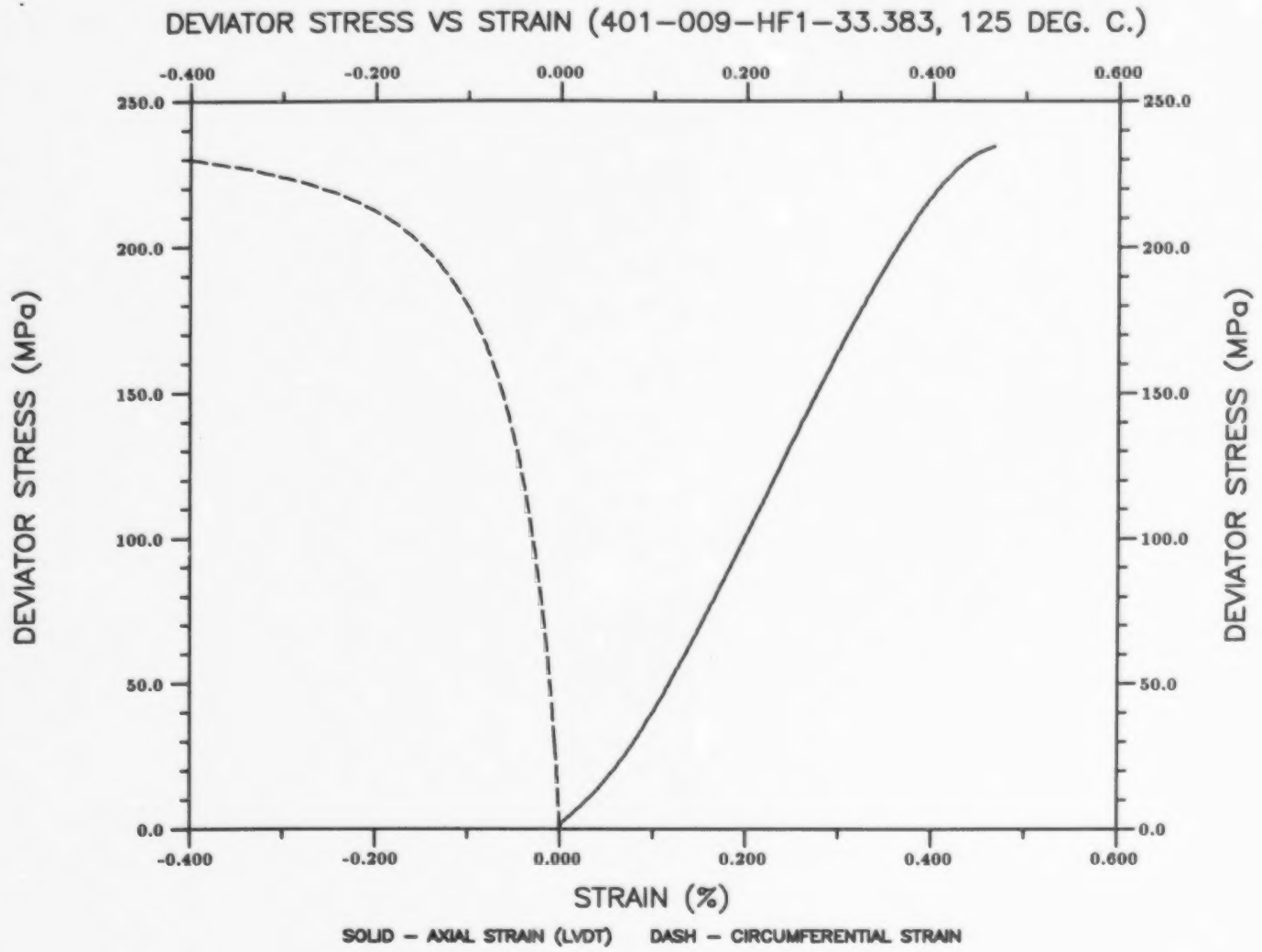

Figure A16. Stress-strain curves for Specimen 401-009-HF1-33.383 tested at 125° C and at $\sigma_3 = 3.5$ MPa.

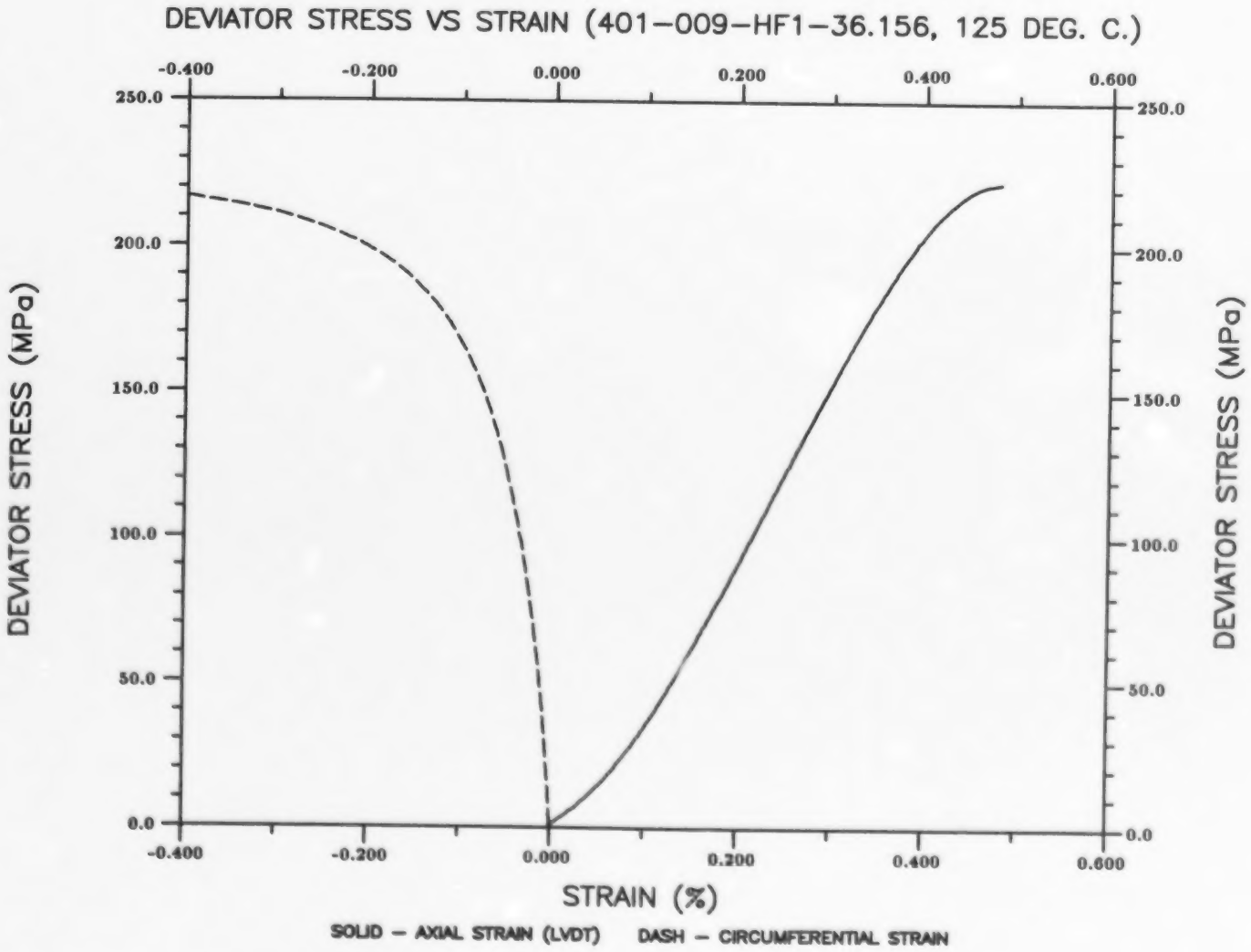

Figure A17. Stress-strain curves for Specimen 401-009-HF1-36.156 tested at 125° C and at $\sigma_3 = 3.5$ MPa.

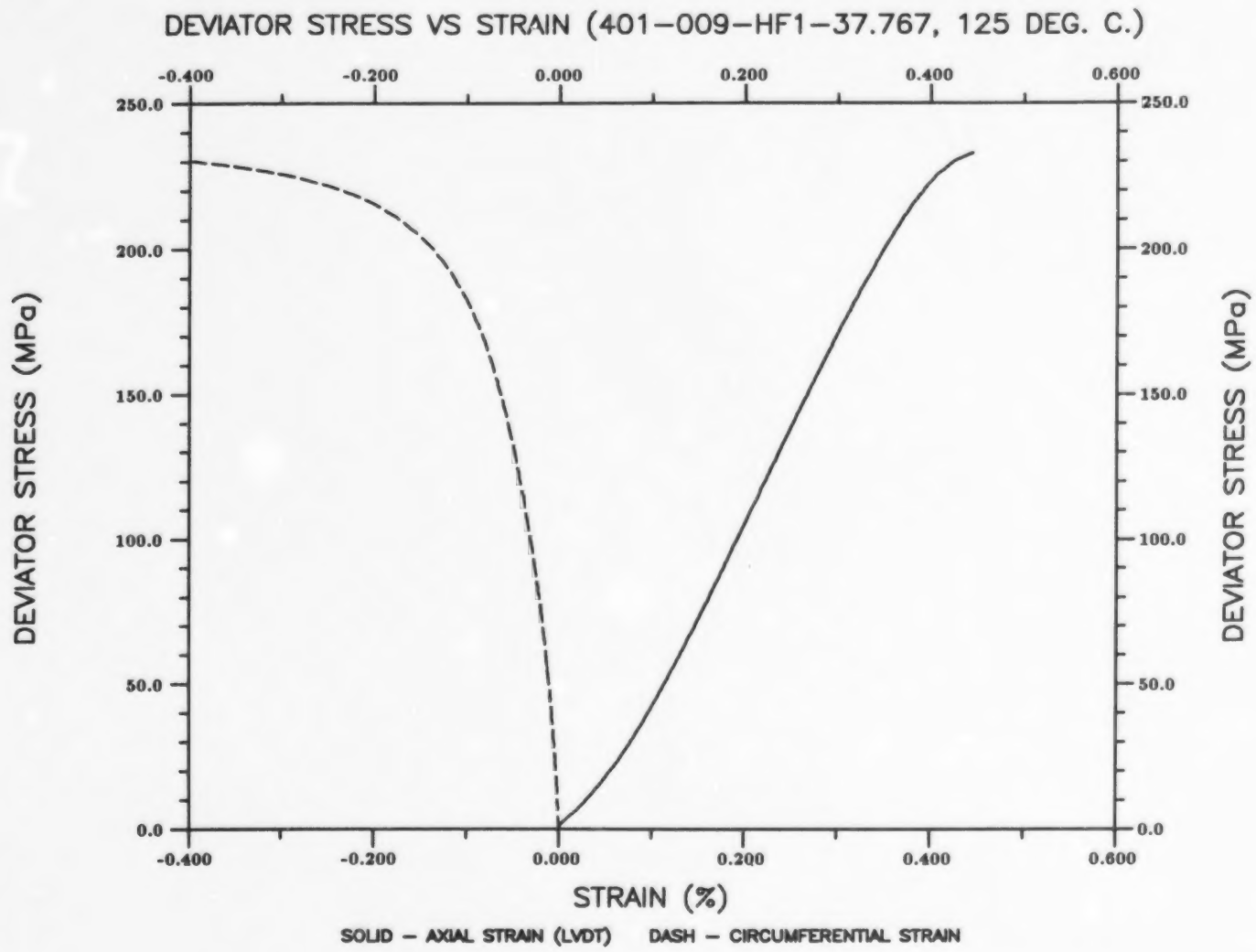

Figure A18. Stress-strain curves for Specimen 401-009-HF1-37.767 tested at 125° C and at $\sigma_3 = 3.5$ MPa.

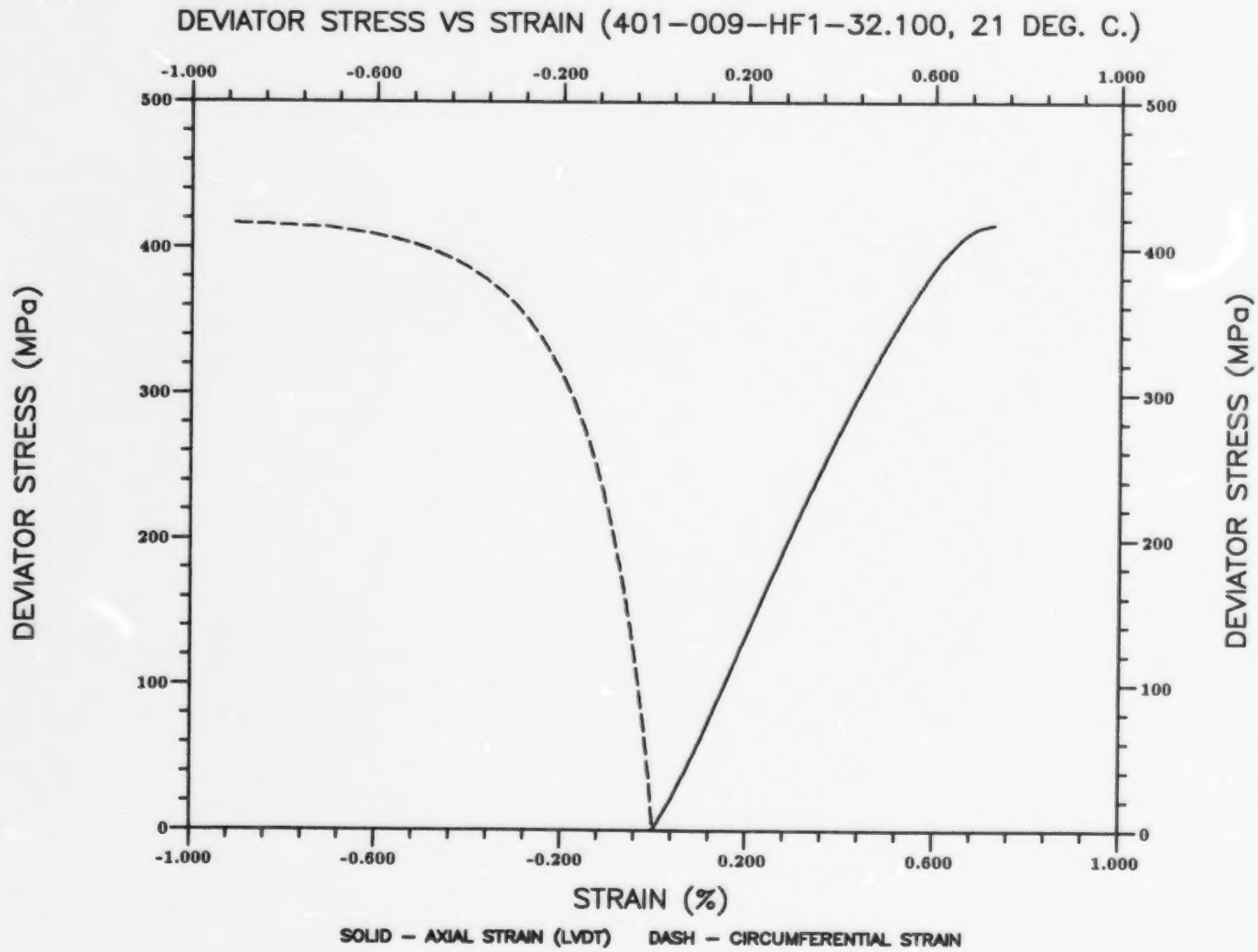

Figure A19. Stress-strain curves for Specimen 401-009-HF1-32.100 tested at 21° C and at $\sigma_3 = 17.0$ MPa.

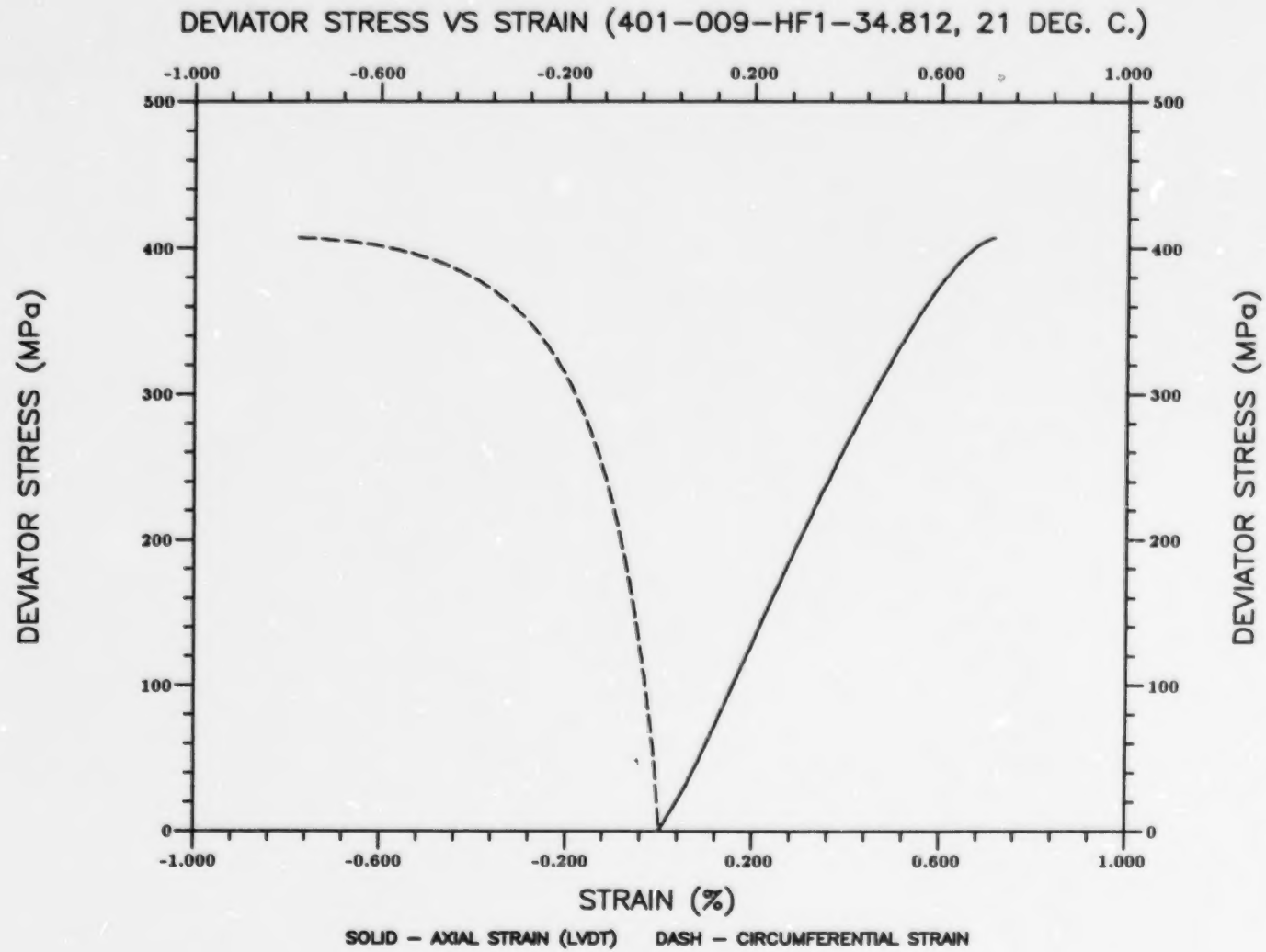

Figure A20. Stress-strain curves for Specimen 401-009-HF1-34.812 tested at 21° C and at $\sigma_3 = 17.0$ MPa.

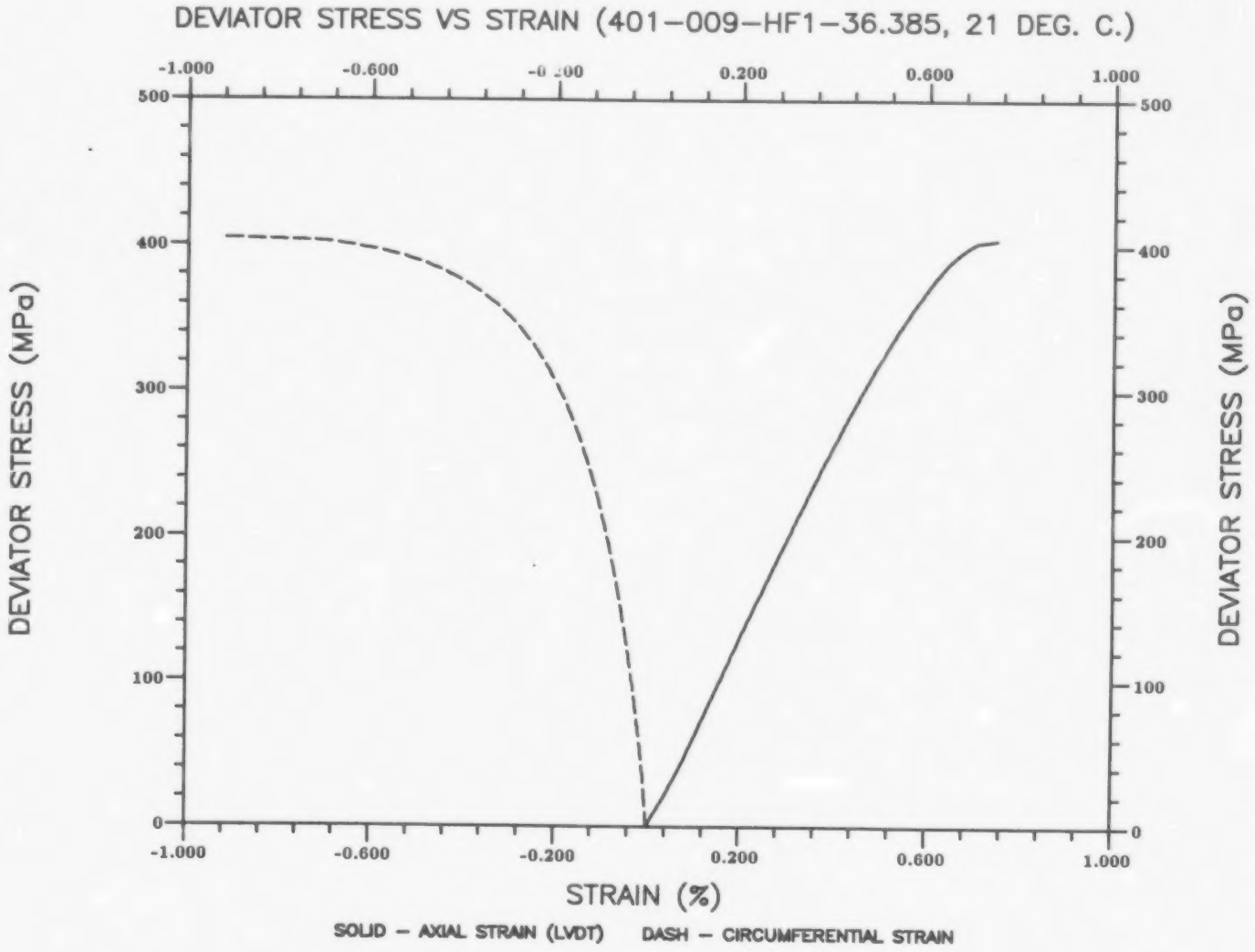

Figure A21. Stress-strain curves for Specimen 401-009-HF1-36.385 tested at 21° C and at $\sigma_3 = 17.0$ MPa.

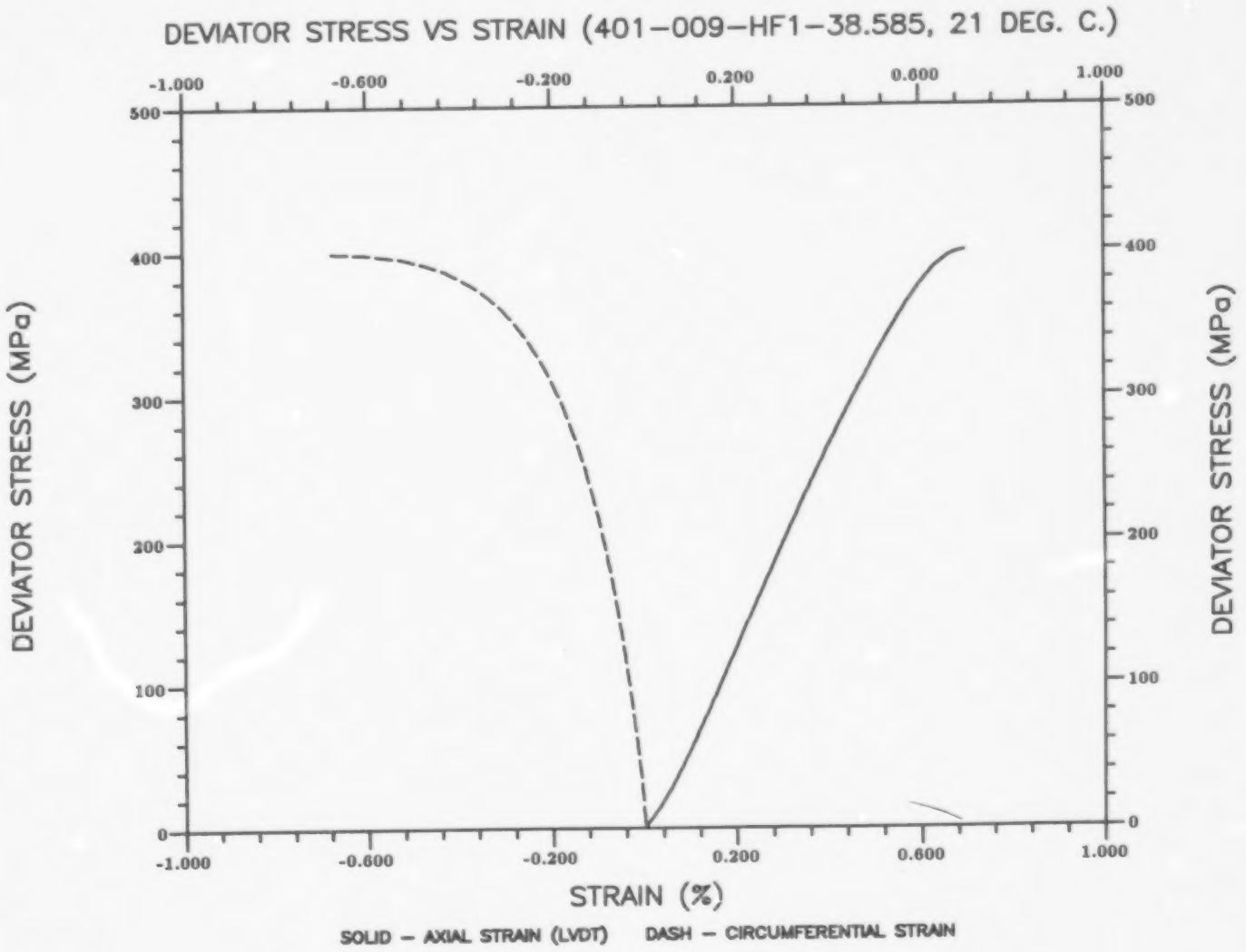

Figure A22. Stress-strain curves for Specimen 401-009-HF1-38.585 tested at 21° C and at $\sigma_3 = 17.0$ MPa.

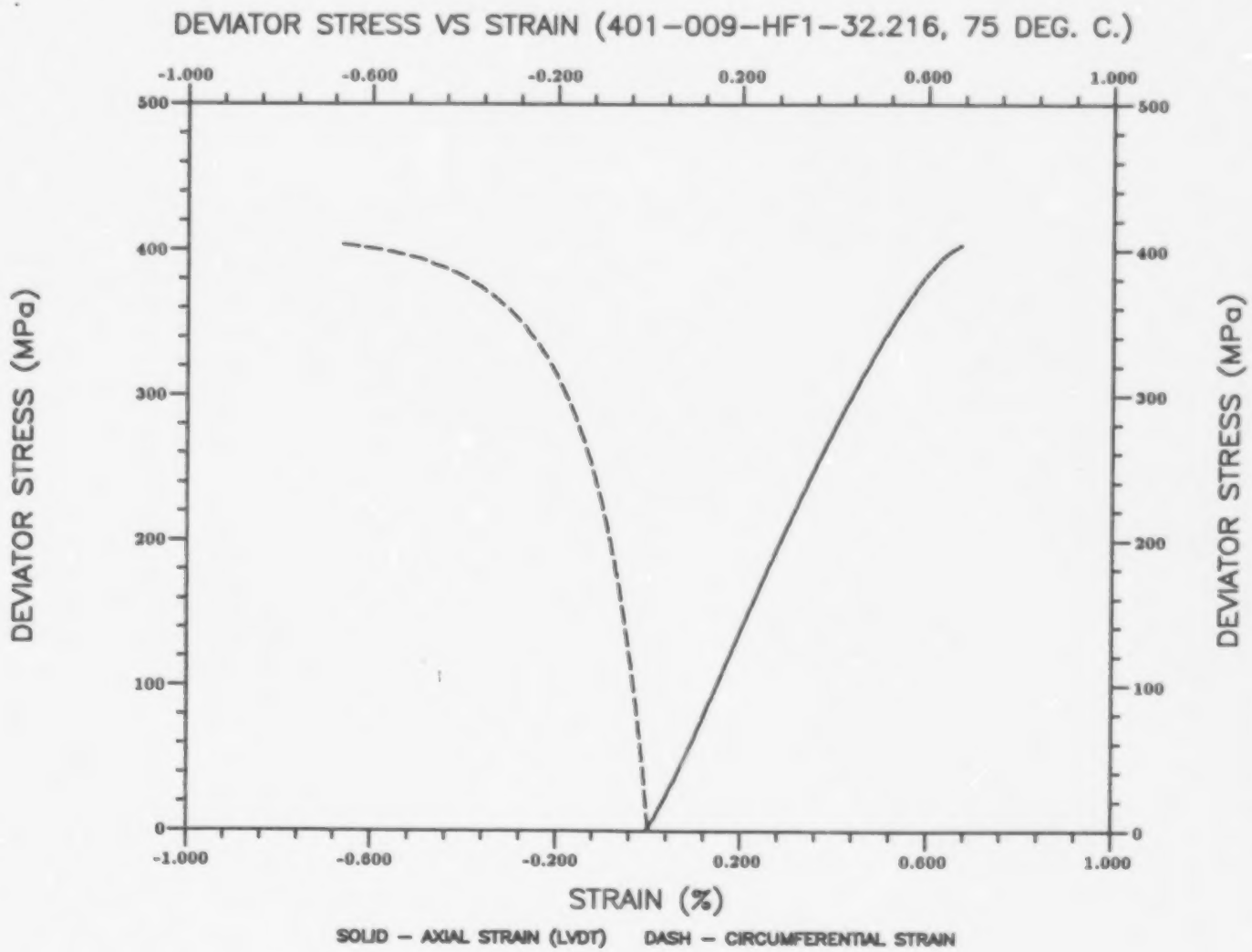

Figure A23. Stress-strain curves for Specimen 401-009-HF1-32.216 tested at 75° C and at $\sigma_3 = 17.0$ MPa.

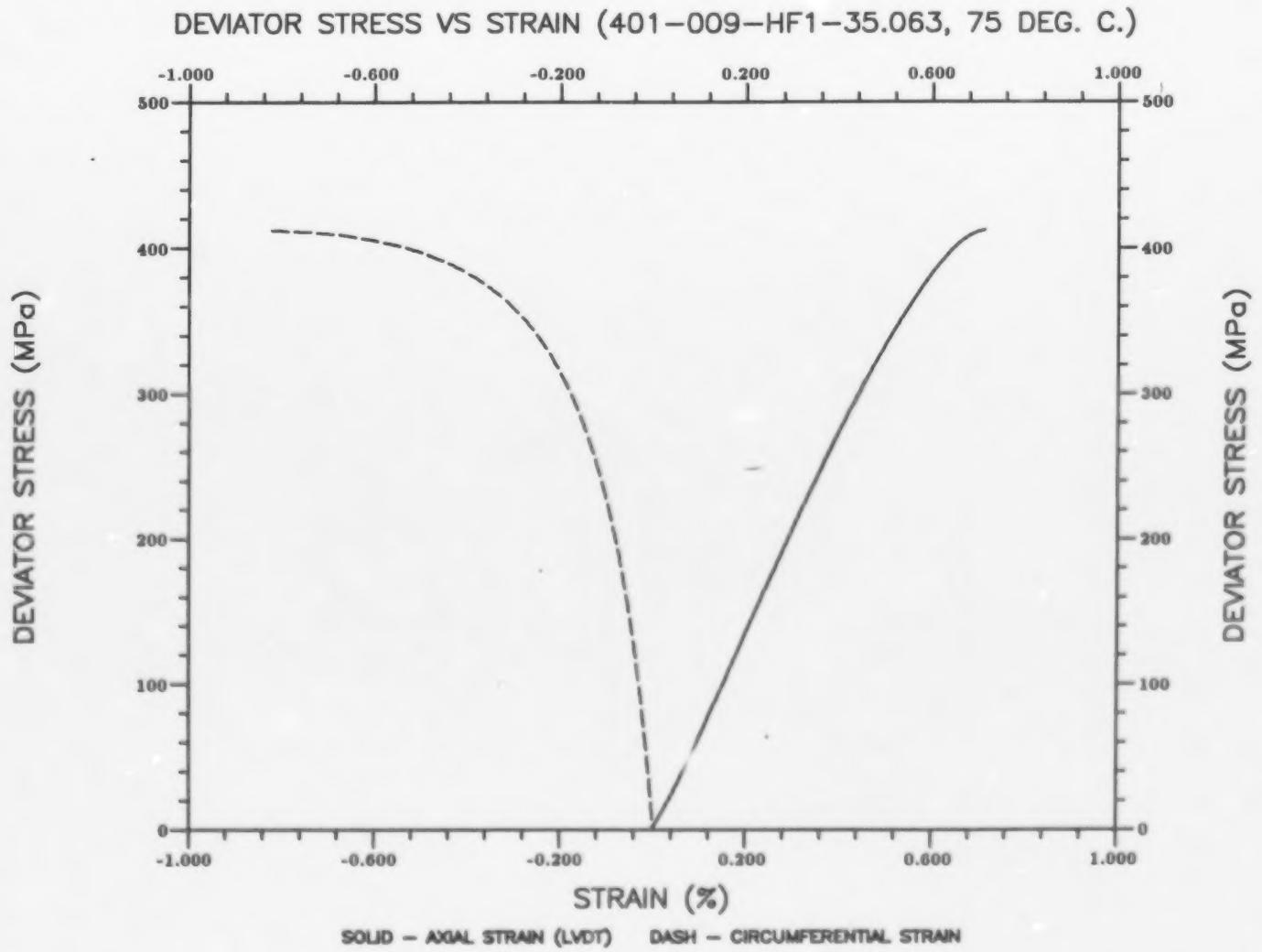

Figure A24. Stress-strain curves for Specimen 401-009-HF1-35.063 tested at 75° C and at $\sigma_3 = 17.0$ MPa.

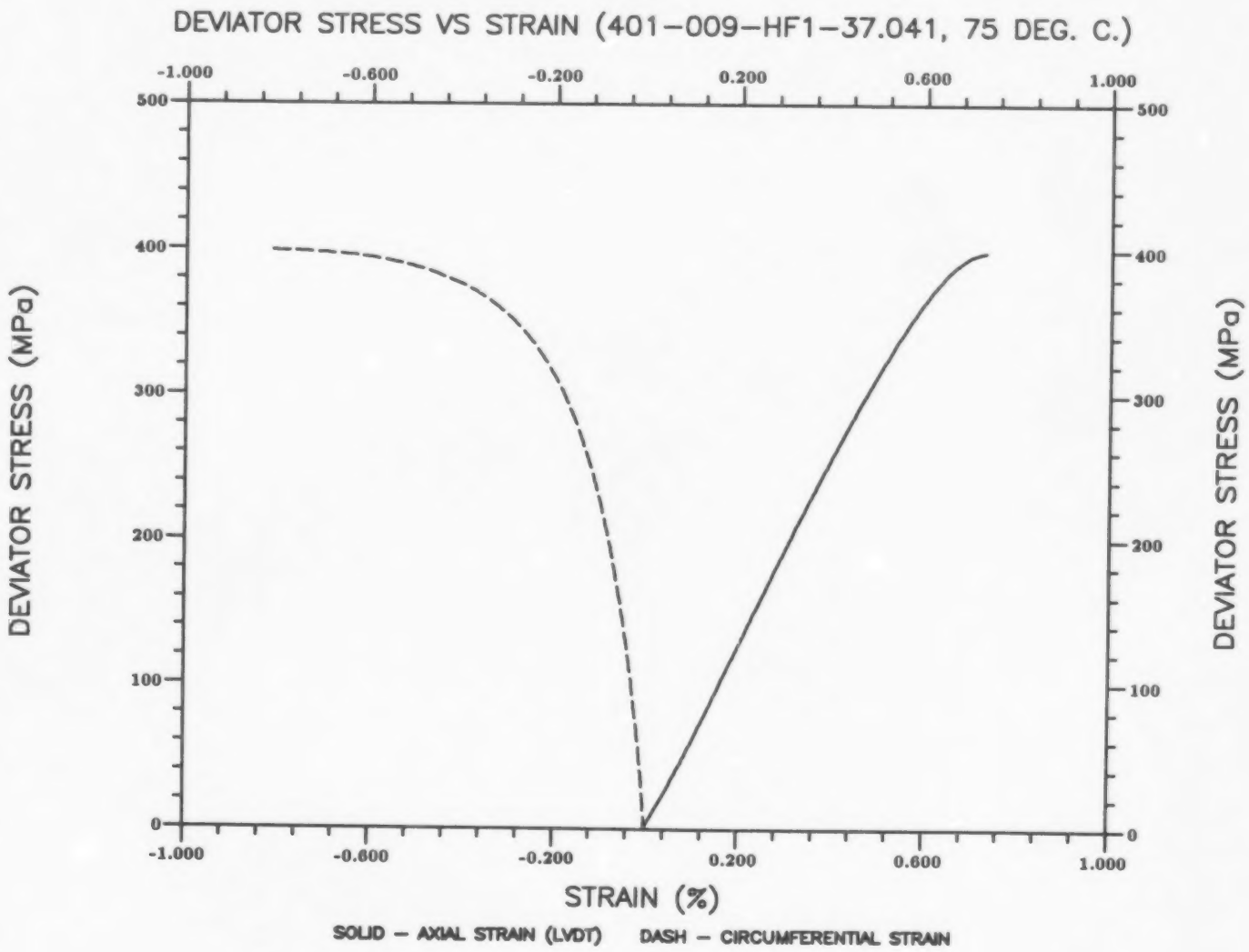

Figure A25. Stress-strain curves for Specimen 401-009-HF1-37.041 tested at 75° C and at $\sigma_3 = 17.0$ MPa.

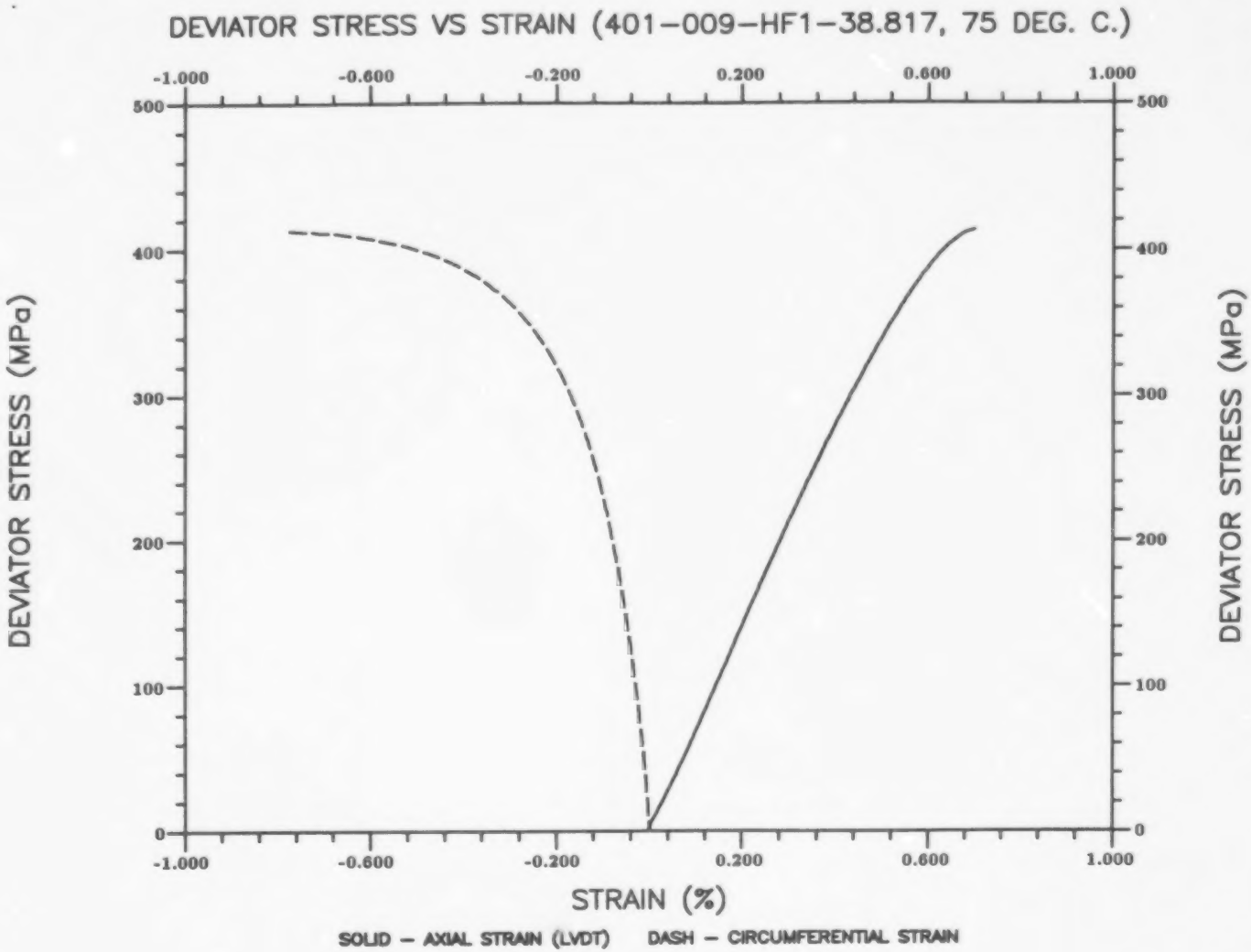

Figure A26. Stress-strain curves for Specimen 401-009-HF1-38.817 tested at 75° C and at $\sigma_3 = 17.0$ MPa.

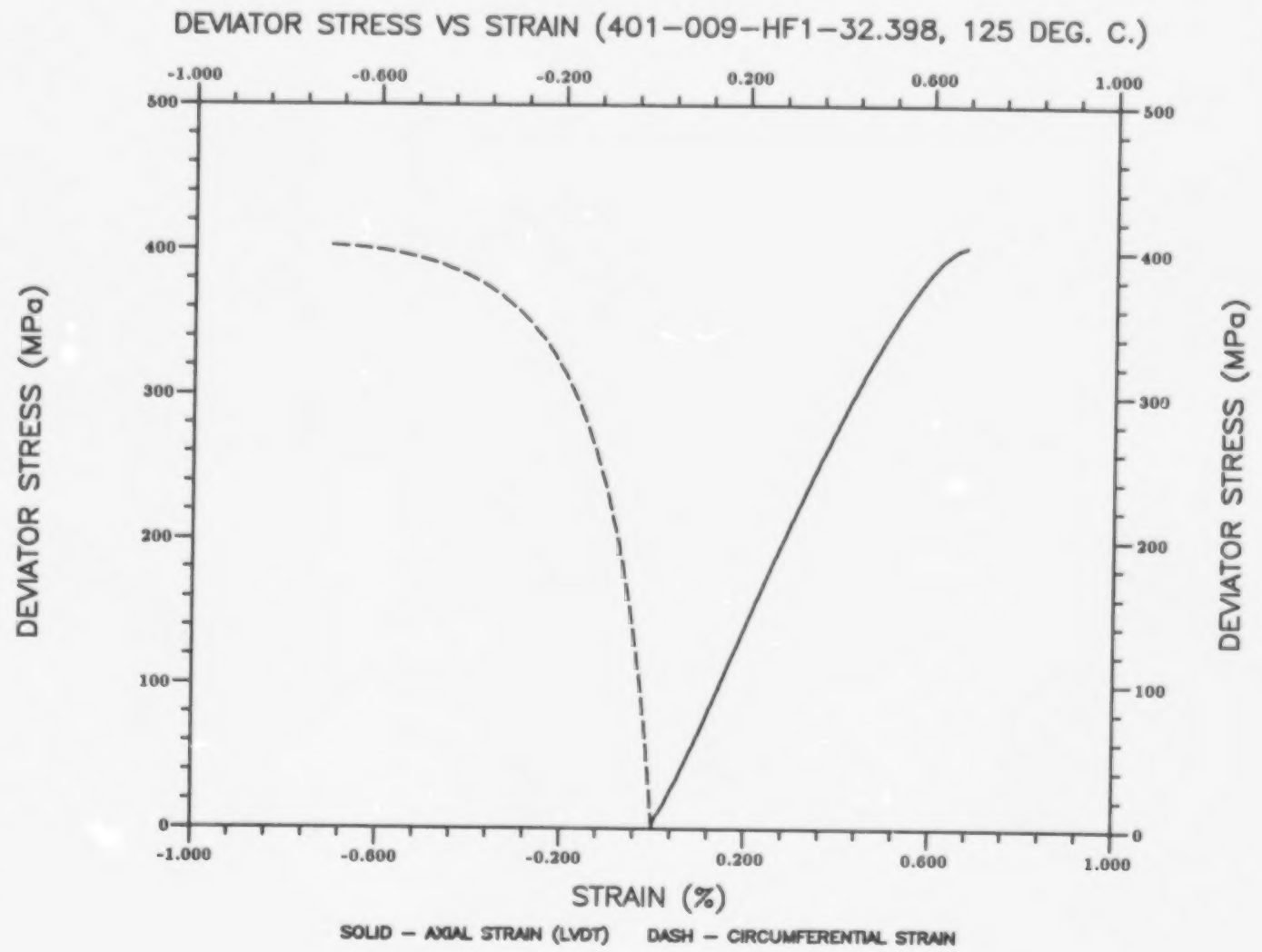

Figure A27. Stress-strain curves for Specimen 401-009-HF1-32.398 tested at 125° C and at $\sigma_3 = 17.0$ MPa.

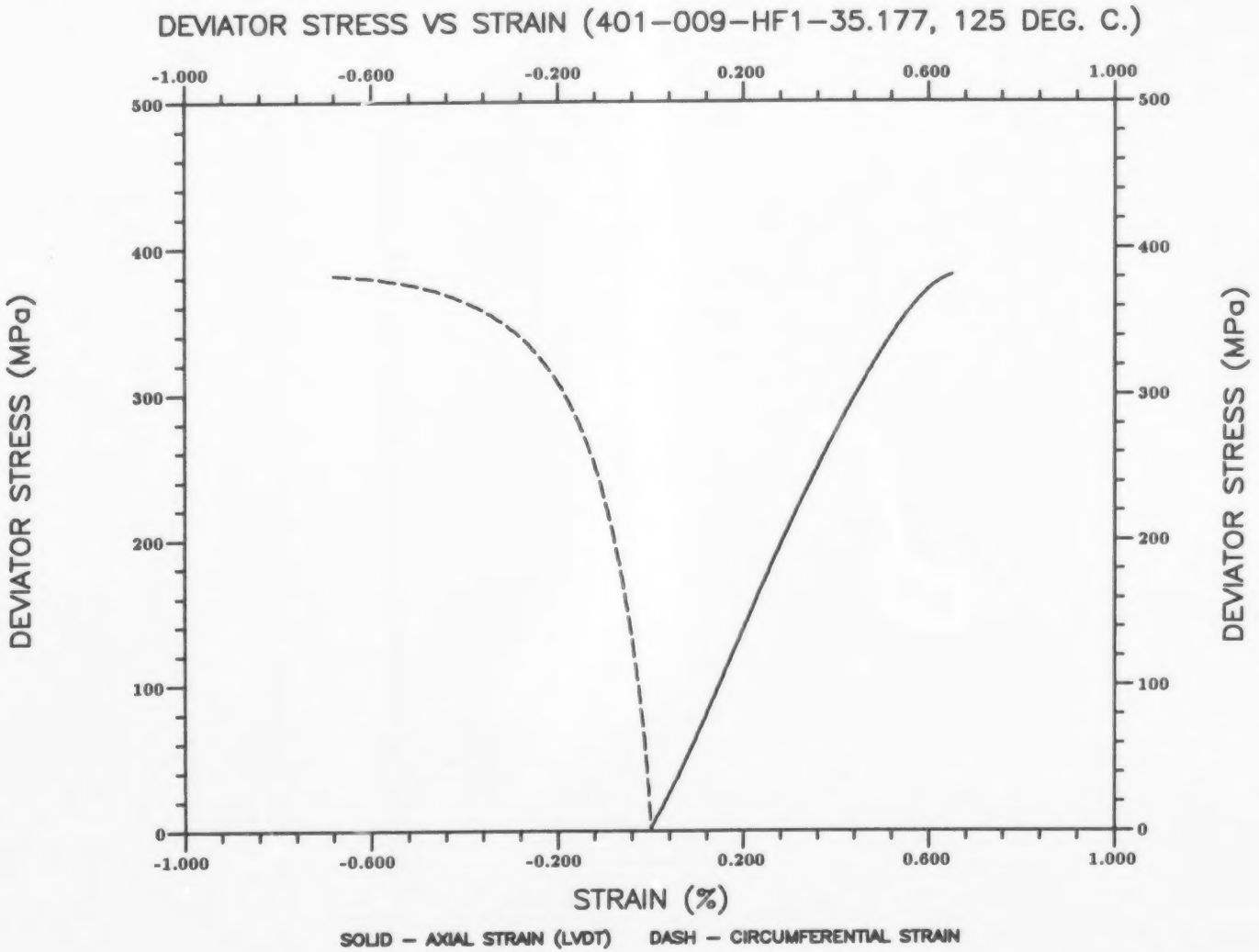

Figure A28. Stress-strain curves for Specimen 401-009-HF1-35.177 tested at 125° C and at $\sigma_3 = 17.0$ MPa.

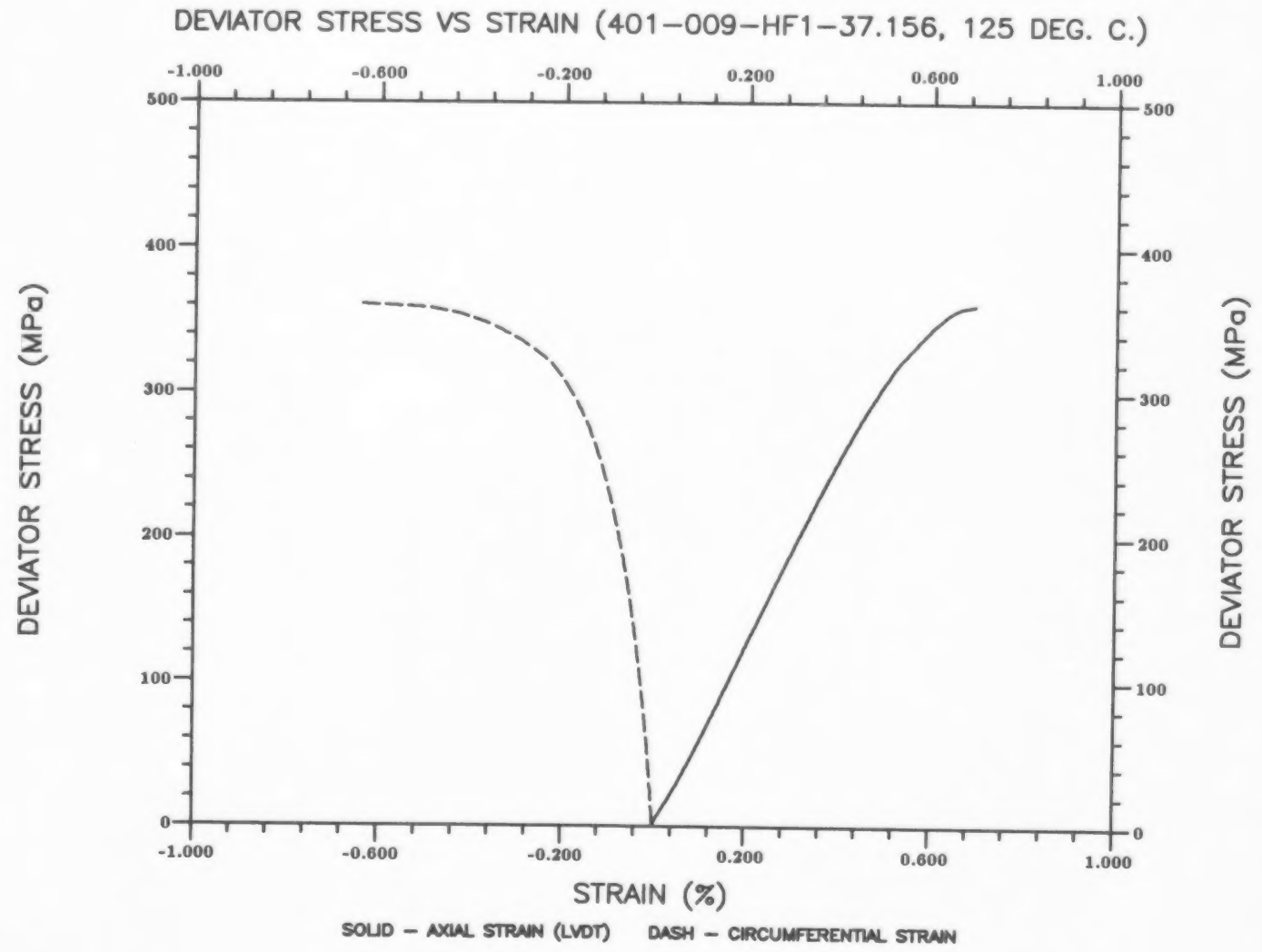

Figure A29. Stress-strain curves for Specimen 401-009-HF1-37.156 tested at 125° C and at $\sigma_3 = 17.0$ MPa.

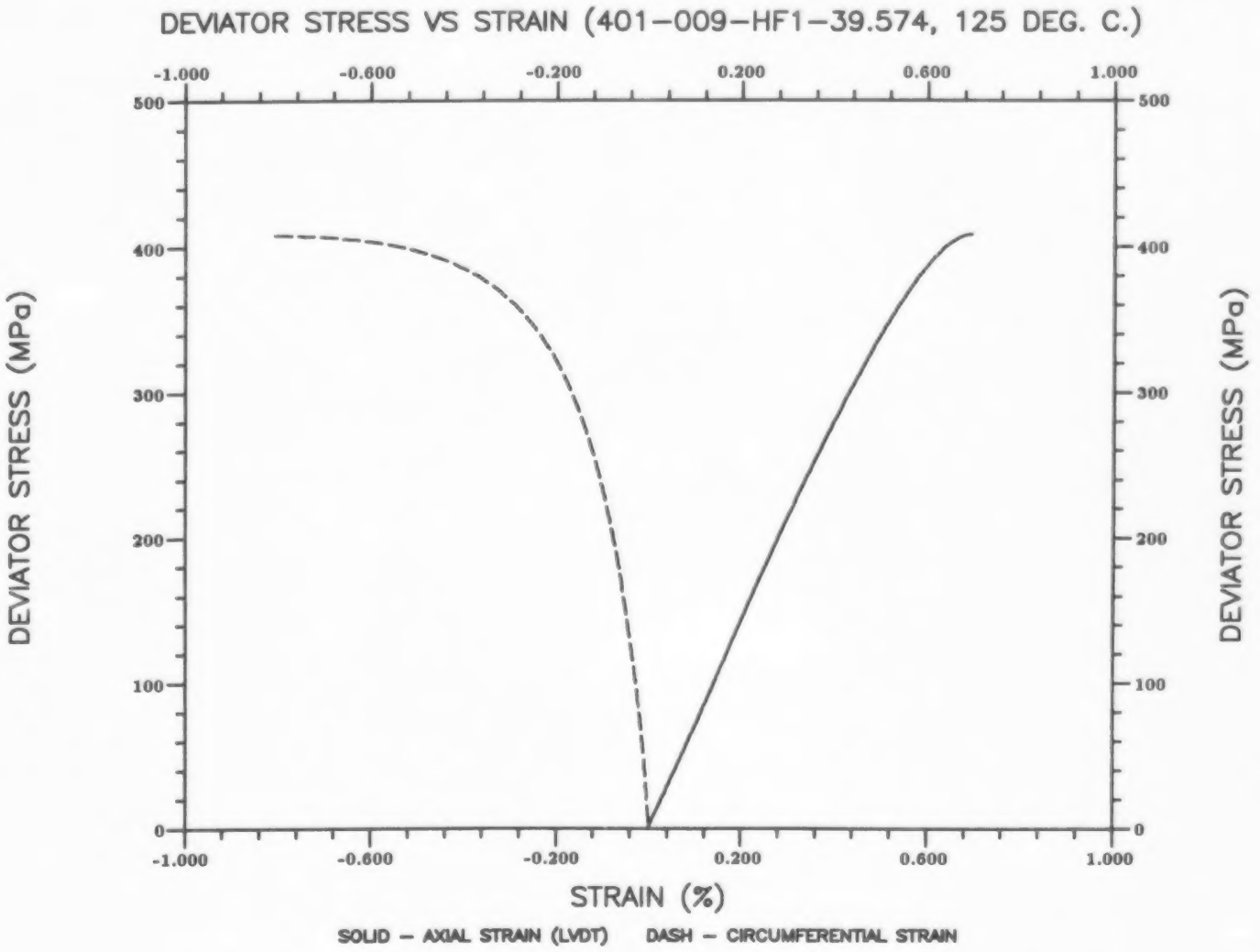

Figure A30. Stress-strain curves for Specimen 401-009-HF1-39.574 tested at 125° C and at $\sigma_3 = 17.0$ MPa.

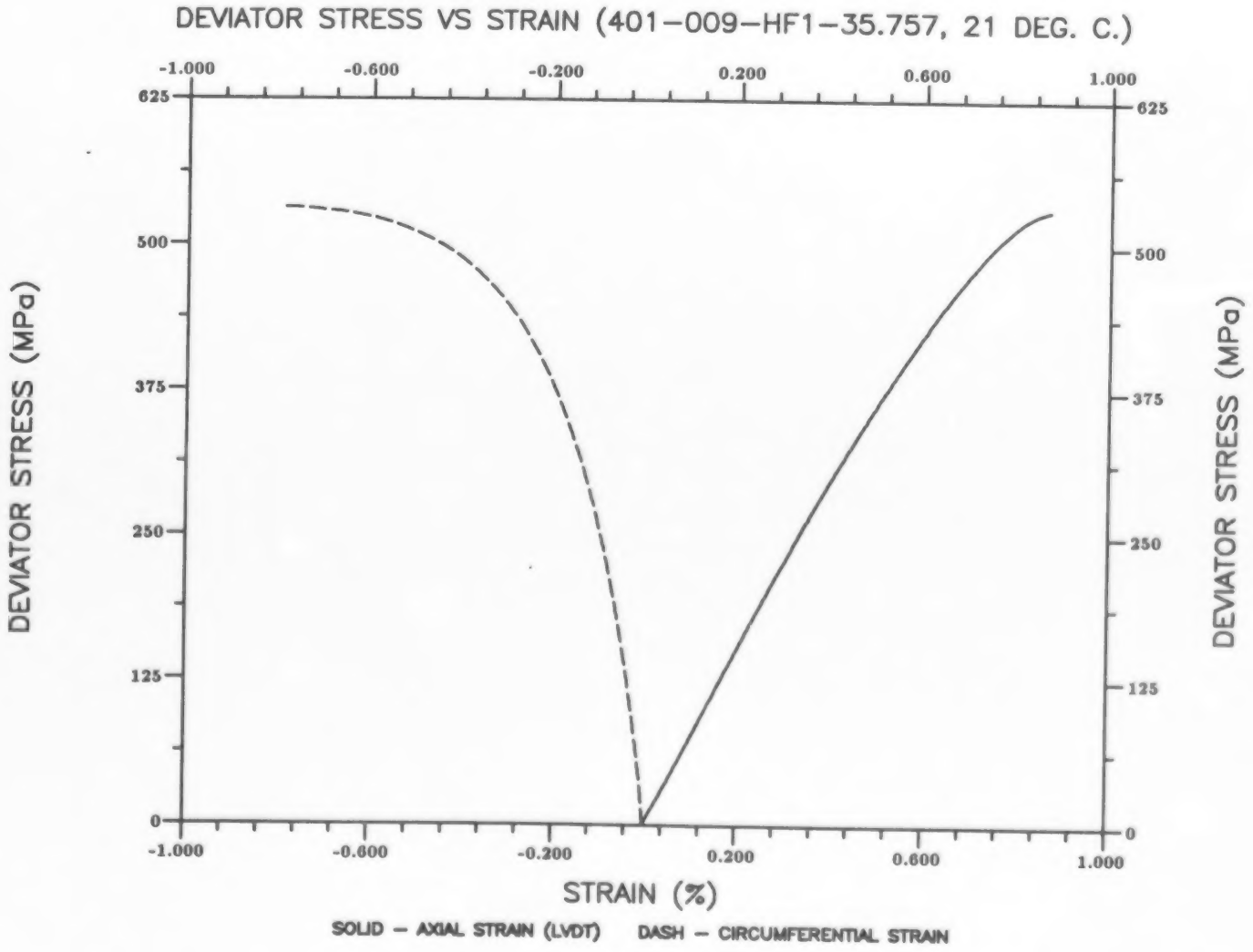

Figure A31. Stress-strain curves for Specimen 401-009-HF1-35.757 tested at 21° C and at $\sigma_3 = 35.0$ MPa.

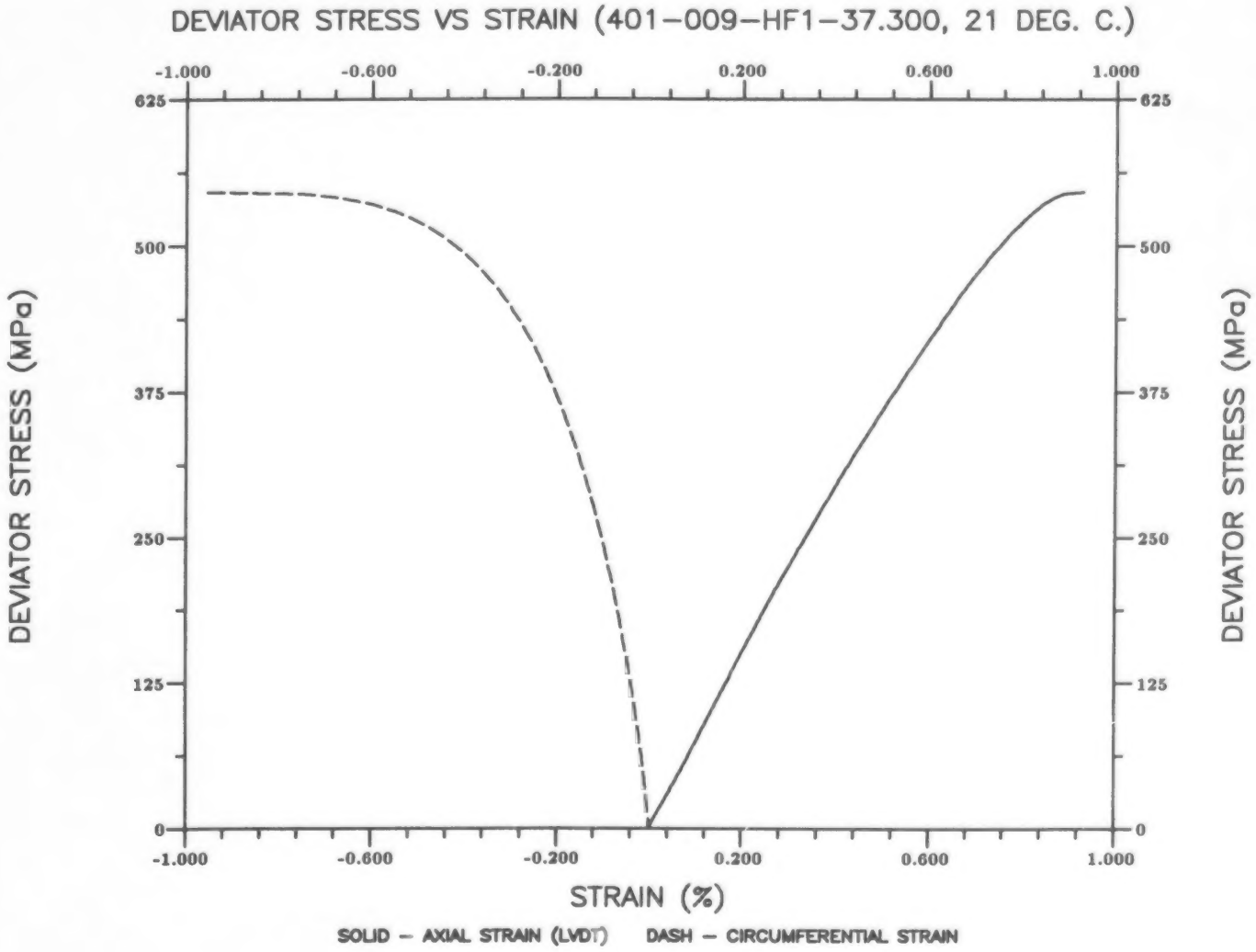

Figure A32. Stress-strain curves for Specimen 401-009-HF1-37.300 tested at 21° C and at $\sigma_3 = 35.0$ MPa.

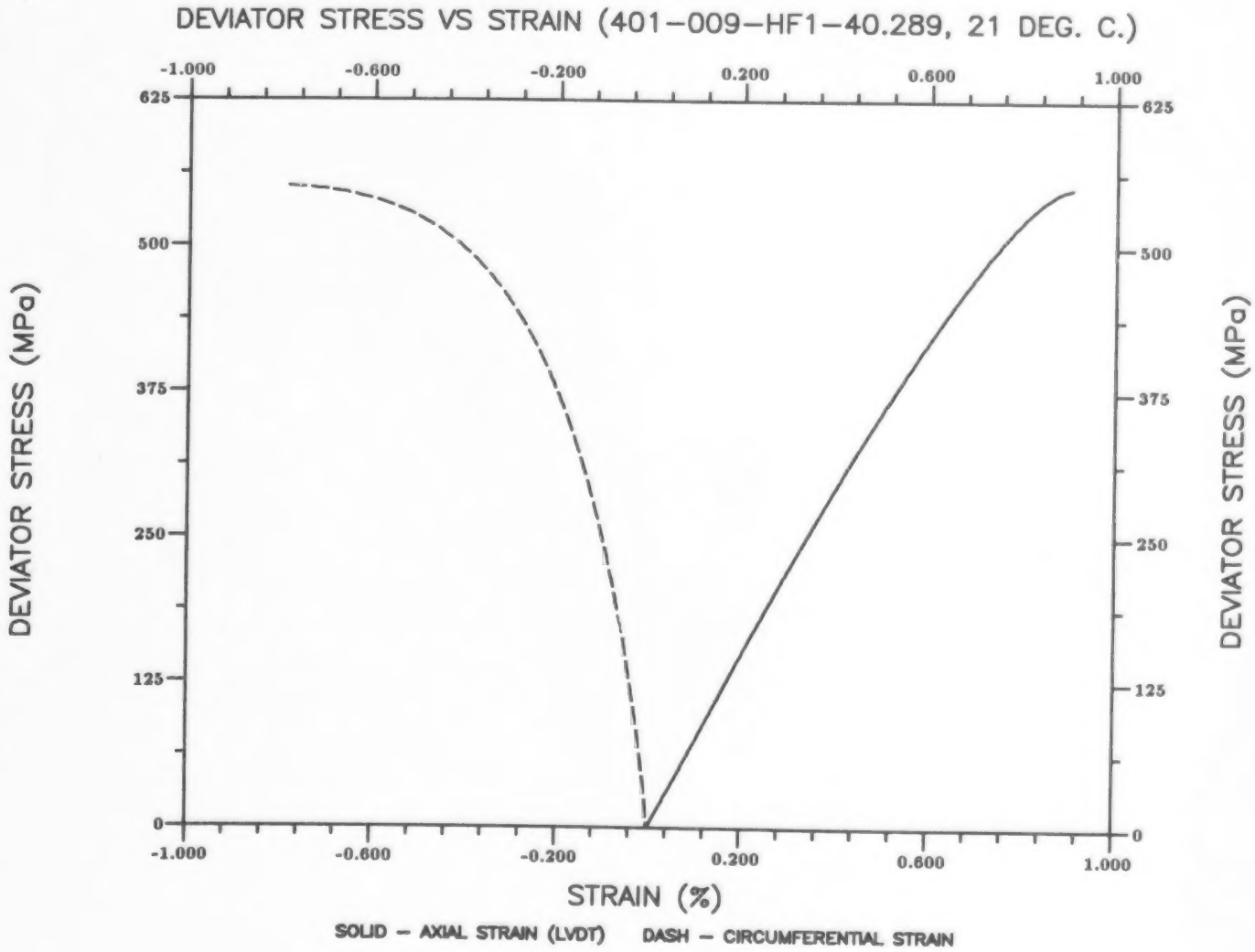

Figure A33. Stress-strain curves for Specimen 401-009-HF1-40.289 tested at 21° C and at $\sigma_3 = 35.0$ MPa.

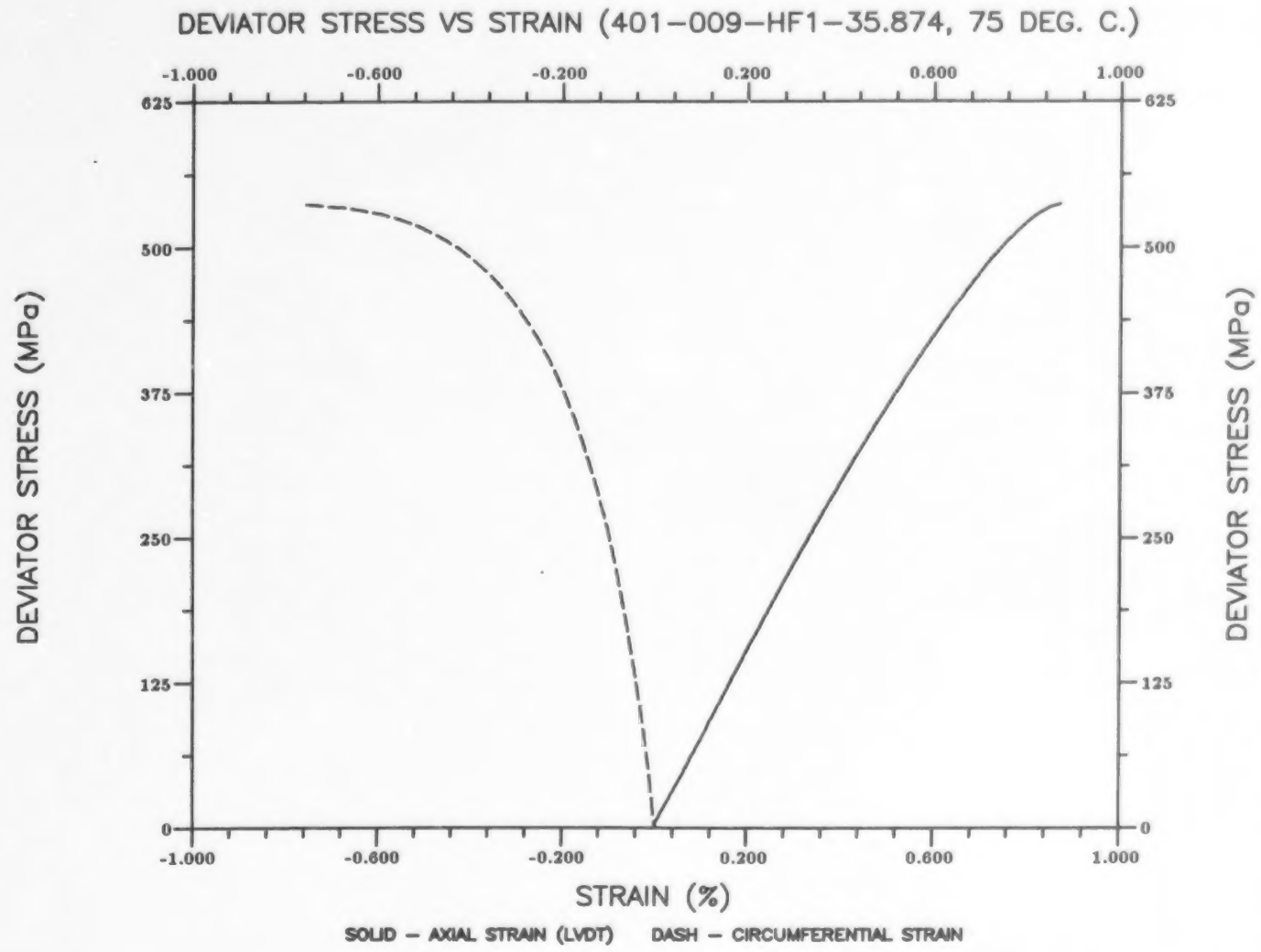

Figure A34. Stress-strain curves for Specimen 401-009-HF1-35.874 tested at 75° C and at $\sigma_3 = 35.0$ MPa.

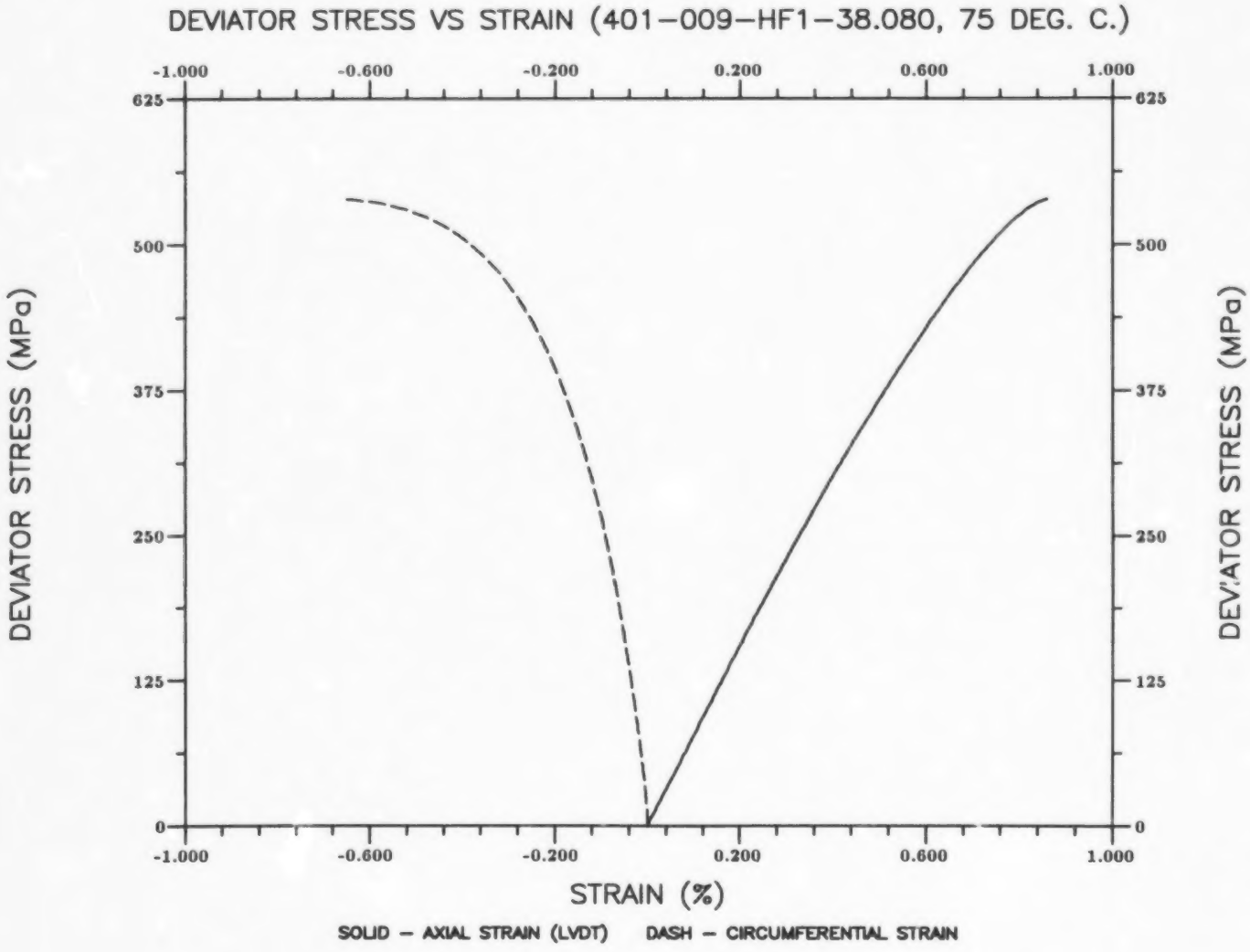

Figure A35. Stress-strain curves for Specimen 401-009-HF1-38.080 tested at 75° C and at $\sigma_3 = 35.0$ MPa.

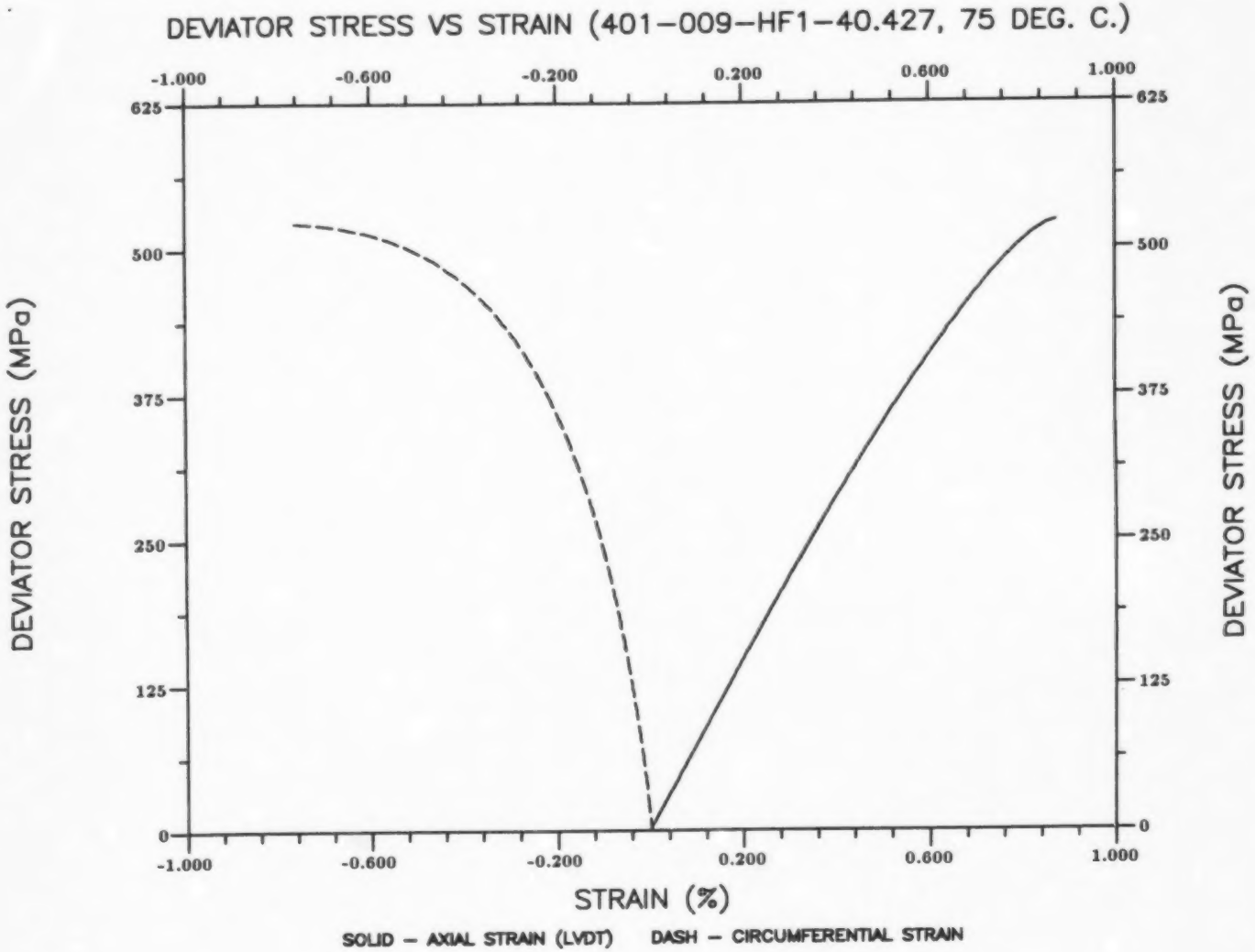

Figure A36. Stress-strain curves for Specimen 401-009-HF1-40.427 tested at 75° C and at $\sigma_3 = 35.0$ MPa.

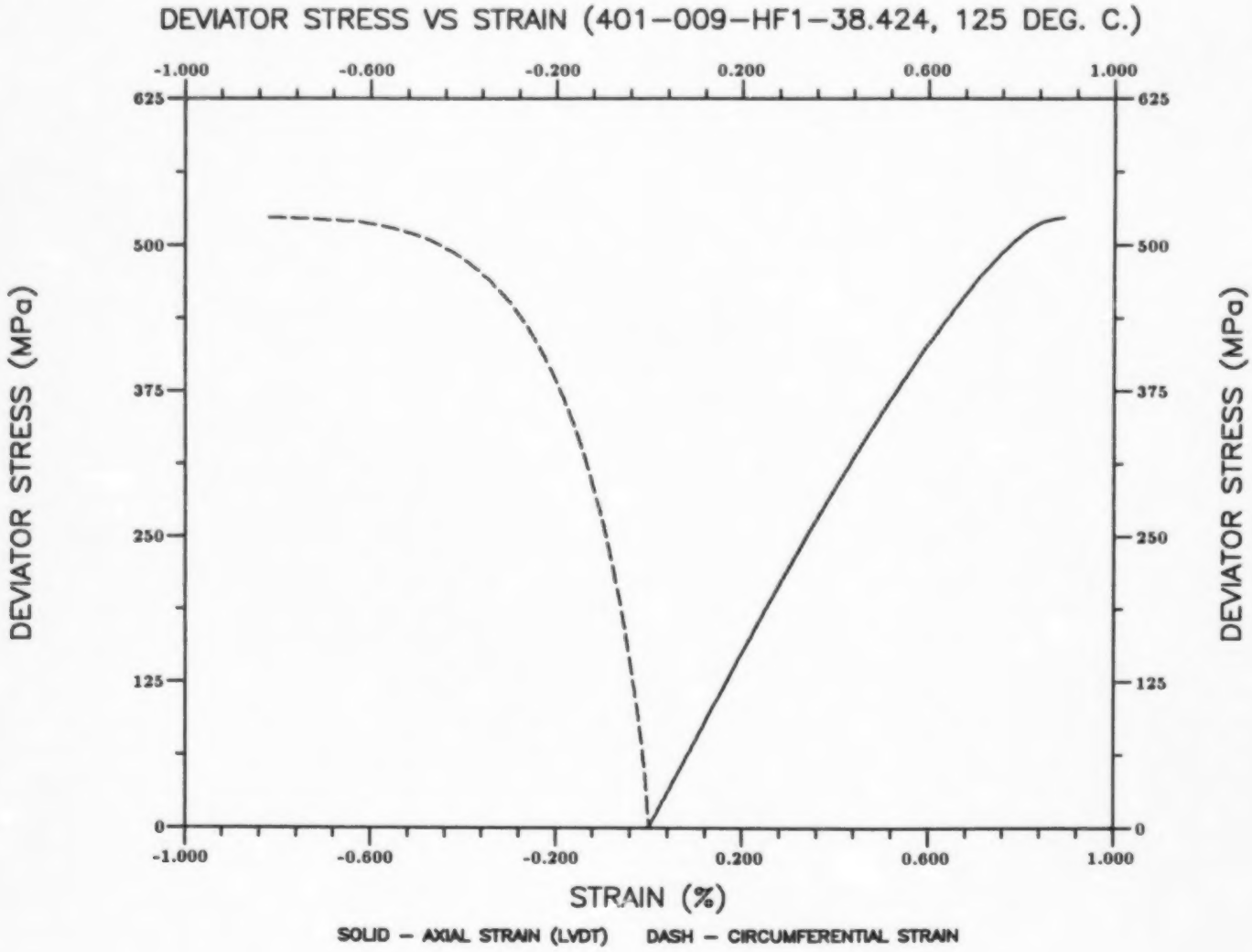

Figure A37. Stress-strain curves for Specimen 401-009-HF1-38.424 tested at 125° C and at σ_3 = 35.0 MPa.

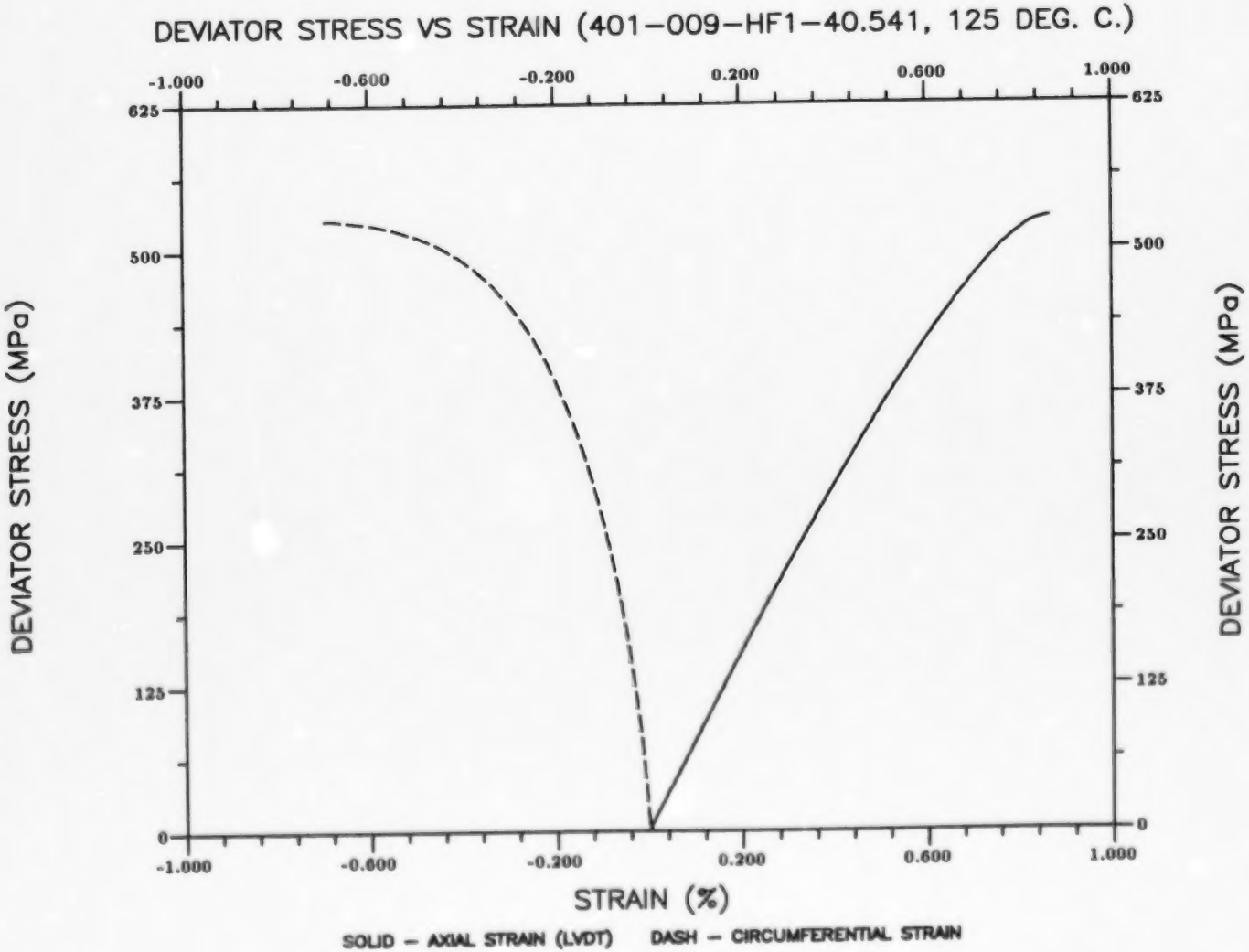

Figure A38. Stress-strain curves for Specimen 401-009-HF1-40.541 tested at 125° C and at $\sigma_3 = 35.0$ MPa.

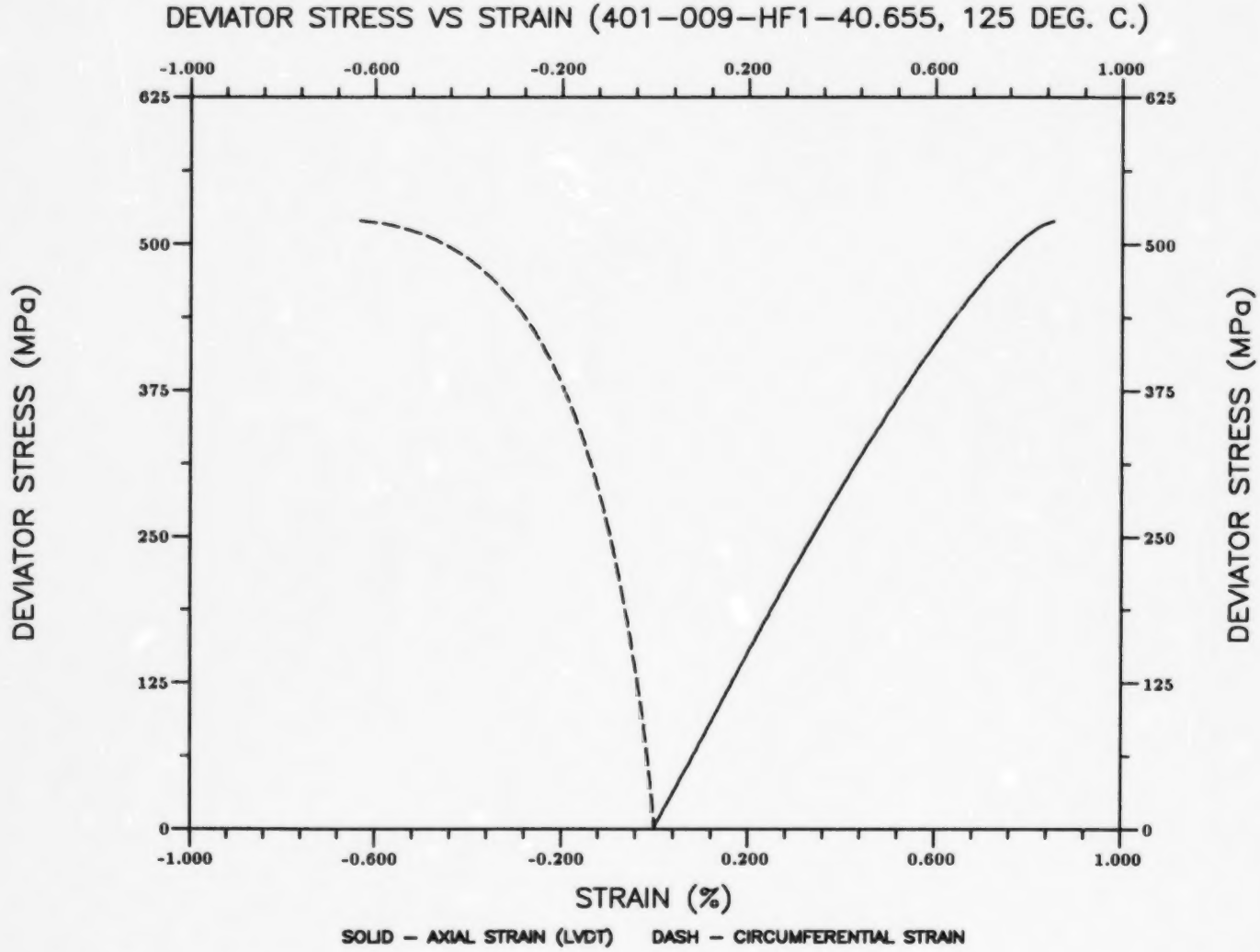

Figure A39. Stress-strain curves for Specimen 401-009-HF1-40.655 tested at 125° C and at $\sigma_3 = 35.0$ MPa.